

August 23, 2021

TO: Todd Mooney, P.E.
Geotechnical Office

FROM: Brice Exley, P.E.; Jeff Bruce, P.E.
WSDOT Geotechnical Office Consultants

SUBJECT: I-90/Easton Hill to W Easton I/C Phase 3 – Add Lanes/Wildlife Bridges,
MP 64.48-70.60, XL5479
Results of Numerical Modeling

PROJECT SUMMARY

This report summarizes Hart Crowser's, a division of Haley & Aldrich (Hart Crowser), numerical modeling of a tiered mechanically stabilized earth (MSE) and soldier pile wall for the I-90 expansion project from Cabin Creek to West Easton, Washington. We completed two-dimensional (2D) finite element modeling (FEM) of the proposed upper MSE Wall lower adjacent soldier pile and tieback wall using the software Plaxis 2D and at the following four roadway stations with the approximate equivalent Wall 2 design station shown in parenthesis:

- LE STA 1772+60 (STA 16+29)
- LE STA 1774+50 (STA 18+25)
- LE STA 1778+50 (STA 22+32)
- LE STA 1781+50 (STA 25+25)

The Washington State Department of Transportation (WSDOT) Construction Division, Geotechnical Office selected these four stations as four of the critical locations with respect to soil properties and/or size of the proposed structures. Additionally, we understand Station 1772+60 will be instrumented to collect performance data during and after construction. WSDOT provided the design profiles for each analysis section. We present these design profiles in Attachment 1.

The following memorandum documents our model assumptions, inputs, verification against historical wall performance records, and model results. Figure 1 shows a site plan with the locations of the modeled sections. Figures 2 through 5 show the subsurface profile of the existing conditions for stations STA 1772+60, STA 1774+50, STA 1779+50, and STA 1781+50.

Note, all load values presented from the results of the Plaxis analysis represent unfactored loads. Plaxis calculates these values with no load or resistance factors applied to any of the soil or structural properties.

SITE SOIL AND GROUNDWATER CONDITIONS

The WSDOT Geotechnical Office provided representative subsurface cross sections at the four analysis locations that we incorporated into our finite element models. The soil conditions for the analysis sections generally consisted of historical fill, colluvium, glacial till, and basalt and andesite bedrock. As the site sits in the foothills of the Cascade Mountains, basalt and andesite rock make up the majority of the slope structure. Glacial till overlies the bedrock with varying thickness of colluvium above the till and along the face of the slope. Finally, a fill embankment was placed partway up the slope during the original construction of Interstate-90 (I-90) to establish the grade for the existing I-90 lanes.

Groundwater was encountered in the majority of borings relevant to the four analysis sections. The interpretation of the design groundwater table was provided by the WSDOT Geotechnical Office based on groundwater levels measured from these borings.

PLAXIS MODEL INPUTS

The finite element model created for this project was focused on capturing behavior of the internal forces of the MSE reinforcement, the deflection of the MSE face, the internal forces and deflection of the soldier pile wall, and the loads in the tiebacks. The model was created in Plaxis 2D (Version 21.01.00.479).

Approach to Soldier Piles and Tiebacks

The proposed soldier piles and MSE wall facing were modeled as plate elements, with axial and bending stiffness values based on structural sizes provided by the WSDOT structural engineer. Embedded beams were originally used for the embedded portion of the soldier piles, but to facilitate comparison to traditional lateral earth pressure approaches, plate elements were used in the final models.

The proposed tieback anchors were modeled using two structural elements: node-to-node (N2N) anchors representing the unbonded zone of the tieback, and embedded beam elements representing the bonded zone of the tieback. The axial stiffness of the N2N anchors was defined based on seven strands required for the design tieback loads provided by the WSDOT structural engineer. The embedded beam elements were modeled using our design anchor pullout resistances based on published data for basalt bedrock in the Federal Highway Administration (FHWA) Geotechnical Engineering Circular No. 4. We defined the bonded zone stiffness based on the strand anchor's elastic properties, discounting the grout stiffness to account for a fully cracked condition while the anchor is put into tension. However, the stiffness is reduced to accommodate the diameter of the anchors when installed to capture spacing effects. This results in spring stiffnesses that are consistent with the derivation of the embedded beam to account for three dimensional effects as documented by Plaxis.

Approach to Geosynthetic Facing and Reinforcement

We modeled the MSE wall with two different design approaches: a permanent geosynthetic wrapped face wall system and a proprietary Hilfiker welded wire wall

system. The WSDOT Geotechnical Office provided the design reinforcement length for the MSE structure at the four design locations. Each of the modeled stations included a tiered truncated base geometry with reinforcement lengths at the base equal to 0.4 times the wall height that stepped up to 0.55, 0.7, and finally 0.8 times the wall height.

The MSE reinforcement for the geosynthetic wrapped face wall consisted of material properties consistent with Tensar UX1100MSE geosynthetic spaced vertically in one-foot increments. We modeled the geosynthetic reinforcement as geogrid elements in Plaxis. We defined the geogrid stiffness in the model as the low strain creep stiffness at 2 percent strain as shown in Appendix D of the WSDOT Qualified Products List. Similarly, the tensile capacity of the geogrid elements was based off the long-term tensile strength value shown in the same publication. We applied interfaces to the geogrid elements with a reduction on the interface friction equal to the Pullout Resistance Factor, F^* , equal to $2/3$ times the tangent of the friction angle multiplied by the scale effect correction factor, α , equal to 0.8. We included a four-foot section of secondary geogrid reinforcement from the top of each lift face extending backward into the backfill at an approximately 8H:1V angle to match WSDOT Standard Plans for wrapped face geosynthetic walls.

The face of the wrapped face wall was modeled using plate elements with the same low strain creep stiffness value at 2 percent. The plate element was selected to capture the lateral stiffness of the facing without needing to explicitly capture membrane effects in the 2D FEM model with an updated mesh. In the field, the membrane effect will occur during the initial construction staging for each lift, which does not require deformation of the wall once constructed. Reasonably capturing this effect in Plaxis would necessitate some degree of deformation that is inconsistent with what occurs during construction. In order to estimate the stiffness of the face, we back calculated an equivalent bending stiffness of the geogrid facing using Plaxis and modeling a length of geogrid as a simply supported beam. To accomplish this, we took a vertical one-foot length of geogrid with one end fixed in both x and y directions and the other end fixed in just the x direction. We applied varying distributed loads and noted the deformations calculated in Plaxis. This allowed for back calculation of the bending stiffness using elastic beam theory. Exhibit 1 (shown below) presents the constructed plate calibration model for the geogrid wall facing. The model presented in this exhibit is orientated with the same directions as our primary Plaxis models (i.e. the x direction is horizontal and the y direction is vertical).

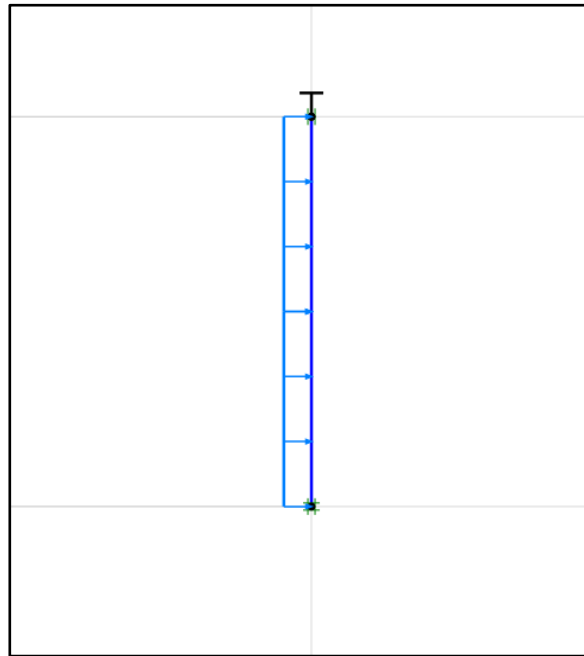


EXHIBIT 1. GEOGRID WALL FACING PLATE CALIBRATION MODEL EXCERPT

We calibrated the bending stiffness, EI , from the results of this model using the following equation:

$$\text{displacement} = -\frac{5wL^4}{384EI}$$

Where w equals the distributed load applied to the geogrid in the model, L equals the length of the geogrid in the model (1 foot), and displacement comes from the measured displacement from the model at the center of the geogrid. This equation is solved for EI to be used as an input to the geogrid wall face constitutive model.

Iterations to the Geogrid Modeling Approach

This model configuration for the wrapped face geosynthetic wall was the result of several iterations of modeling approaches to calibrate the wall deformations and internal forces to historical wall measurements (detailed in the following section of this report) and to internal force calculations performed by the WSDOT Geotechnical Office. The following modeling approaches were attempted:

- Wall face modeled as a semi-circular geotextile element for each MSE layer to prescribe the “pillowing” effect observed in wrap faced walls and reduce the deformation required to achieve a membrane effect with an updated mesh analysis.
- Wall face modeled as a vertical geotextile element with and without an updated mesh analysis.
- Temporary construction forms for the wall face modeled by fixing lateral displacements at various point/segments along the geotextile.
- Small lateral force applied to the top of each geotextile layer attempting to model the contractor pulling the geotextile tight between lifts.

- Surcharge loads applied to each lift to model compaction effort.
- Reinforcement layers modeled as embedded beam elements.
- Reinforcement layers modeled with both linear and non-linear modulus properties.

Approach to Hilfiker Facing and Reinforcement

Details for the Hilfiker welded wire reinforced wall were based on the Hilfiker Standard Drawings for “Welded Wire Retaining Wall” publicly available on the Hilfiker website and WSDOT Geotech’s design spreadsheets for the internal design of the welded wire wall system.

Welded wire mesh reinforcement systems (steel grid) can have F^* coefficients that are very small, with values ranging from 0.1 to 0.15 for this design. As such, incorporating the equivalent friction angle of the interface is approximately 7 degrees. Applying an interface with such a low friction angle on a continuous element that is part of the FEM mesh results in a very low strength sliding plane. However, the steel grid is not truly full coverage ratio, there is soil-soil contact between the bars or wires within the steel grid zone. Therefore, while the effective pullout resistance of the steel grid is relatively low, it does not introduce a particularly weak slip plane in the wall. To overcome this, we modeled the welded wire reinforcement using embedded beam elements in Plaxis. The embedded beam elements are structural elements that are located “in front of” the FEM mesh and are connected to the mesh using elasto-plastic springs. The use of the element avoids introducing a weak slip plane within the model, while also allowing for the pullout resistances to be consistent with the American Association of State Highway and Transportation Officials (AASHTO) methodologies. However, the embedded beam does carry compressive forces, which are not normally considered in the design of MSE walls. To overcome accumulating significant compressive loads in the reinforcement, up to four 6-inch-long N2N anchors (structural elements that do not carry compressive forces or moments) were spaced along the length of the embedded beam elements. Stiffness properties of the embedded beam elements were based on the elastic modulus of steel and the welded wire bar diameter, spacing, and size provided by the WSDOT Geotechnical Office.

We were required to make one adjustment to the input properties of the Hilfiker reinforcement due to how Plaxis models horizontal embedded beams. Plaxis assumes that embedded beam elements are used as vertical elements (i.e., pile foundations) and automatically calculates the normal force on the embedded beam based on horizontal stresses. However, for horizontal embedded beam elements, this needs to be adjusted to account for the contribution of the vertical stress to the normal force on the embedded beam. To correct this, we applied a correction factor to the horizontal spacing of the longitudinal bars based on a ratio of the average horizontal stress to the vertical stress. This allowed for Plaxis to incorporate the correct stress profile in the pullout resistance of the embedded beam.

The facing of the Hilfiker system in the model incorporated the welded wire mesh as well as the welded wire backing mat as shown in the Rock Facing Detail of sheet 2 in Hilfiker’s standard drawings. We modeled these two meshes as a single plate element with composite properties accounting for the combined stiffnesses of both meshes.

Exhibits 2 through 4 document the final structural properties of the elements included in our Plaxis 2D model.

EXHIBIT 2: STRUCTURAL (PLATE) INPUT PROPERTIES FOR SOLDIER PILES AND MSE WALL FACING

Structural Element	Poisson Ratio, ν	Axial Stiffness, EA (lb/ft) ^a	Bending Stiffness, EI (lb-ft ² /ft) ^b
Hilfiker Facing Lower ^c	0.30	1.02E7	3.32E2
Hilfiker Facing Middle ^c	0.30	9.12E6	2.60E2
Hilfiker Facing Upper ^c	0.30	8.88E6	2.48E2
Geogrid Facing	0.30	2.45E4	2.00E2
W14x109 ^d	0.30	1.03E8	2.78E7
W14x132 ^d	0.30	1.25E8	3.42E7
W14x145 ^d	0.30	1.38E8	3.83E7
W14x193 ^d	0.30	1.83E8	5.37E7

Notes:

- a) lb/ft = pound per foot
- b) lb-ft²/ft = pound-foot squared per foot
- c) Hilfiker facing properties vary based on changes in the facing reinforcement detail per the WSDOT provided design spreadsheet
- d) Soldier pile properties adjusted to account for the design spacing of 9 feet

EXHIBIT 3: STRUCTURAL (EMBEDDED BEAM) INPUT PROPERTIES FOR BONDED TIEBACK LENGTHS AND HILFIKER REINFORCEMENT

Element	Spacing (feet)	Area, A (in ²) ^a	Unit Weight (pcf) ^b	Elastic Modulus, E (psf) ^{c,d}	Axial Skin Resistance (lb/ft) ^e	Axial Stiffness Factor	Lateral Stiffness Factor	Base Stiffness Factor
Tieback	9	51	10	1.25E8	5.00E4	--	--	--
F* = 0.10	2.70	0.13	1.00	1.13E10	1.10E4	2.70	2.70	2.70
F* = 0.11 base	2.46	0.17	1.00	1.03E10	1.10E4	2.46	2.46	2.46
F* = 0.11 mid	2.46	0.08	1.00	1.03E10	1.10E4	2.46	2.46	2.46
F* = 0.12	2.25	0.08	1.00	9.41E9	1.10E4	2.25	2.25	2.25
F* = 0.13	2.08	0.08	1.00	8.69E9	1.10E4	2.08	2.08	2.08
F* = 0.14	1.93	0.08	1.00	8.07E9	1.10E4	1.93	1.93	1.93
F* = 0.15	1.80	0.08	1.00	7.53E9	1.10E4	1.80	1.80	1.80
F* = 0.16	1.69	0.08	1.00	7.06E9	1.10E4	1.69	1.69	1.69
F* = 0.17	1.59	0.08	1.00	6.64E9	1.10E3	1.59	1.59	1.59
F* = 0.32	0.84	0.08	1.00	3.53E9	1.10E4	0.84	0.84	0.84
F* = 0.34	0.80	0.08	1.00	3.32E9	1.10E4	0.80	0.80	0.80

Notes:

- a) in² = inches squared
- b) pcf = pounds per cubic foot
- c) psf = pounds per square foot

- d) Elastic modulus for tiebacks is reduced proportionally by the area of the steel relative to the area of the hole
- e) lbf/ft = pound force per foot

EXHIBIT 4: STRUCTURAL (N2N ANCHOR) INPUT PROPERTIES FOR UNBONDED TIEBACK LENGTHS AND WALL FACE CONNECTIONS

Structural Element	Spacing (feet)	Axial Stiffness, EA (pounds)	Maximum Tensile Force, Fmax, tens (pounds)
Tieback	9	4.38E7	--
Hilfiker Lower	1	3.73E6	2.25E14
Hilfiker Mid	1	2.65E6	2.25E14
Hilfiker Upper	1	2.40E6	2.25E14
Geogrid	1	2.45E4	--

Notes:

- a) Hilfiker properties vary based on changes in the reinforcement detail per the WSDOT provided design spreadsheet

Approach to Soil Elements

The subsurface profiles defined for the 2D model were based on sections provided by the WSDOT Geotechnical Office. We determined soil properties based on values provided by the WSDOT Geotech office for unit weight and friction angle of the soil properties and Hoek-Brown model inputs for the rock properties. More advanced soil properties for granular soil units were based off published correlations to relative density. Some model geometries required the introduction of small quantities of effective cohesion to the constitutive models to address numerical instabilities resulting in unrealistic soil failures. We limited the effective cohesion to a maximum of 50 pounds per square foot so as not to introduce unreasonable increases to the soil strengths.

Native Soils

The major distinct soil layers identified for the four analysis sections consisted of: historical fill, colluvium, glacial till, and basalt and andesite bedrock. We modeled the historical fill, colluvium, and glacial till using the Hardening Soil small (HSsmall) model. A key benefit of the HSsmall model is that it accounts for the small strain stiffness of soils and provides an adjustable shear modulus degradation curve based on the Hardin and Drnevich relationship (Plaxis 2014). Additionally, the model accounts for stress-dependent stiffness (i.e. stiffness as a function of confining pressure) as well as cap and hardening yield surfaces (i.e. yield criteria that can expand due to plastic straining) to capture the stress history of the soil. The HSsmall parameters for the existing soils were determined using published correlations between relative density and the primary constitutive model parameters as documented in *Validation of Empirical Formulas to Derive Model Parameters for Sands* by Brinkgreve, Engin and Engin (2010).

We modeled the basalt and andesite bedrock using the Hoek-Brown model incorporated into Plaxis. As previously stated, engineering values for this model were provided by the WSDOT Geotechnical Office.

MSE Backfill

Backfill for both the Hilfiker and geosynthetic walls was assumed to consist of WSDOT Gravel Borrow. We modeled gravel borrow using the Hardening Soil model. Similar to the HSsmall model, the hardening soil model accounts for stress-dependent stiffness as well as a cap and hardening yield surface. The Hardening Soil model differs from the HSsmall model in that the Hardening Soil model does not have a small strain overlay applied to it. The Hardening Soil model was used for the wall backfill due to the larger anticipated relative strains within the MSE structure and for better efficiency in the model calculations.

We modeled the gravel borrow using two different friction angles: 38 degrees based on standard values published in the Geotechnical Design Manual (GDM) and 47 degrees based on historical results of isotropically consolidated undrained triaxial compression tests (CICU) performed in similar material by Yu, Allen, and Bathurst (Yu et. al 2016) and the Federal Highway Administration (FHWA 2013). The higher friction angle is also more consistent with published documentation for gravel fill materials. Results of the 38-degree models were compared against the geotechnical design performed by the WSDOT Geotechnical Office. The results of the 47-degree model gave a more realistic estimate of the behavior of the structural system assuming similar strengths suggested by the historical test results. Converting the CICU derived effective friction angle to a plane strain compression (PSC) friction angle was not completed, which is conservative as the PSC friction angle is typically approximately 14 percent greater than the CICU friction angle.

Input parameters for the Hardening Soil model for gravel borrow were based on published correlations to relative density. We calibrated the relative density, and model parameters, to the 38-degree and 47-degree friction angle assumptions, which are consistent with published journal articles assessing the performance of MSE walls by Dr. Bathurst.

Exhibit 5 documents the estimated or measured engineering soil properties for each unit for the respective stations.

EXHIBIT 5: SOIL PROPERTIES

Element	Soil Unit						
	Existing Fill ^a	Colluvium ^b	Till	Basalt ^c	Andesite ^c	Gravel Borrow: 38 phi	Gravel Borrow: 47 phi
Constitutive Model	HS small	HS small	HS small	Hoek-Brown	Hoek-Brown	Hardening Soil	Hardening Soil
Drainage Type	Drained	Drained	Drained	Drained	Drained	Drained	Drained
Saturated Unit Weight (pcf)	125	125	145	171	173	135	135
Friction Angle, ϕ' (degrees)	33 – 35	34 - 37	41	--	--	38	47
Effective Cohesion, C (psf)	40	25 – 40	0	--	--	30	42
Reference Elastic Modulus at 50 percent Strain (psf)	5.72E5 to 6.94E5	7.76E5 to 8.77E5	1.21E6	--	--	2.00E6	1.70E6

Element	Soil Unit						
	Existing Fill ^a	Colluvium ^b	Till	Basalt ^c	Andesite ^c	Gravel Borrow: 38 phi	Gravel Borrow: 47 phi
Reference Elastic Modulus Constrained (psf)	5.72E5 to 6.94E5	7.76E5 to 8.77E5	1.21E6	--	--	1.50E6	1.70E6
Reference Elastic Modulus During Unload/Reload (psf)	1.72E6 to 2.08E6	2.33E6 to 2.63E6	3.63E6	--	--	4.00E6	5.10E6
Reference Small Strain Shear Modulus, G _o (psf)	1.90E6 to 2.04E6	2.13E6 to 2.25E6	2.63E6	--	--	--	--
Shear Strain Corresponding to 30% Secant Shear Modulus Reduction, Gamma _{0.7}	1.50E-4 to 1.45E-4	1.38E-4 to 1.30E-4	0.10E-3	--	--	--	--
E' _{rm}	--	--	--	1.45E8	2.78E8	--	--
Sigma _{mi}	--	--	--	1.08E6	1.79E6	--	--
GSI	--	--	--	25	25	--	--
D	--	--	--	35	35	--	--
	--	--	--	0	0	--	--

Notes:

- Existing fill properties based on the design friction angle for each station as follows: 35 degrees for 1772+60, 33 degrees for 1774+50, and 34 degrees for 1779+50 and 1781+50
- Colluvium properties based on the design friction angle for each station as follows: 37 degrees for 1774+50 and 34 degrees for 1772+60, 1779+50, and 1781+50
- Basalt properties used for the models at stations 1774+50, 1779+50, and 1781+50. Andesite properties used for the model at station 1772+60

Approach to Staged Construction

The Plaxis model includes several sequential construction stages. The full model sequential construction stages are shown as story boards in Attachment 2 for one example model for Geogrid model and Attachment 3 for one example model for Hilfiker model.

We defined the construction staging based on conversations with the WSDOT Geotechnical Office WSDOT standard plans for the construction of wrapped face geosynthetic MSE walls. The standard plans specify the use of temporary forms to support the soil backfill at the facing until the next layer of reinforcement can be placed. We modeled these forms by incorporating fixed lateral displacements in the x direction along the face of each newly activated lift. These fixed displacements were then removed upon activation of the next stage of overlying lifts.

A detailed breakdown of the construction sequencing in the models is as shown below. Please refer to the story boards in Attachments 2 and 3 for figures presented how these stages were constructed in the model.

- Excavate a 2 horizontal to 1 vertical (2H:1V) slope and create a bench for soldier pile installation.
- Activate the soldier pile.

3. Backfill behind the soldier pile to a minimum of 2 feet over the first tieback level, install the first tieback, and stress the first tieback. Perform these three construction procedures over three stages. Continue this sequence until all tiebacks have been activated and pre-stressed and the backfill grade reaches the bottom of the MSE elevation.
4. Activate the first two lifts of geogrid and backfill (one foot vertical spacing) or one layer of Hilfiker and backfill (two-foot vertical spacing) and the facing. Activate the face displacement that fixes the facing in the x-direction to simulate the construction form.
5. Activate the next two layers of geogrid and backfill (one foot vertical spacing) or one layer of Hilfiker and backfill (two foot vertical spacing) and the facing. Activate the face displacement at the same time for the newly activated backfill lift. Deactivate the face displacement for the previous two lifts.
6. The sequence continues until reaching the top lift of reinforcement and backfill.
7. Deactivate the last face displacement.

We defined the construction staging to attempt modeling the application of loads as close to reality as possible given the constraints of the constitutive model. We would not anticipate significant changes to our results for minor alterations to this sequencing. However, significant changes to the application of loads (i.e. excessive lift sizes, application of several rows of the MSE wall at once, etc.) would likely impact the results. We do not expect sensitivity to construction methodology different than what is typically observed in the construction of typical MSE walls.

VALIDATION OF MODELING APPROACH TO HISTORICAL WALL PERFORMANCE DATA

We validated our modeling approach against two historical MSE projects performed by WSDOT: a 12.6-meter-high geotextile wall constructed along Rainier Avenue in Seattle, WA, and a 10.7-meter-high geogrid reinforced modular block retaining wall along State Route 18 (SR-18) near Seattle, WA. Both projects instrumented their wall stations allowing for validation against post-construction inclinometer and discrete strain gauge data.

Rainier Avenue

The Rainier Avenue project consisted of the design and construction of a wrapped face geotextile MSE wall with heights of up to 12.6 meters. Details on the design and construction of the walls and the results of the monitoring program for the wall were published in the 1992 paper, "*Performance of a 12.6-meter-high Geotextile Wall in Seattle, WA*," by Allen, Bathurst, and Holtz. Using details provided in the paper, we replicated the instrumented wall section in Plaxis 2D.

Based on review of the 1992 paper, we understand the wall was designed for a reinforcement length equal to 80 percent of the wall height, a vertical spacing of 0.38 meters, and design geotextile strengths and stiffnesses that varied with depth. Exhibit 6 (shown below) presents the geometry of the instrumented section.

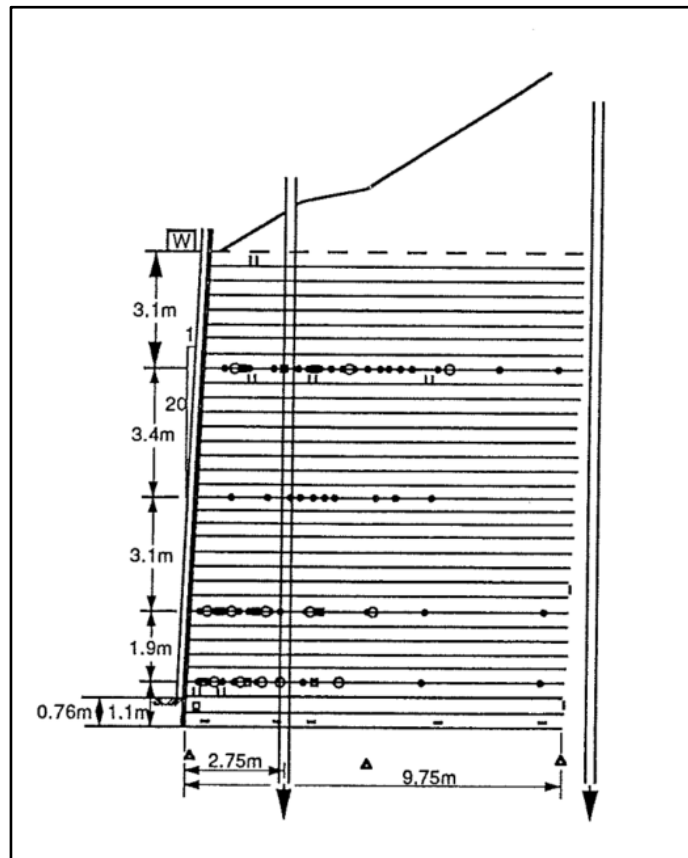


**EXHIBIT 6. HISTORICAL RAINIER AVENUE INSTRUMENTED WALL CROSS SECTION
(EXCERPT FROM FIGURE 3. OF PERFORMANCE OF A 12.6 M HIGH GEOTEXTILE WALL IN
SEATTLE, WA, ALLEN ET. AL, 1992.)**

To validate our proposed modeling approach for the I-90 project, we used the same structural elements and staged construction techniques as our I-90 model when building the Rainier Avenue model. We based the geometry for the model off the instrumented section of the Rainier Avenue wall presented in Exhibit 6 (shown above). We modeled the MSE backfill using the Hardening Soil constitutive model for 47-degree gravel borrow based on laboratory test data performed for the project. Properties for the geotextile were based on the published wide width strength and modulus values presented in the 1992 paper. The paper included design values for the 4 zones of geogrid reinforcement for the wide width tensile strength and the modulus at 5 percent strain. Exhibit 7 (shown below) presents the constructed 2D Plaxis model at the instrumented wall section.

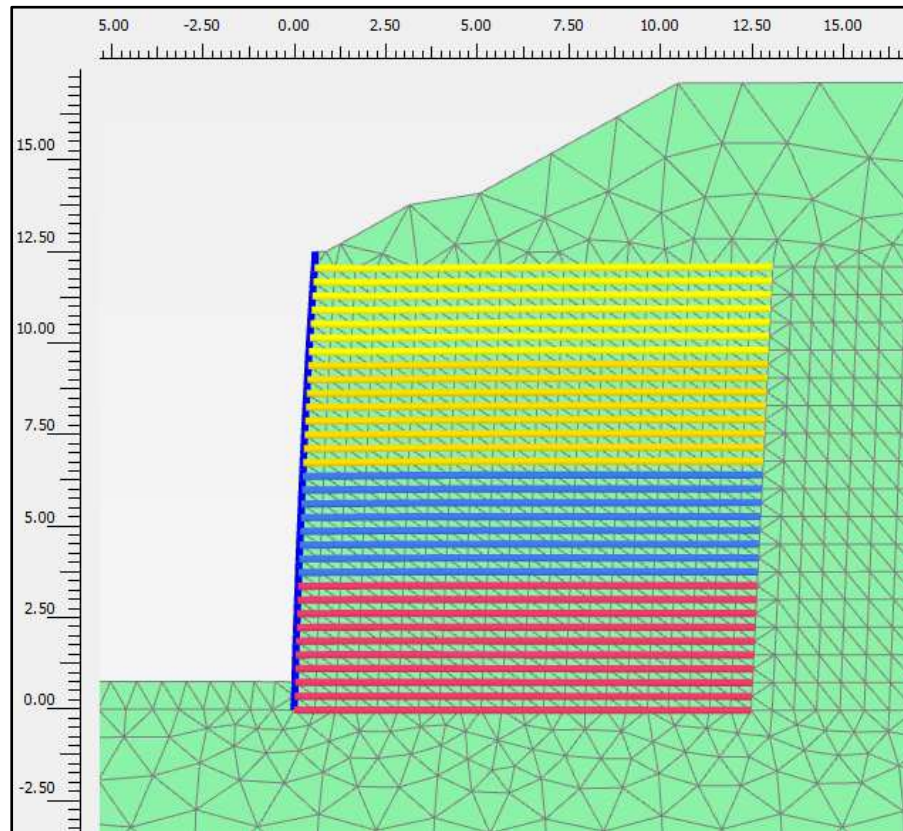


EXHIBIT 7. PLAXIS 2D FINITE ELEMENT MODEL CONFIGURATION FOR RAINIER AVENUE INSTRUMENTED WALL SECTION (SCALE IN METERS)

We compared the Plaxis results to the published performance data for the deformation of the wall face and the strains in the geotextile reinforcement. The published wall face deformation data included the results of optical surveys, extensometer plate surveys, and photogrammetry surveys performed during construction. We plotted these results against the lateral deformations predicted by Plaxis for the accumulated deformations of the wall face during phased construction of the MSE layers. The Plaxis deformations account for the elongation of the geotextile reinforcement and the deformation of the wall face elements. Exhibit 8 (shown below) presents this comparison. The results show the Plaxis estimates to match the general shape and magnitude of the deformations measured from the three field surveys.

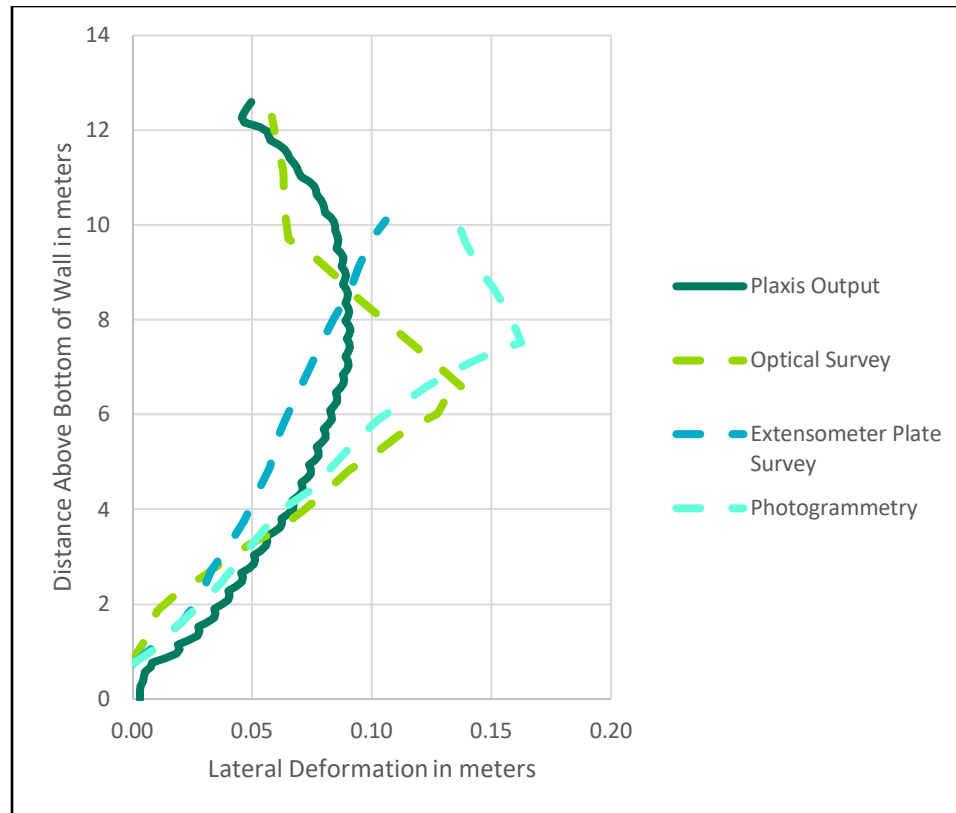


EXHIBIT 8. COMPARISON OF MSE WALL FACE DEFORMATION BETWEEN PLAXIS RESULTS AND FIELD MEASUREMENTS FOLLOWING CONSTRUCTION

We used the strain gauge data presented for the geogrid layer 9.5 meters from the base of the wall to compare to the internal force per unit width of wall estimated by Plaxis. We back calculated the internal force per unit width of wall of the geogrid using the historical strain data and the presented unit stiffness properties for the geogrid. Exhibit 9 (shown below) presents the results of this comparison. Plaxis appears to overpredict the forces in the geogrid compared to those calculated from the strain measurements in the field. Potential sources for the discrepancy include: the definition of the reference strain in the field, limitations of the constitutive model, the use a linear modulus for the geogrid to define the load, and the input modulus for the geogrid properties based on 5 percent strain. Current WSDOT design standards based on recent studies assume end of construction modulus values associated with 2 percent strains. Incorporating a modulus associated with 2 percent strain would result in stiffer geogrid properties and reduced displacements. Additionally, back calculation of the axial force in the geogrid from strain data depends on an accurate estimate of the modulus of the material. Given the uncertainty in the appropriate stiffness values this could lead to errors in the calculated loads presented in Exhibit 9.

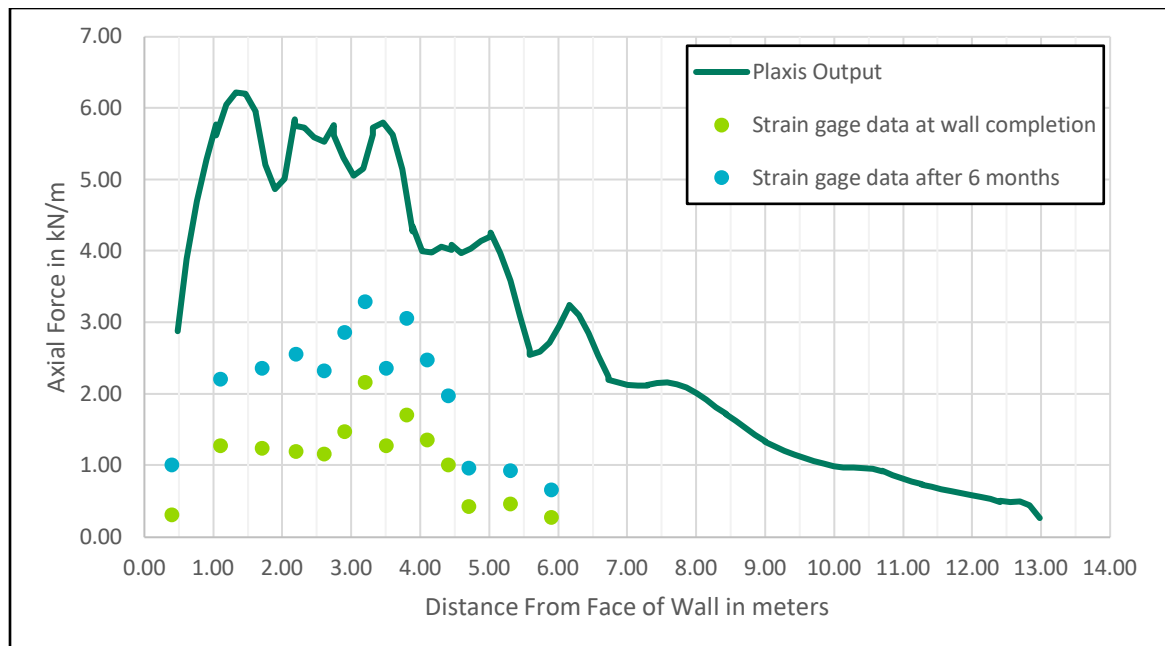


EXHIBIT 9. RAINIER AVENUE INTERNAL GEOGRID AXIAL FORCE COMPARISON: LAYER 9.5 METERS FROM BOTTOM OF WALL

SR-18

The SR-18 project consisted of the design and construction of a geogrid reinforced modular block retaining wall with heights of up to 10.7 meters. A historical finite-difference numerical modeling study was performed and published in the 2016 paper *"Numerical Modeling of the SR-18 Geogrid Reinforced Modular Block Retaining Walls"* by Yu, Bathurst, and Allen. This paper detailed the design and construction of the walls as well as a comparison of the results of the numerical models to the data collected during and following construction.

Based on review of the paper, we understand there were two walls instrumented for this project: Wall C with a height of 10.7 meters and Wall D with a height of 6.4 meters. Using details provided in the paper, we replicated the larger instrumented wall section for Wall C from the project in Plaxis 2D. Wall C was designed for a reinforcement length equal to 8.8 meters, a vertical spacing of 0.6 meters, and design geotextile strengths and stiffnesses that varied with depth. Exhibit 10 (shown below) presents the geometry of the instrumented section.

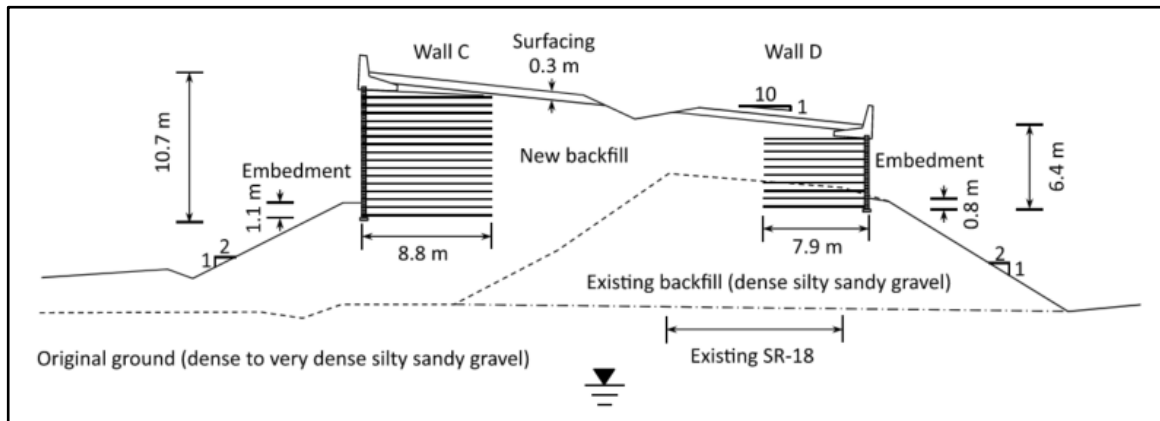


EXHIBIT 10. CROSS SECTION OF HISTORICAL SR-18 MSE WALL CONFIGURATIONS

To validate our proposed modeling approach for the I-90 project, we used the same structural elements and staged construction techniques when building the SR-18 model. We based the geometry for the model off the instrumented section for Wall C presented in Exhibit 10 above. We modeled the MSE backfill using the Hardening Soil constitutive model for the 47-degree gravel borrow based on laboratory test data performed for the project.

We modeled three different geogrid strengths as detailed in the 2016 paper: 115, 70.3, and 54 kN/m ultimate strengths. The paper provided nonlinear relationships for time-dependent secant stiffness and strain based on research performed by Allen and Bathurst (2014). We incorporated these ultimate strengths and nonlinear stiffness relationships into the constitutive model for the geogrid elements.

Exhibit 11 (shown below) presents the constructed 2D Plaxis model at the instrumented wall section.

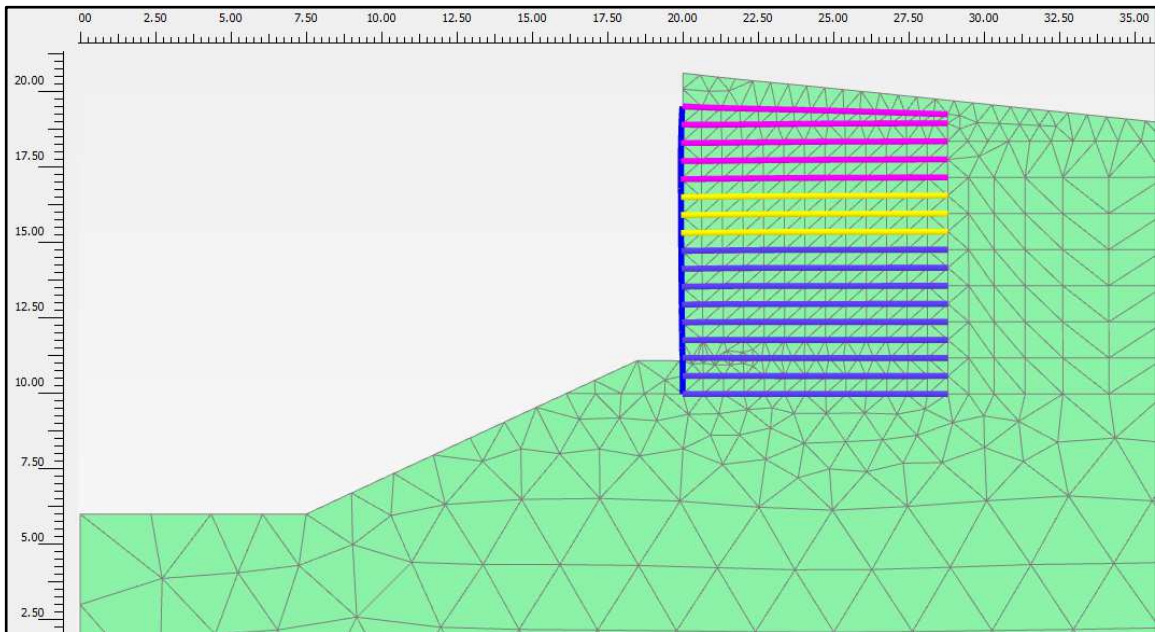


EXHIBIT 11. PLAXIS 2D FINITE ELEMENT MODEL CONFIGURATION FOR SR-18 WALL C (SCALE IN METERS)

We compared the Plaxis results to the results of the historical finite-difference model, the field measurements for the wall deformations, and the maximum measured tensile loads for the reinforcement following construction. Regarding wall deformation results, the historical finite-difference model incorporated both 8 and 16 kilopascal (kPa) surcharge loads to model the effects of compaction on wall face deformations. We plotted the results of the 16-kPa compaction model and the results of the field measurements to compare against the lateral deformations predicted by Plaxis for the accumulated deformations of the wall face during phased construction of the MSE layers. The Plaxis deformations account for the elongation of the non-linear geotextile model and the deformation of the wall face elements. Exhibit 12 (below) presents this comparison.

The results show the Plaxis estimates match the general shape and magnitude of the deformations predicted from the finite difference model. However, both the Plaxis results and the finite difference results overestimated the wall face deformation compared to the measurements taken in the field following construction. Yu, Bathurst, and Allen address this discrepancy in the 2016 paper and comment it may be due to very aggressive methods the contractor used to maintain wall facing alignment, which was observed by Allen and Bathurst (2014). Should the wall have been allowed to deform without aggressive correction by the contractor, the field results likely would better match the results of the finite element and finite difference models.

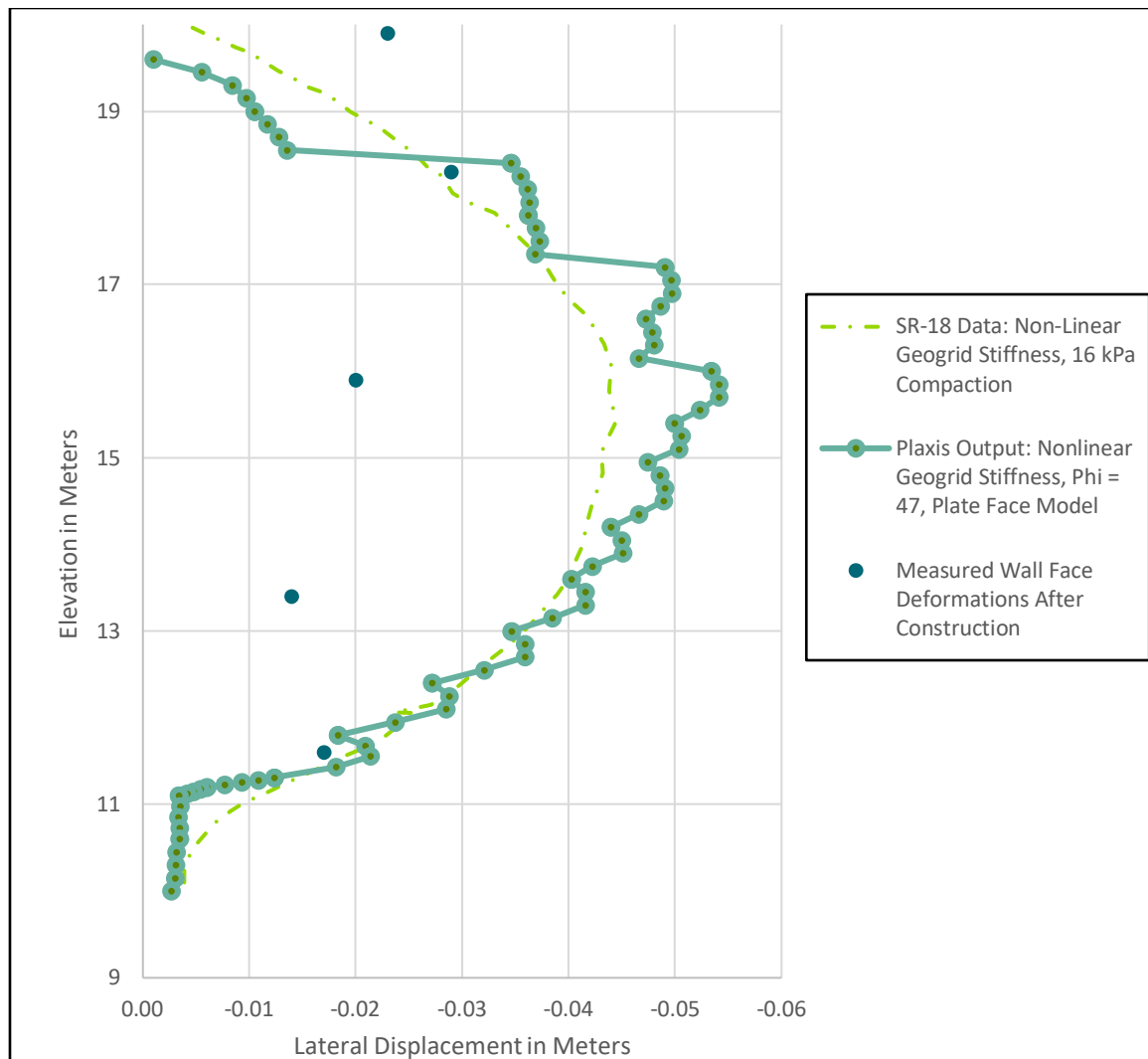


EXHIBIT 12. COMPARISON OF MSE WALL FACE DEFORMATIONS BETWEEN PLAXIS RESULTS AND FIELD MEASUREMENTS FOLLOWING CONSTRUCTION

We used the measured maximum tensile loads presented in Figure 11b of the 2016 paper to compare to the internal forces estimated by Plaxis. Additionally, we compared the results to the results of the historical Finite Difference Model (FDM) estimates (using nonlinear elastic soil properties) as well as to the maximum axial tensile load calculated using the Simplified Stiffness Method and the AASHTO Simplified Method for Wall C. Exhibit 13 (shown below) presents the results of these comparisons. Plaxis appears to match well to the maximum measured axial forces near the top and base of the wall. The model appears to slightly overpredict the maximum axial forces near the middle of the wall. However, this model in general presents a better agreement with the historical data than the Rainier Avenue model previously described. In our opinion this is likely due to the more accurate methodology for modeling the geogrid properties by using the non-linear stiffness relationships published in the 2016 paper.

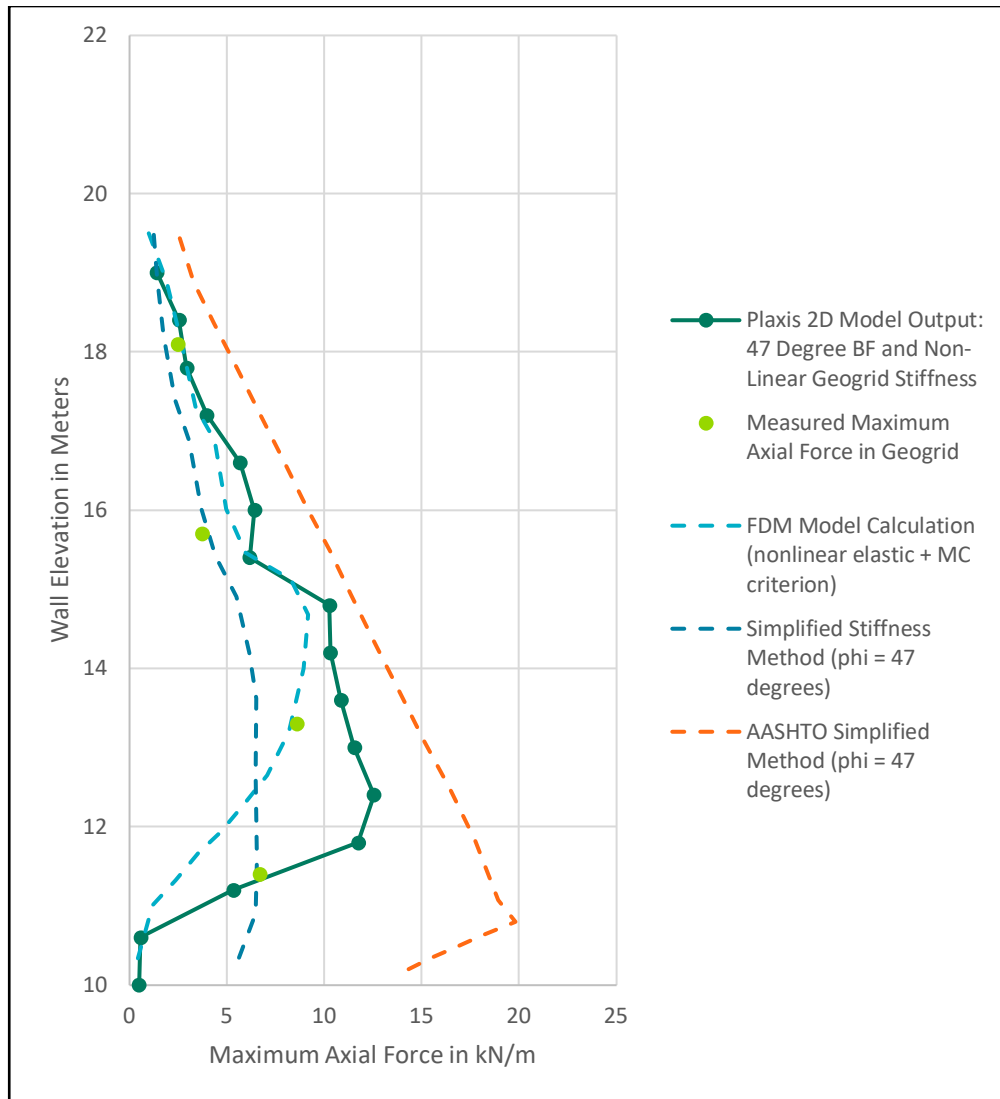


EXHIBIT 13. SR-18 MAXIMUM INTERNAL GEOGRID AXIAL FORCE COMPARISON

Conclusions

Based on the results of our validation models for the SR-18 and Rainier Avenue geosynthetic walls, our modeling and staged construction approach provides wall face deformations in general agreement with the historical field measurements. However, this modeling approach appears to overestimate the maximum axial force in the geogrid reinforcement elements. This overestimation was significantly higher for the Rainier Avenue validation model that used geogrid stiffness properties based off the modulus at 5 percent strain. The SR-18 model utilized the non-linear, time-dependent modulus relationship with results more aligned with a modulus at 2 percent strain. As noted above, the results of this model matched well to the measured maximum axial forces near the top and bottom of the wall and only slightly overpredicted the forces in the middle of the wall. Additionally, the model results from SR-18 overpredicted the forces of the bottom half of the wall compared to the Simplified Stiffness Method, but underpredicted the forces compared to the AASHTO Simplified Method.

Based on these comparisons, the assumed modulus values for the proposed geogrid for the I-90 Plaxis model, based on the modulus at 2 percent strain, should give a reasonable, albeit slightly conservative, estimate of the internal forces of the geogrid reinforcement.

PLAXIS 2D FINITE ELEMENT MODEL RESULTS

We provided representative plots and figures of the results in Figures 6 to 9 at Station 1772+60. Compiled results for all 16 models were provided to the Geotechnical Office via email.

Soldier Pile Results

Output of the enveloped normal forces, shear forces, and bending moments for each section can be found on Figure 6 for STA 1772+60 and within the separately provided spreadsheets for all other models. Horizontal displacement profiles of the soldier pile wall prior to and at the end of the MSE construction for all model iterations are also included in these spreadsheets.

We provided example output of the effective normal stresses on the back and front face of the soldier pile interface elements in Figure 7.

Based on our review of the results the soldier piles appear to perform generally as anticipated. The stress application from the vertical surcharge of the MSE wall is not significantly different than the traditional simplified methods. However, the prestress loads for the tiebacks appear to result in significant lateral deformation of the top of the soldier pile into the retained soils behind the wall. This deformation appears to be sensitive to the assumed friction angle, and thus passive resistance, of the backfill placed behind the wall. We recommend the structural engineer review the soldier pile results for conformity with their design assumptions and adjust the lock-off loads as necessary. Specifying a delay in prestressing the upper tiebacks until additional backfill is placed to increase the passive resistance of the pile is an example of a technique that could be employed that we would not expect to significantly alter the results of the model in a negative way.

Tieback Results

Exhibit 14 presents the design lock-off loads for the proposed tiebacks, as well as the calculated maximum anchor load for each anchor at the end of construction. Cells highlighted in gray are anchors that exceed the lock-off loads by more than 5 kips.

EXHIBIT 14: ANCHOR LOADS

Station	Anchor Elevation (feet)	Pre-Stress Load (kips)	Load at End of Construction with Geogrid Reinforcement (kips)		Load at End of Construction with Hilfiker Reinforcement (kips)	
			Gravel Borrow: 38 phi	Gravel Borrow: 47 phi	Gravel Borrow: 38 phi	Gravel Borrow: 47 phi
1772+60	2488	235	257	251	270	264
	2482		242	251	248	254
	2476		249	257	237	249
1774+50	2491	150	191	161	180	158
	2485		154	149	151	149
	2479		140	145	140	145
1779+50	2497	205	212	211	214	214
	2491		207	209	209	211
1781+50	2491	255	279	277	283	282

In general the results indicate that the tiebacks carry loads above their pre-stress values following construction of the MSE wall. We recommend the structural engineer review these values to confirm this increase does not present a structural concern for the tiebacks.

MSE Facing and Reinforcement Results

Example horizontal displacement profiles of the MSE wall face at Station 1772+60 at the end of construction are shown in Figure 8. Example plots of the internal forces for the geogrid and Hilfiker straps at the end of construction are shown in Figure 9. Exhibit 15 (below) presents the maximum deformation estimated along the MSE wall face for each model and analysis section.

EXHIBIT 15: MAXIMUM CALCULATED MSE WALL FACE DEFORMATION

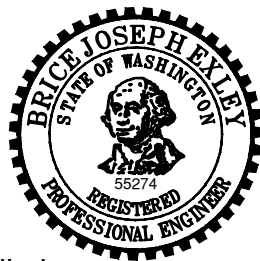
Station	Wall Type	Gravel Borrow Friction Angle	Maximum Wall Face Deformation in inches
1772+60	Geogrid	38	15.7
		47	7.7
	Hilfiker	38	2.5
		47	1.5
1774+50	Geogrid	38	12.0
		47	5.8
	Hilfiker	38	1.6
		47	0.8
1779+50	Geogrid	38	8.3
		47	6.2
	Hilfiker	38	1.1
		47	0.8
1781+50	Geogrid	38	12.2
		47	6.1
	Hilfiker	38	2.0
		47	1.3

The results indicate the anticipated deformation of the wrapped face geogrid wall face to be sensitive to the assumed friction angle of the backfill soils. As a result, gravel borrow with friction angles at or above values historically tested for similar walls (i.e. 47 degrees) may be required to achieve similar wall performance as historically measured. To validate this, WSDOT should collect and test representative samples from the proposed gravel source prior to construction.

CLOSURE


This report has been prepared to provide the details and results of the numerical modeling performed at select Stations for the subject project. It should not be used, in part or in whole for other purposes without contacting the Geotechnical Office for a review of the applicability of such reuse. This memorandum should be made available to prospective contractors for their information or factual data only, and not as a warranty of ground conditions.


If you have questions or require further information, please contact Brice Exley at (206) 860-5554.



Preliminary

Prepared By: Brice Exley, P.E.
By: Principal Geotechnical
Engineer

Reviewed By: 
Todd Mooney, P.E.
Geotechnical Design Project
Development Engineer

Agency Approval Authority: 
Tony Allen, P.E.
State Geotechnical Engineer

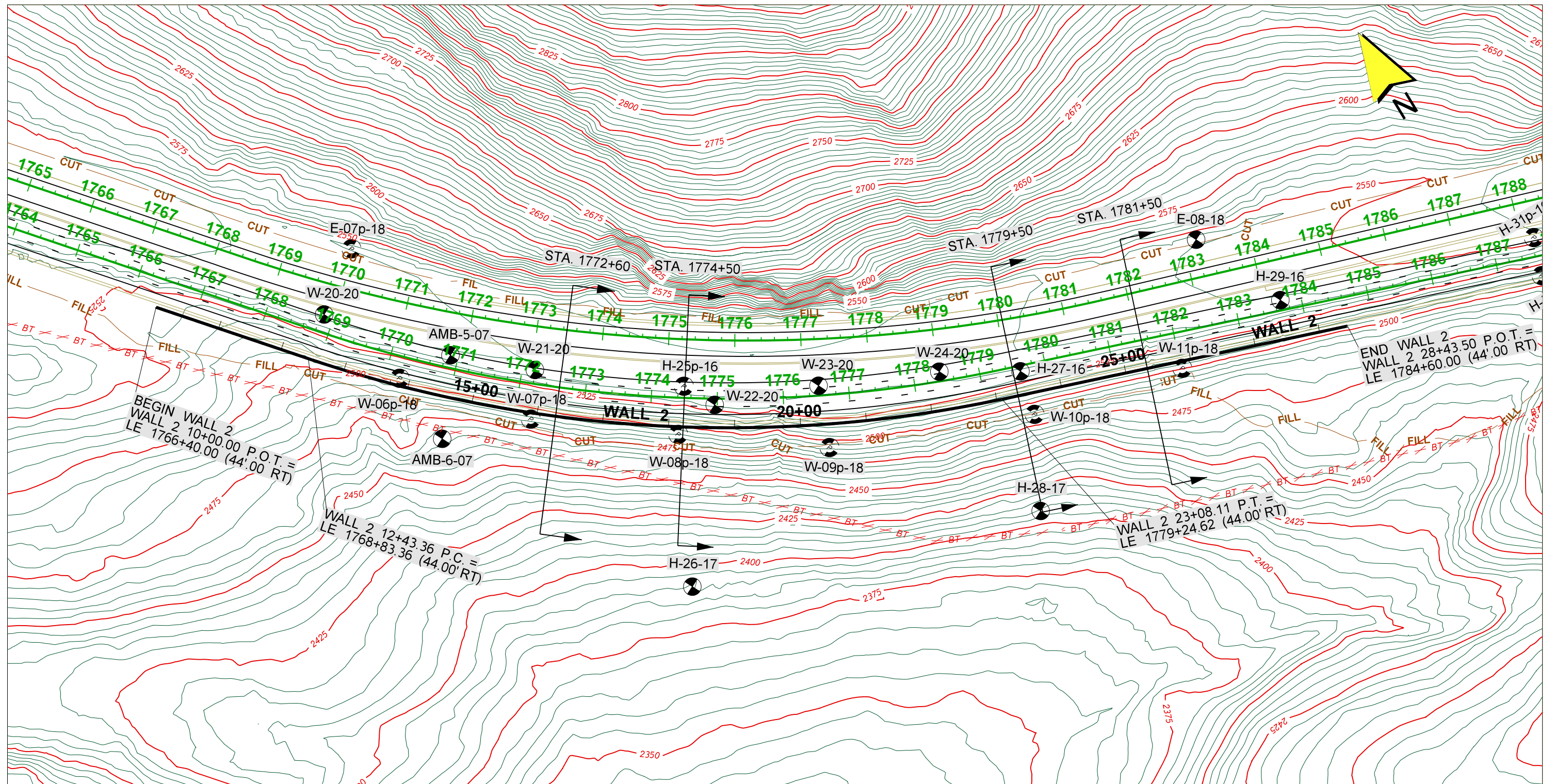
TJM:RBH/be:jsb:snb

Figures:



- Figure 1 – Site Plan
- Figure 2 – Station 1772+60 Plaxis Cross Section: Existing Conditions
- Figure 3 – Station 1774+50 Plaxis Cross Section: Existing Conditions
- Figure 4 – Station 1778+50 Plaxis Cross Section: Existing Conditions
- Figure 5 – Station 1781+50 Plaxis Cross Section: Existing Conditions
- Figure 6 – Representative Output STA 1772+60: Soldier Pile Internal Forces
- Figure 7 – Representative Output STA 1772+60: Effective Normal Stress on Back and Front Face of Soldier Pile
- Figure 8 – Representative Output STA 1772+60: MSE Wall Face Deformations
- Figure 9 – Representative Output STA 1772+60: MSE Reinforcement Maximum Axial Force

Attachments:

- Attachment 1 – WSDOT Provided Design Sections
- Attachment 2 – Plaxis Storyboard: Geogrid Example
- Attachment 3 – Plaxis Storyboard: Hilfiker Example



"Plaxis 2D Analysis Section"

-  H-1-19 Test Boring Location
-  H-1p-19 Test Boring And Piezometer Location

0 75 150
SCALE IN FEET

JOB# XL5479 STATE ROUTE 090 MILEPOST(S) 00.00 - 00.00

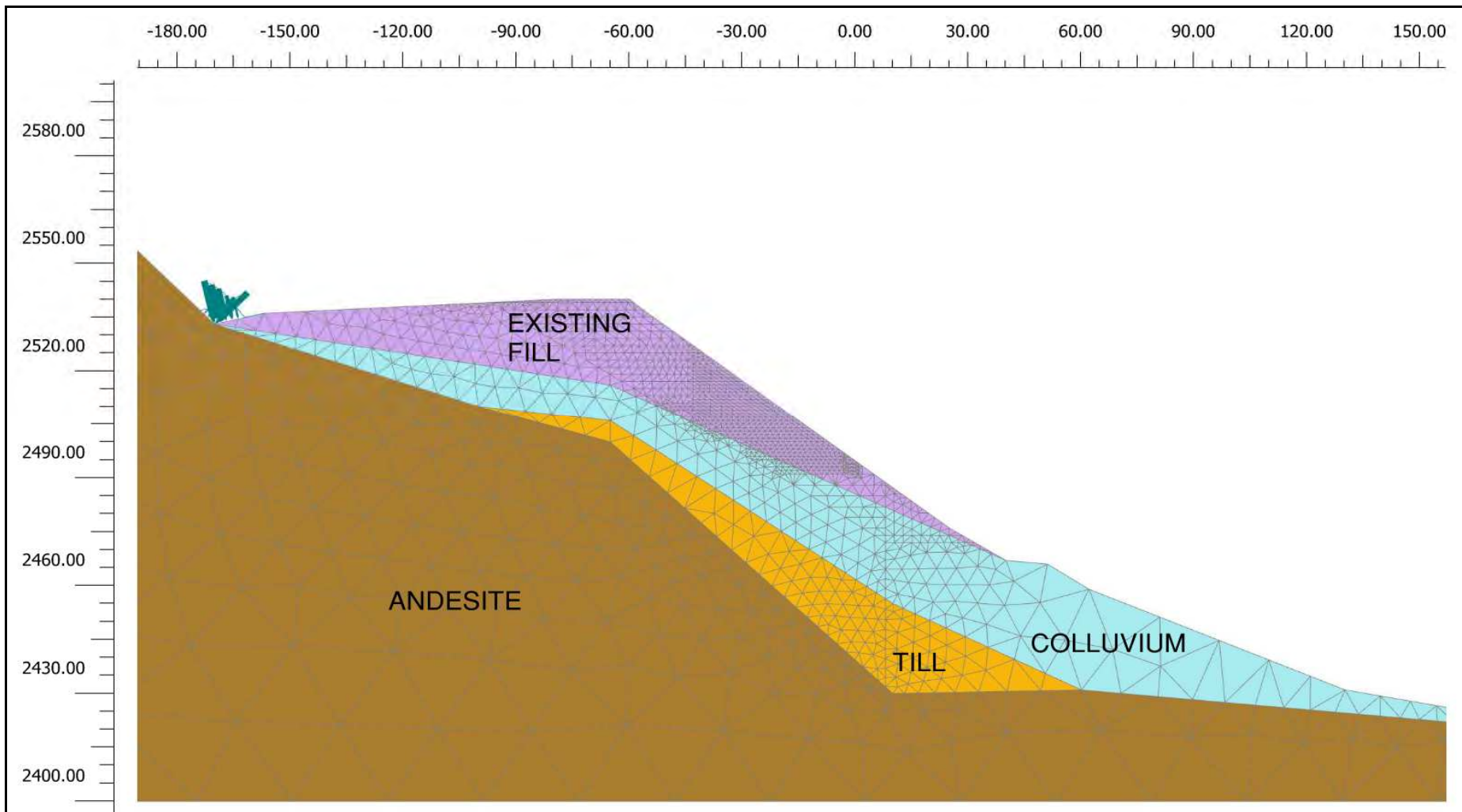
FIGURE 1: SITE MAP - WALL 2

I-90/Easton Hill To W Easton I/C Phase 3 -
Add Lanes/Wildlife Bridges

 **WSDOT** GEOTECHNICAL OFFICE

PREPARED BY William Montgomery

DATE July, 2021



NOTES:

JOB# XL-5479 STATE ROUTE 90 MILEPOST(S) 107.5

FIGURE 2: STA 1772+60 PLAXIS CROSS SECTION: EXISTING CONDITIONS

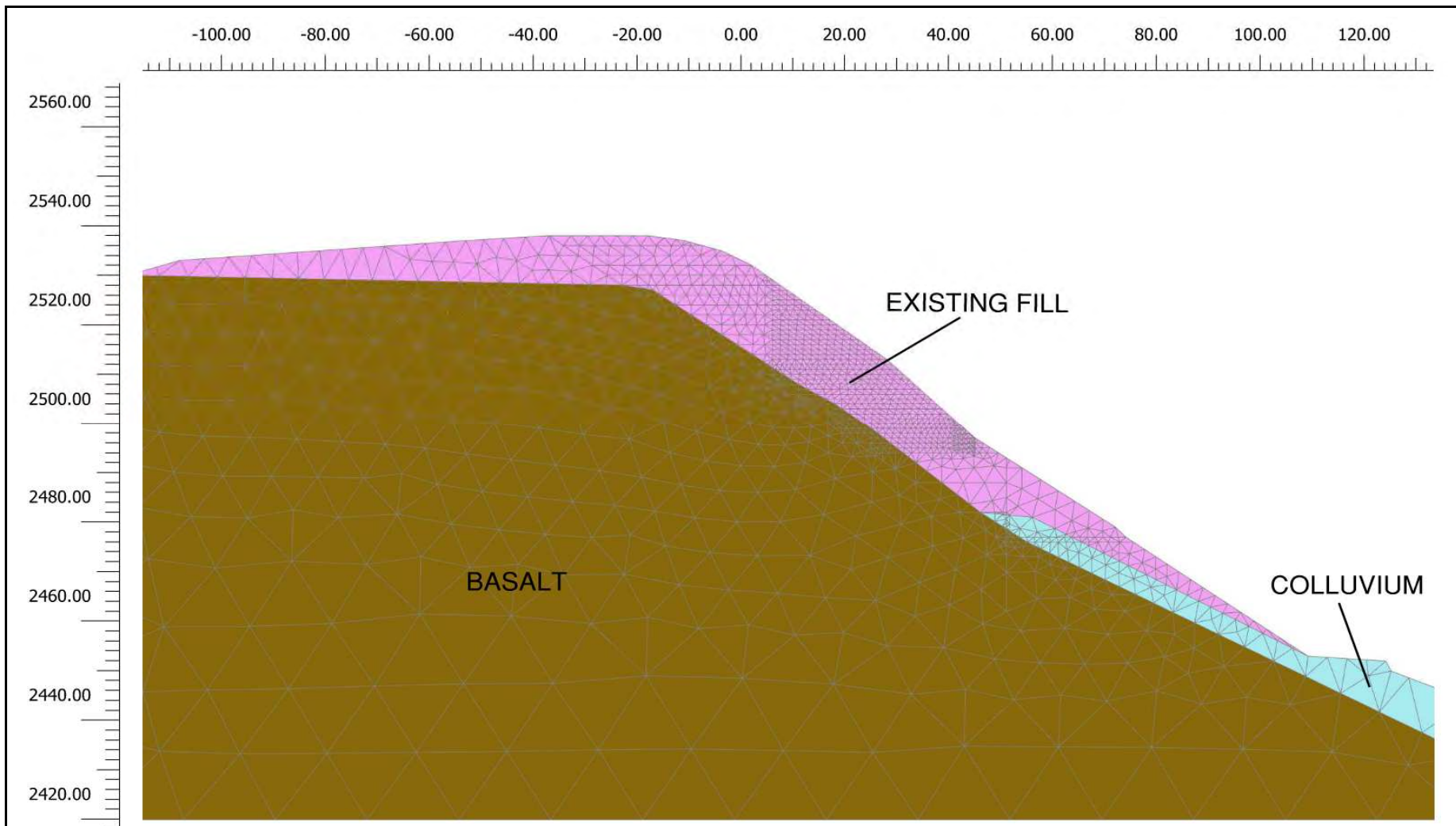
I90/EASTON HILL TO W EAST I/C PHASE 3
ADD LANES/WILDLIFE BRIDGES



GEOTECHNICAL OFFICE

PREPARED BY J. Bruce

DATE 7/2021



NOTES:

JOB# XL-5479	STATE ROUTE 90	MILEPOST(S) 107.5
--------------	----------------	-------------------

**FIGURE 3: STA 1774+50 PLAXIS
CROSS SECTION: EXISTING CONDITIONS**

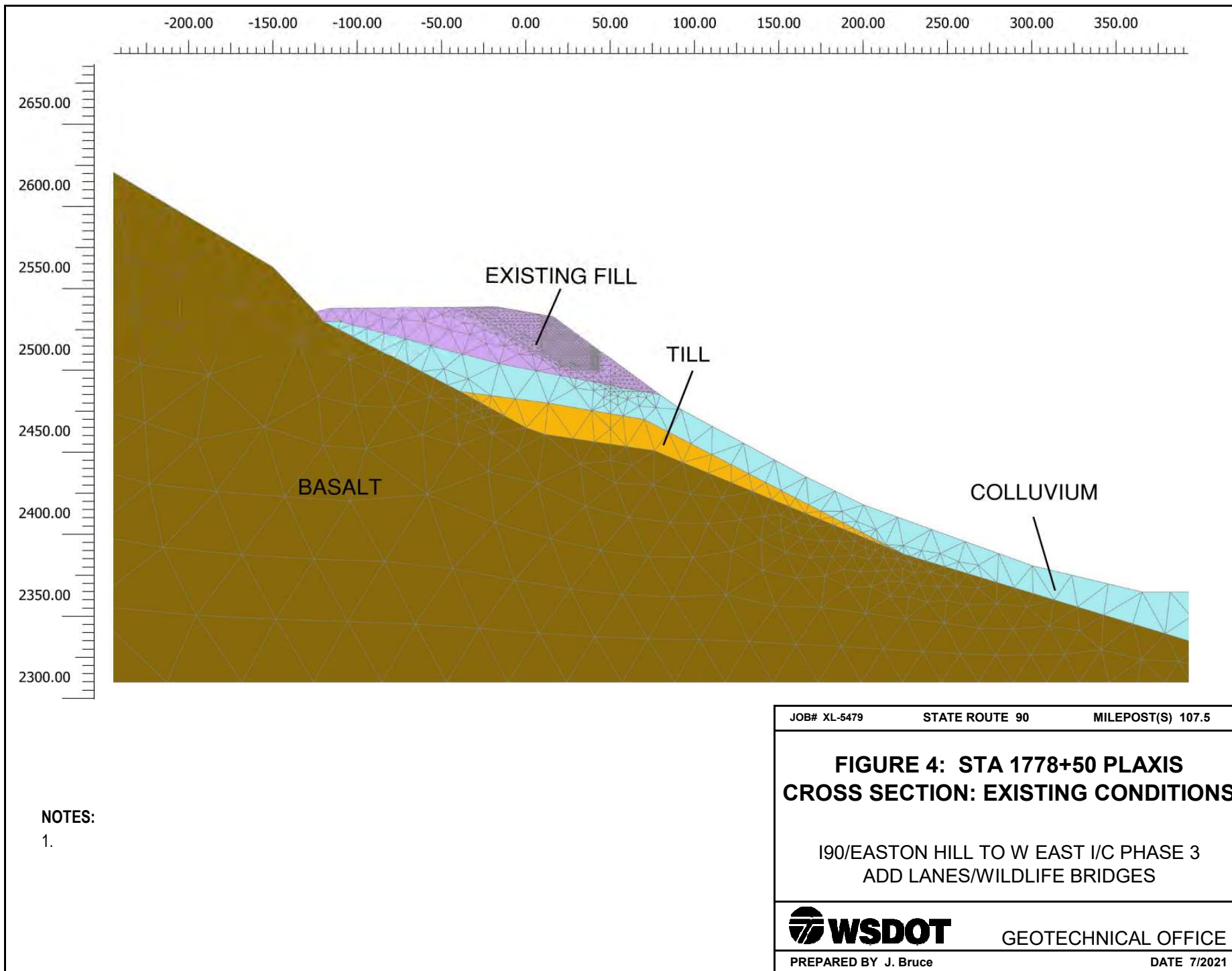
I90/EASTON HILL TO W EAST I/C PHASE 3
ADD LANES/WILDLIFE BRIDGES

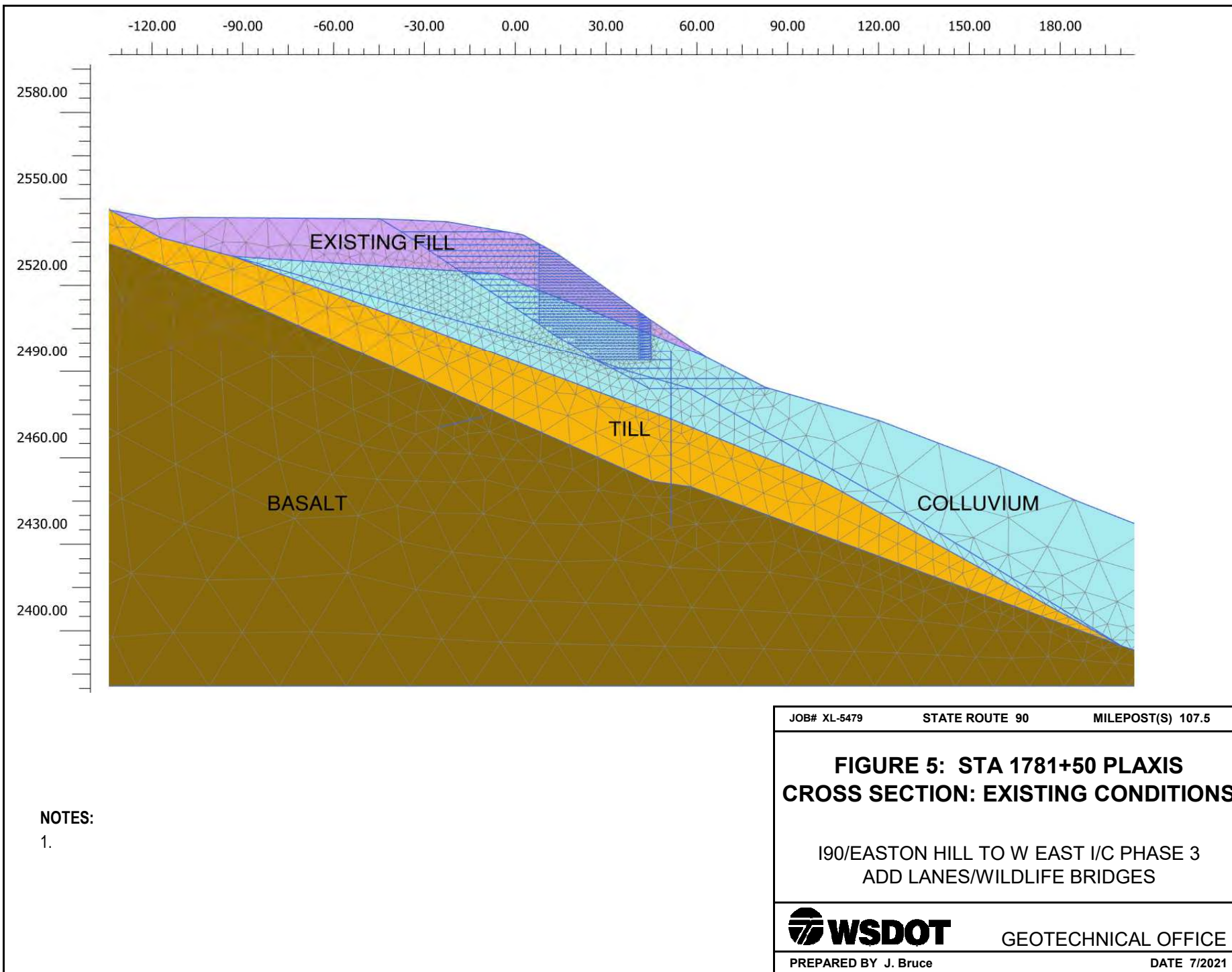


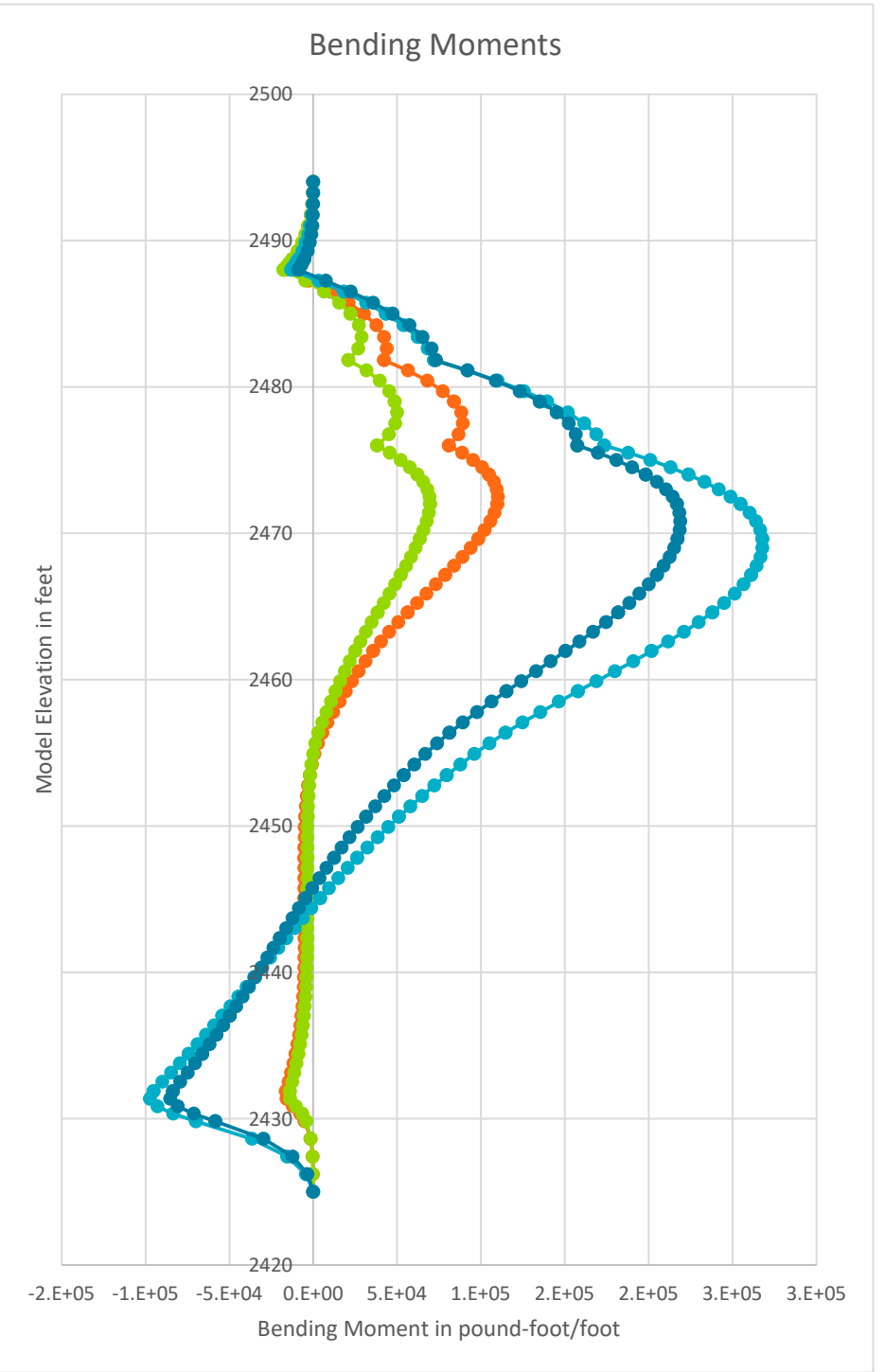
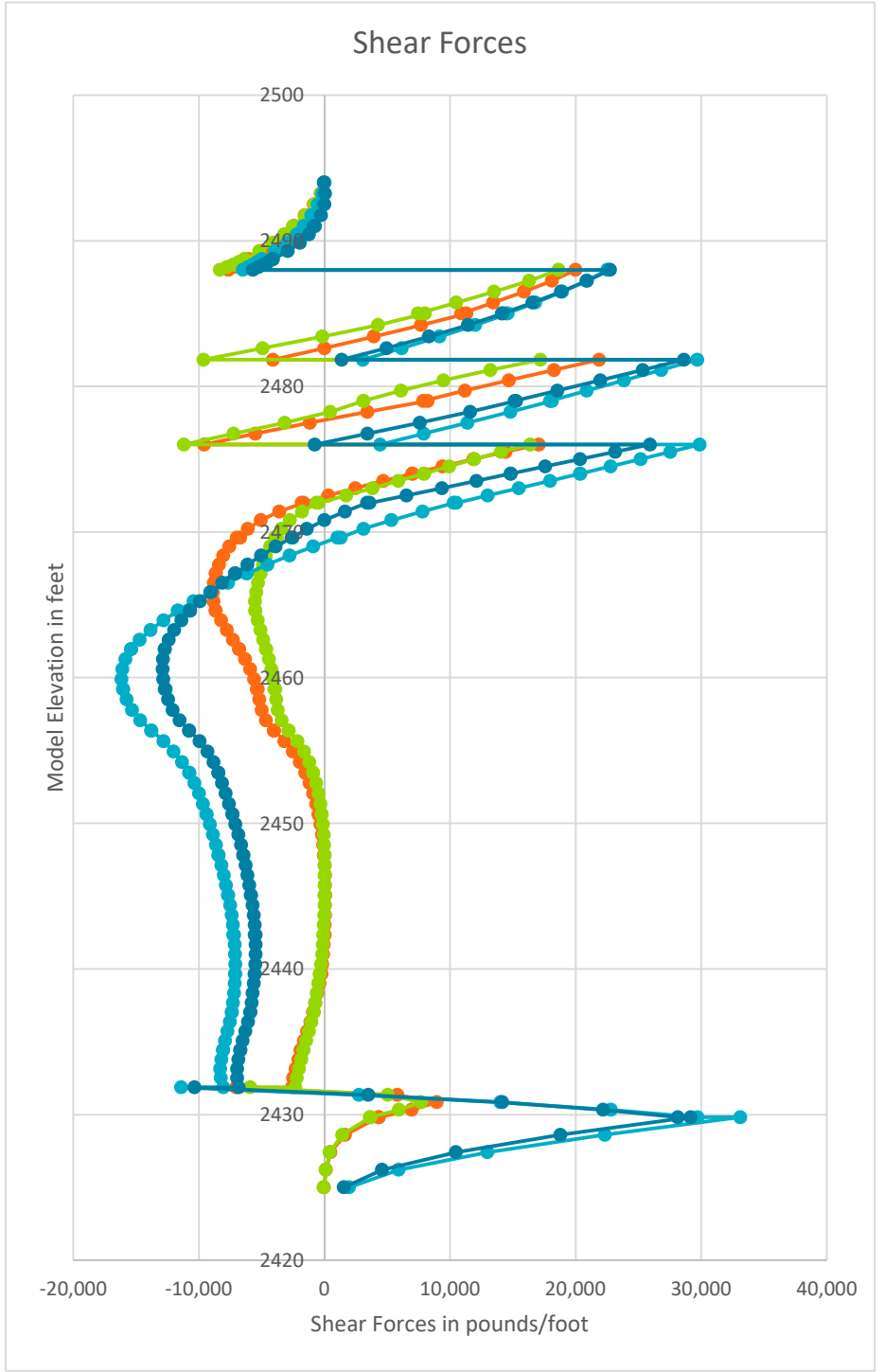
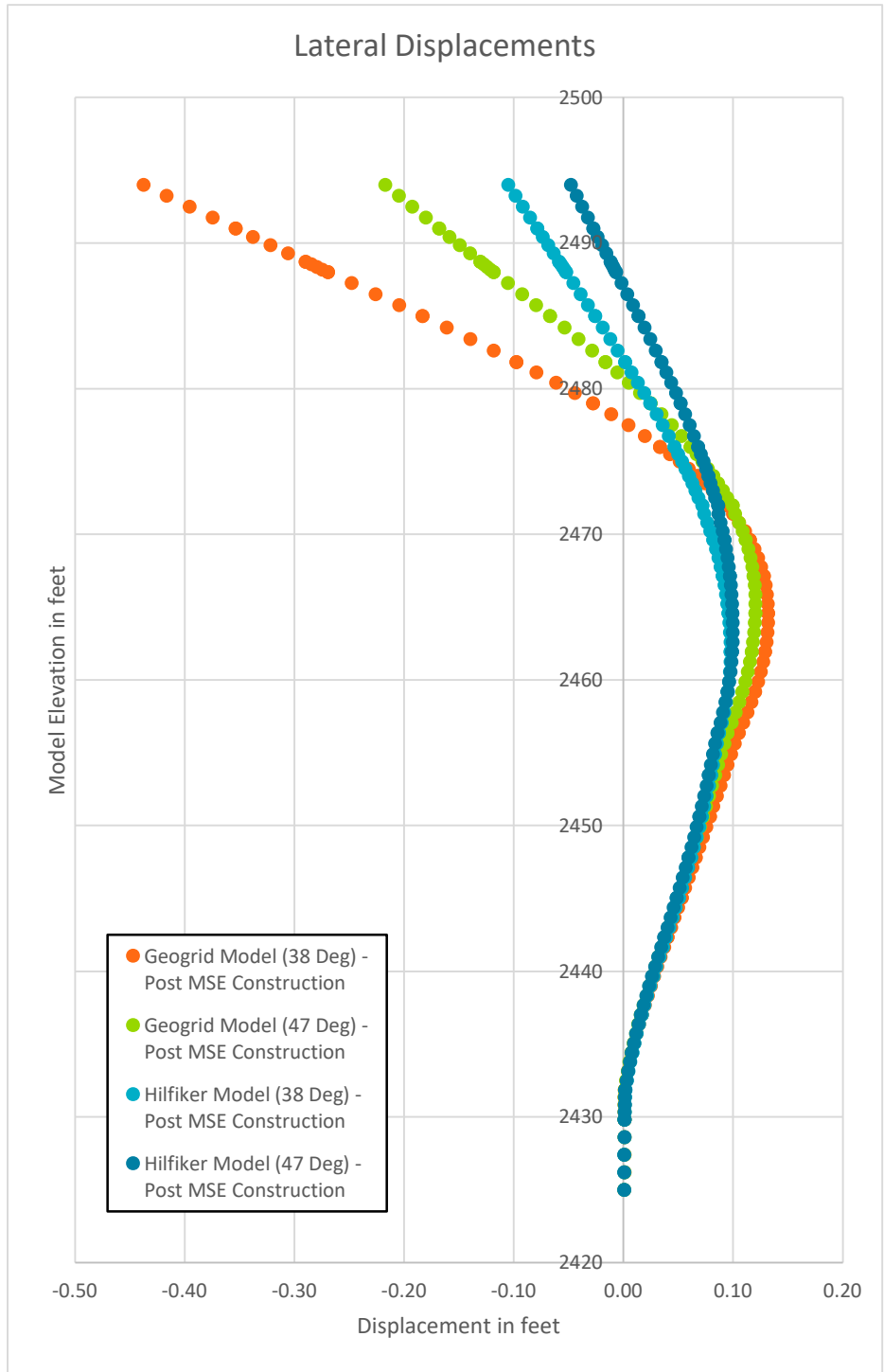
GEOTECHNICAL OFFICE

PREPARED BY J. Bruce


DATE 7/2021



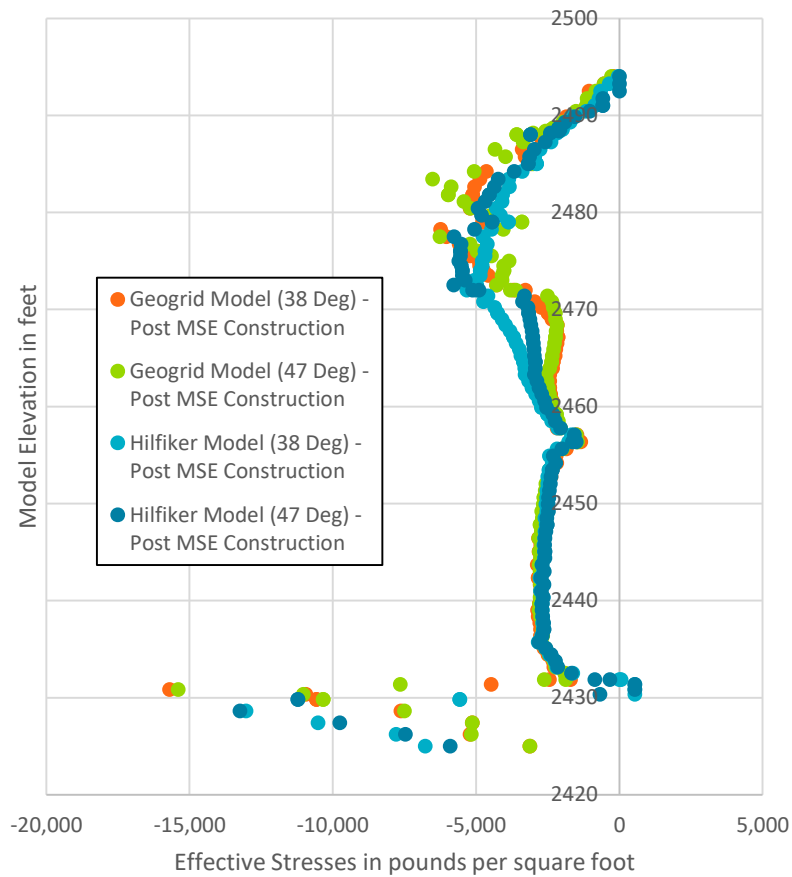




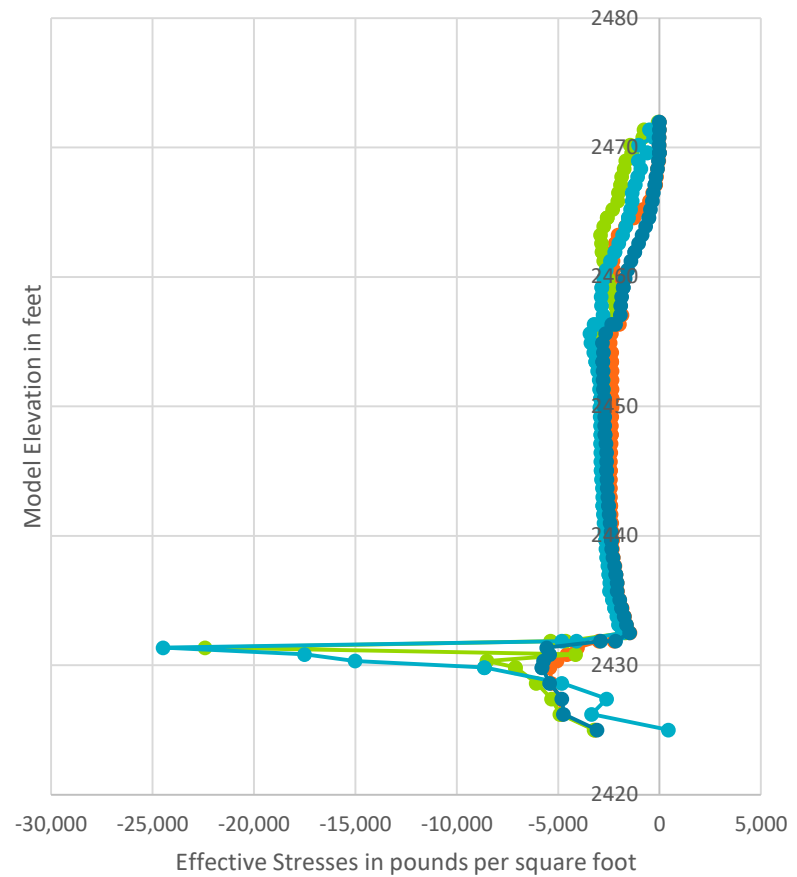
- NOTES:**
1. Compression is negative.
 2. Friction angles presented in the legend correspond to the modeled friction angle for the gravel borrow backfill.

JOB# XL-5479	STATE ROUTE 90	MILEPOST(S) 107.5
FIGURE 6: REPRESENTATIVE OUTPUT STA 1772+60 SOLDIER PILE INTERNAL FORCES		
190/EASTON HILL TO W EAST I/C PHASE 3 ADD LANES/WILDLIFE BRIDGES		
		GEOTECHNICAL OFFICE
PREPARED BY J. Bruce		DATE 7/2021

Effective Normal Stresses on Back of Pile



Effective Normal Stresses on Front of Pile



NOTES:

1. Friction angles presented in the legend correspond to the modeled friction angle for the gravel borrow backfill.

JOB# XL-5479 STATE ROUTE 90 MILEPOST(S) 107.5

**FIGURE 7: REPRESENTATIVE OUTPUT STA
1772+60
EFFECTIVE NORMAL STRESS ON SOLDIER PILE**

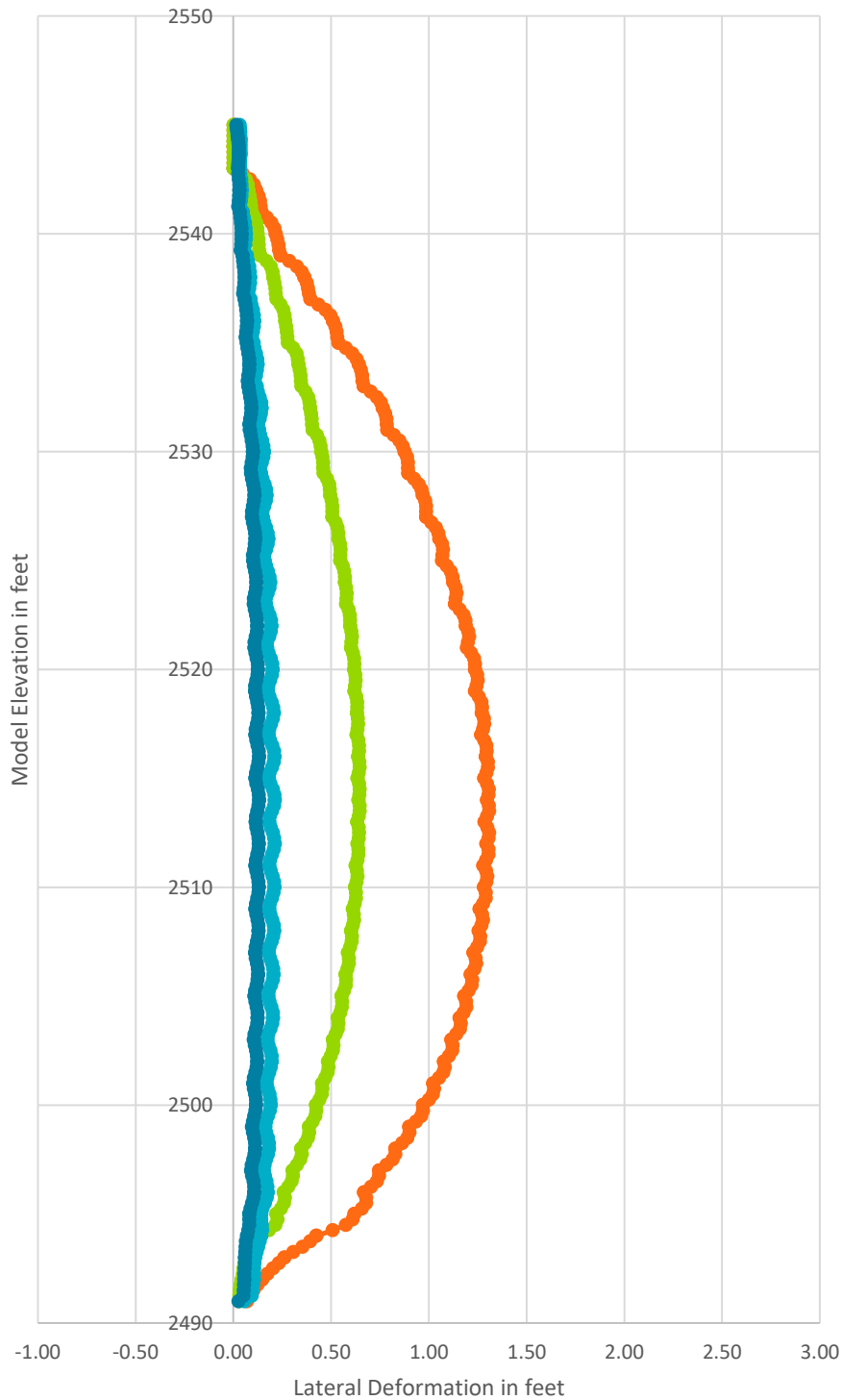
I90/EASTON HILL TO W EAST I/C PHASE 3
ADD LANES/WILDLIFE BRIDGES



GEOTECHNICAL OFFICE

PREPARED BY J. Bruce

DATE 7/2021



NOTES:

1. Friction angles presented in the legend correspond to the modeled friction angle for the gravel borrow backfill.

JOB# XL-5479 STATE ROUTE 90 MILEPOST(S) 107.5

**FIGURE 8: REPRESENTATIVE OUTPUT
STA 1772+60
MSE WALL FACE DEFORMATIONS**

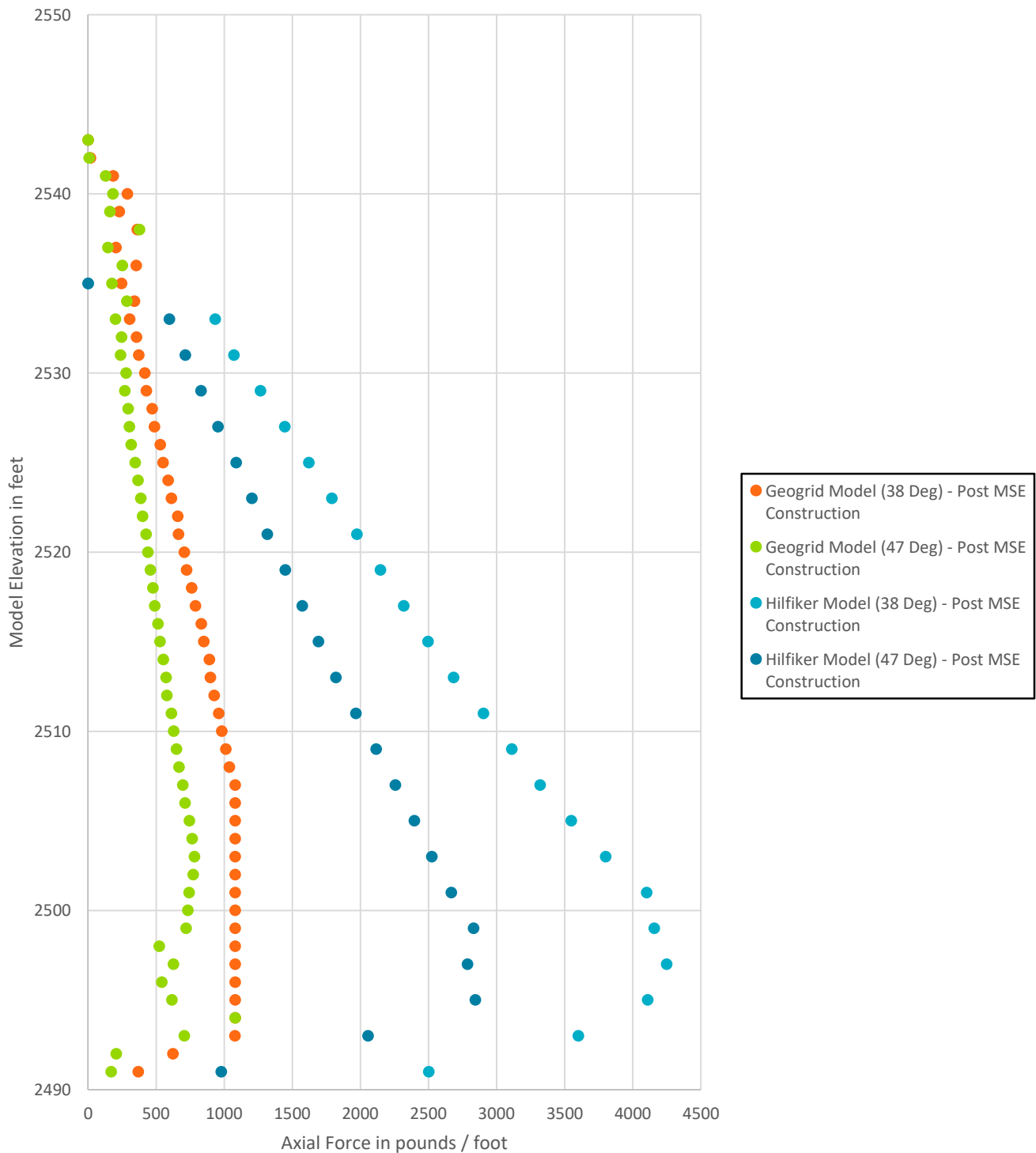
I90/EASTON HILL TO W EAST I/C PHASE 3
ADD LANES/WILDLIFE BRIDGES



GEOTECHNICAL OFFICE

PREPARED BY J. Bruce

DATE 7/2021



NOTES:

- Friction angles presented in the legend correspond to the modeled friction angle for the gravel borrow backfill.

JOB# XL-5479

STATE ROUTE 90

MILEPOST(S) 107.5

**FIGURE 9: REPRESENTATIVE OUTPUT STA
1772+60
MSE REINFORCEMENT MAXIMUM AXIAL FORCE**

I90/EASTON HILL TO W EAST I/C PHASE 3
ADD LANES/WILDLIFE BRIDGES

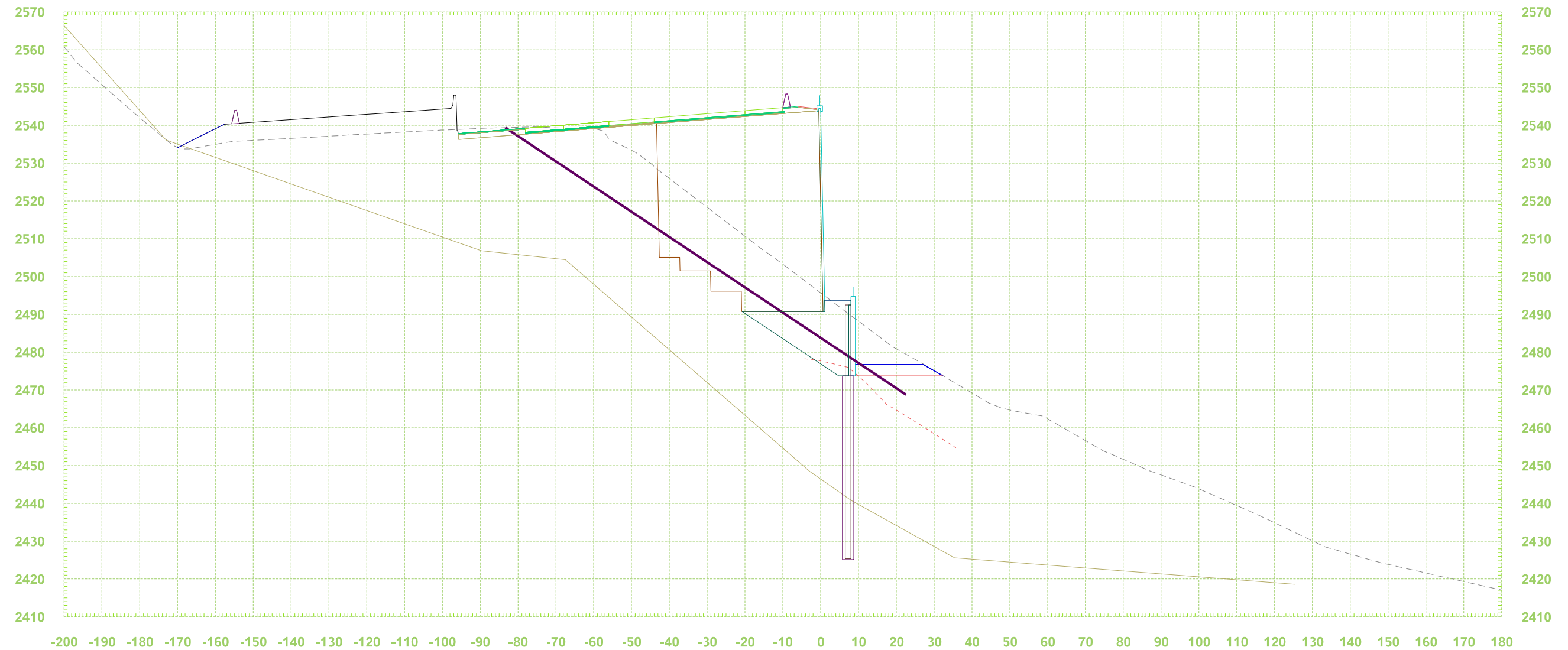


GEOTECHNICAL OFFICE

PREPARED BY J. Bruce

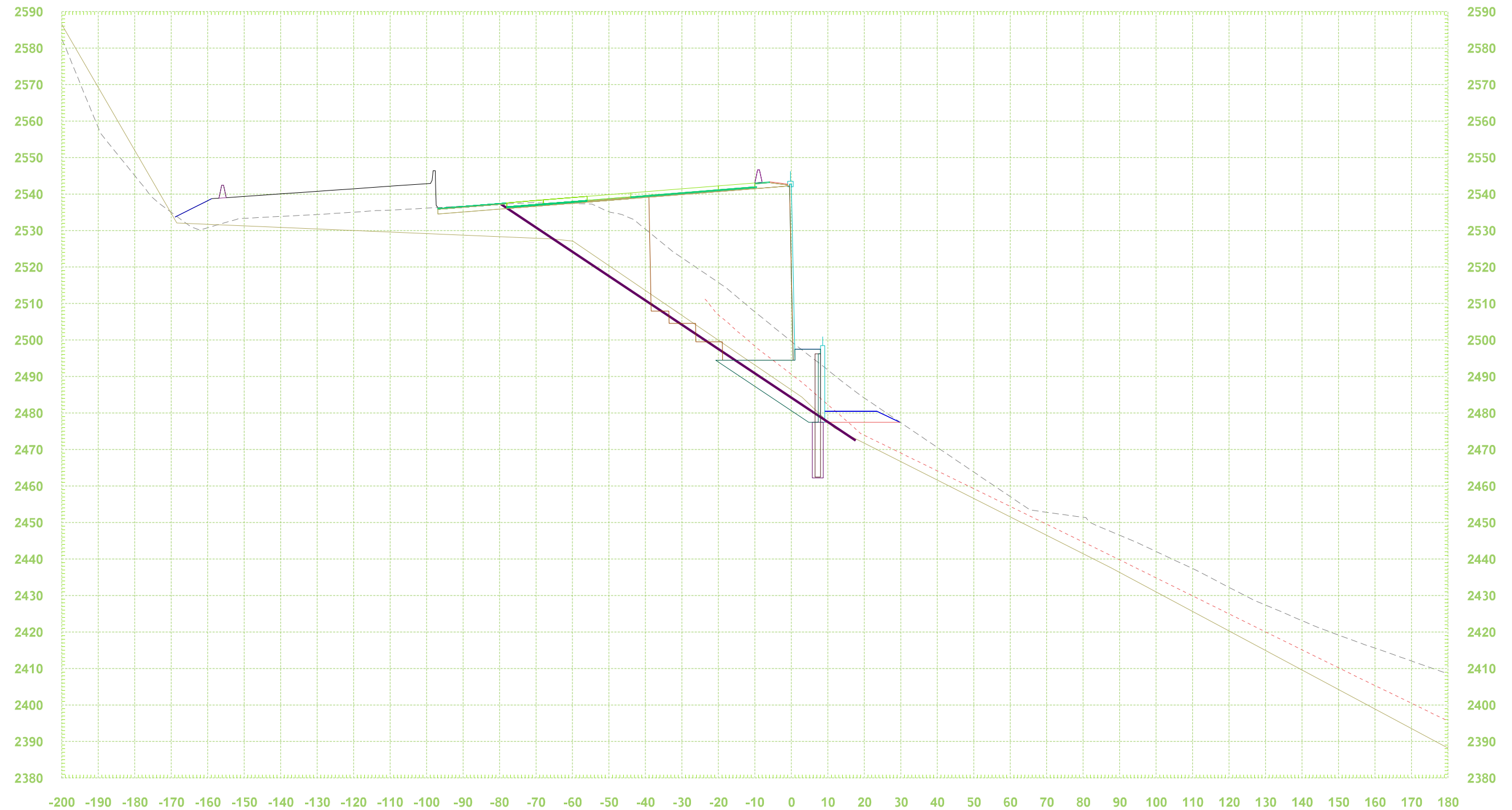
DATE 7/2021

ATTACHMENT 1: WSDOT PROVIDED DESIGN SECTIONS



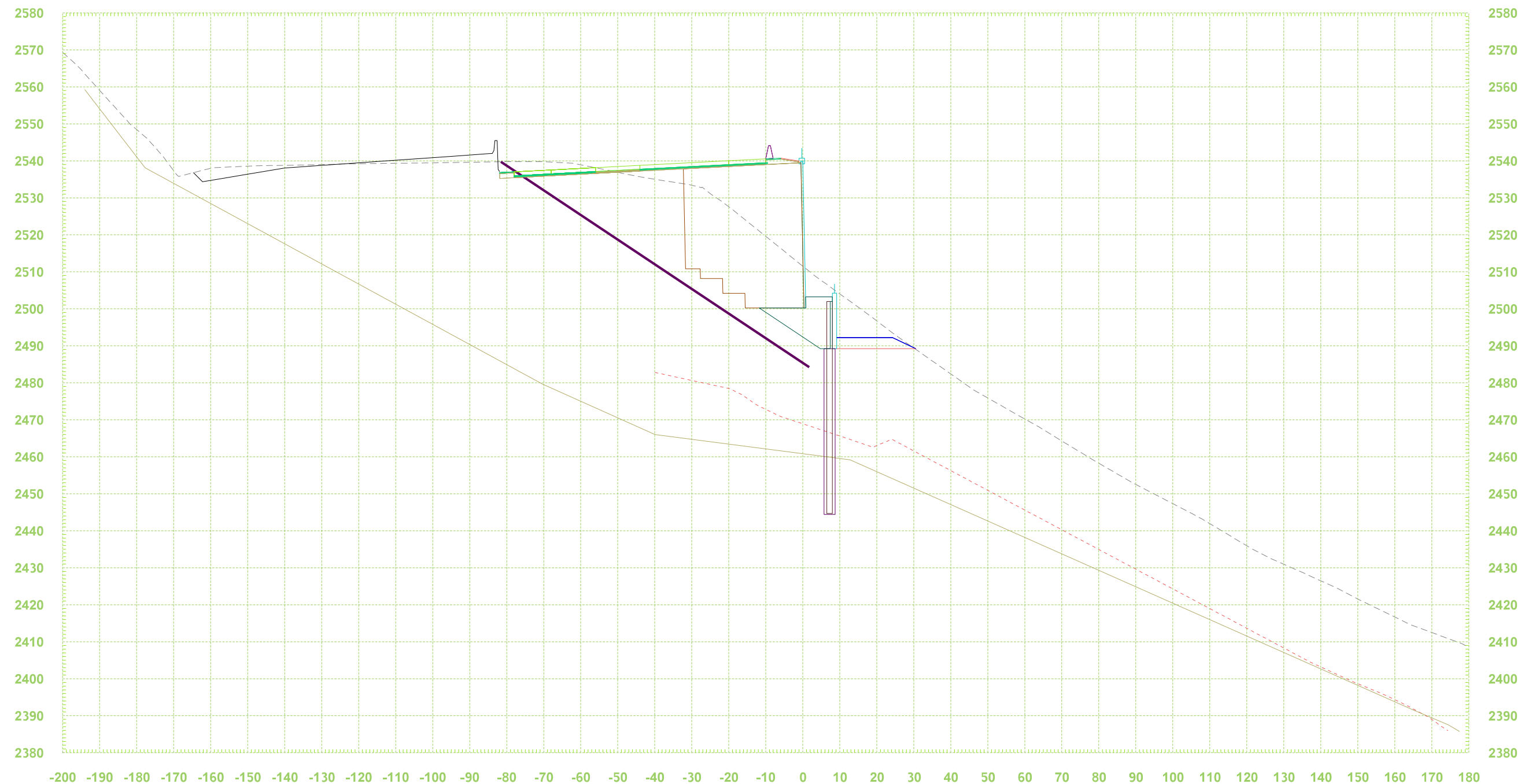
WALL 2 16+25
STATION 1772+60

FILE NAME	C:\Users\GipnerM\OneDrive - Washington State Department of Transportation\Desktop\Wall 2 Design I X-sections & Profile 2021-06-16.dgn			
TIME	11:25:23 AM	Informational use only Not intended for Contract Plans	 Washington State Department of Transportation	Cross Sections
DATE	6/16/2021			
DESIGNED BY	GipnerM			



WALL 2 18+25
STATION 1774+50

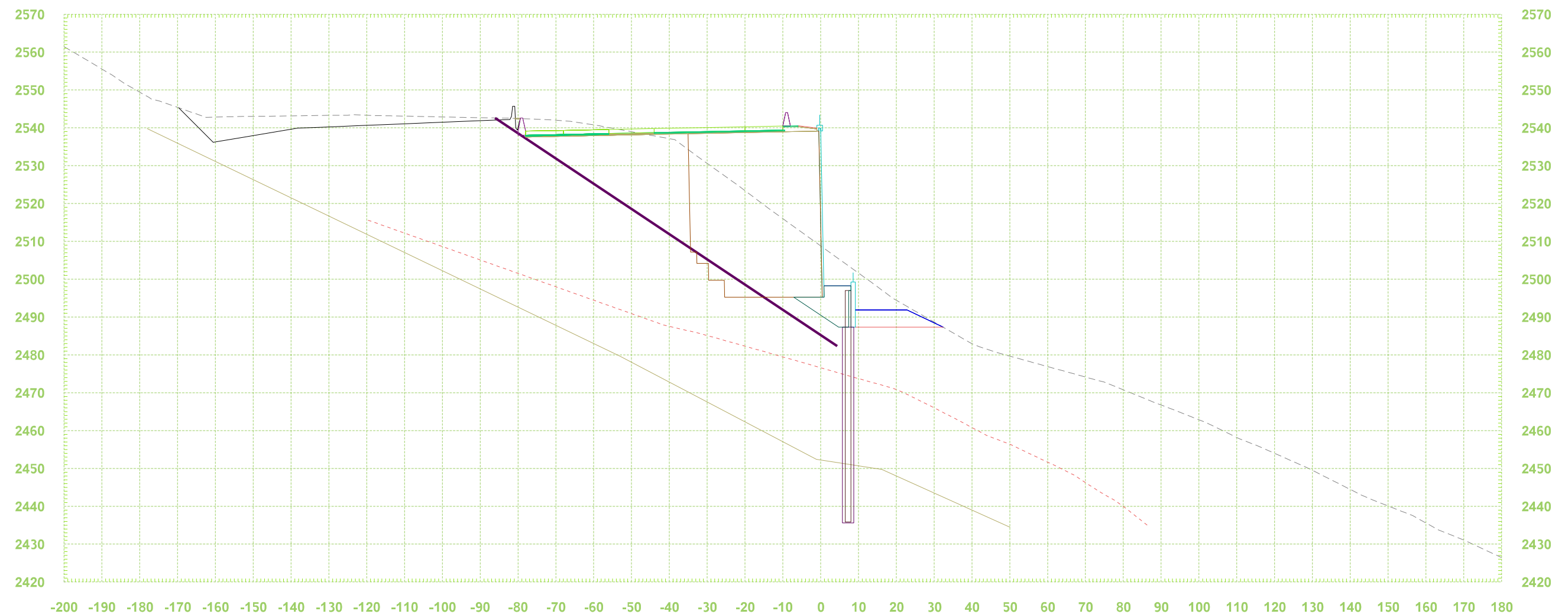
FILE NAME	C:\Users\GipnerM\OneDrive - Washington State Department of Transportation\Desktop\Wall 2 Design I X-sections & Profile 2021-06-16.dgn			
TIME	11:25:26 AM	Informational use only Not intended for Contract Plans	 Washington State Department of Transportation	Cross Sections
DATE	6/16/2021			
DESIGNED BY	GipnerM			



WALL 2 23+25
STATION 1779+50

FILE NAME	C:\Users\GipnerM\OneDrive - Washington State Department of Transportation\Desktop\Wall 2 Design I X-sections & Profile 2021-06-16.dgn		
TIME	11:25:34 AM	Informational use only Not intended for Contract Plans	 Washington State Department of Transportation
DATE	6/16/2021		
DESIGNED BY	GipnerM		

Cross Sections

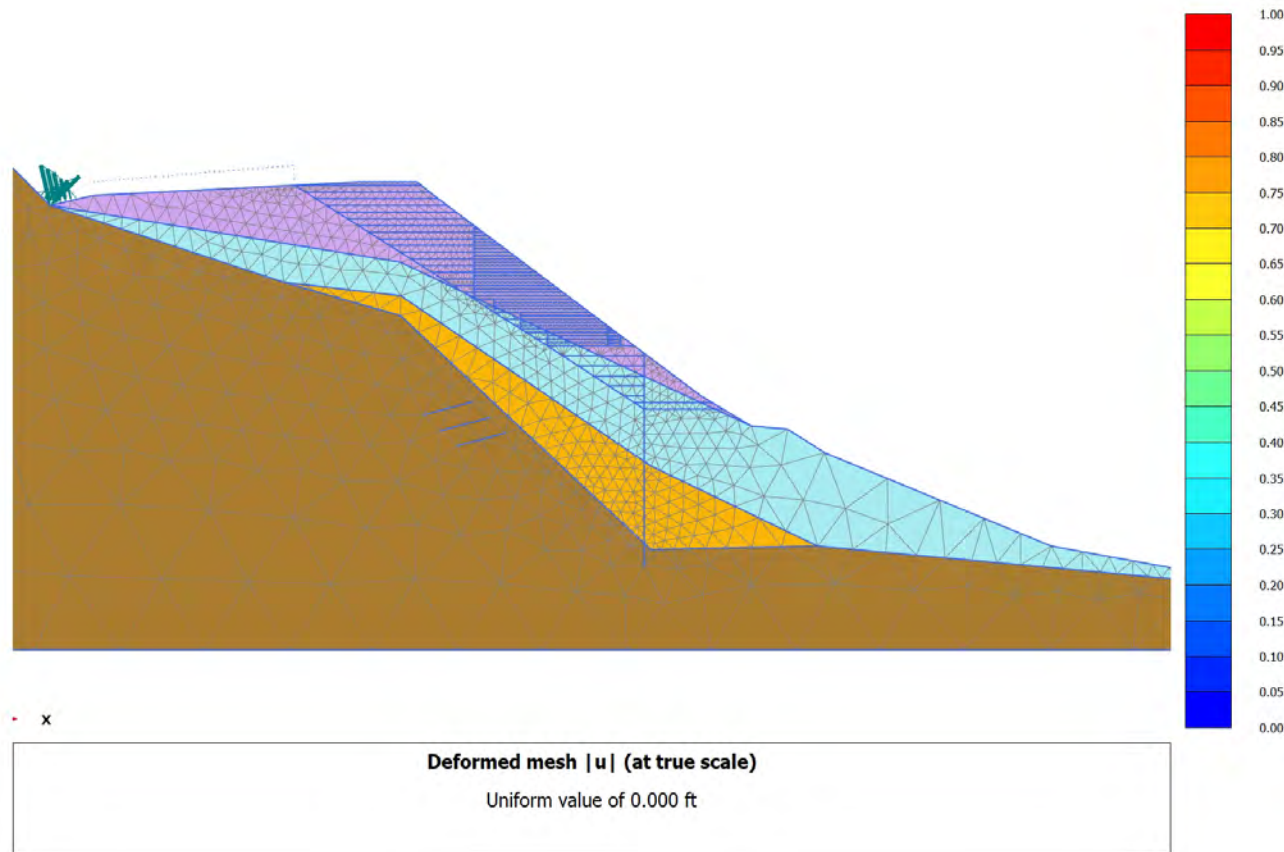


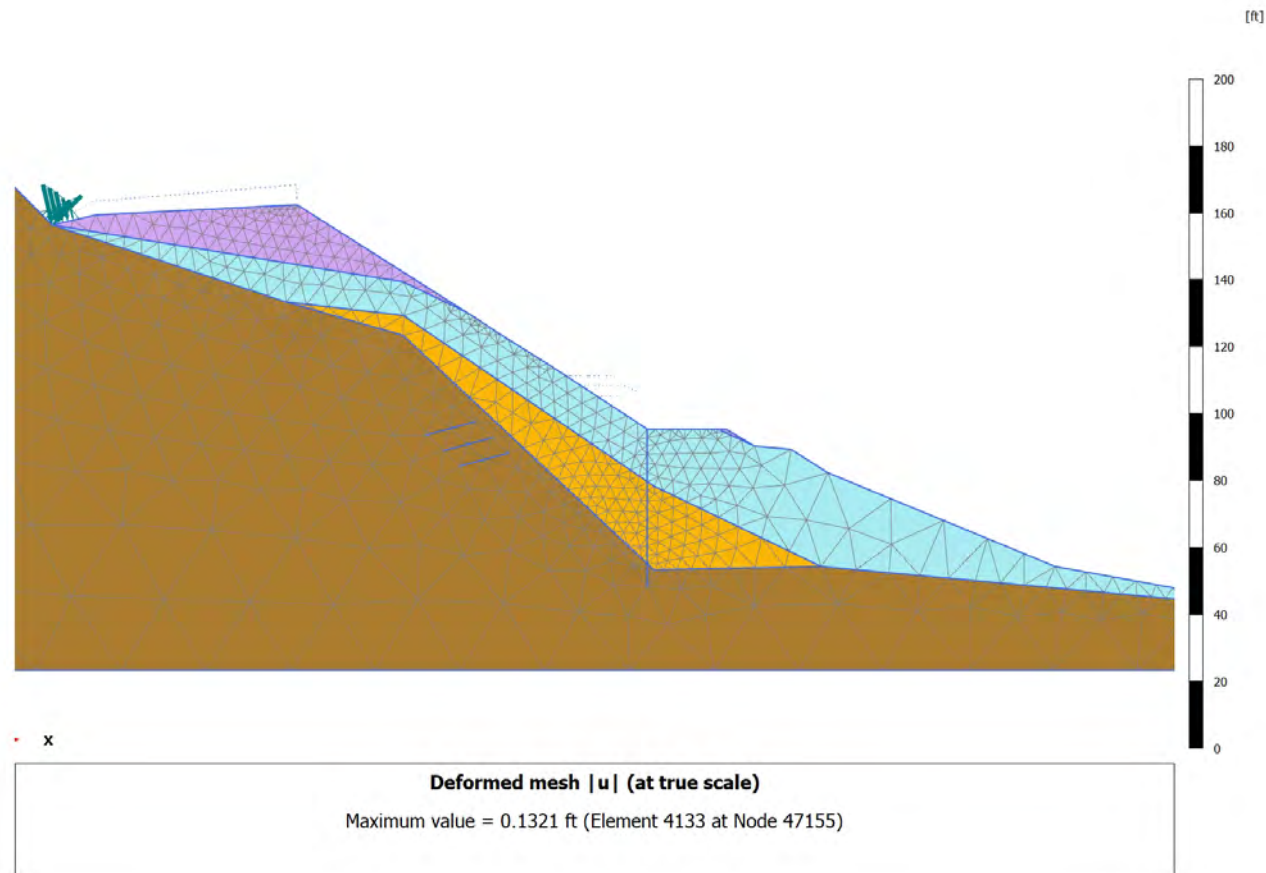
WALL 2 25+25
STATION 1781+50

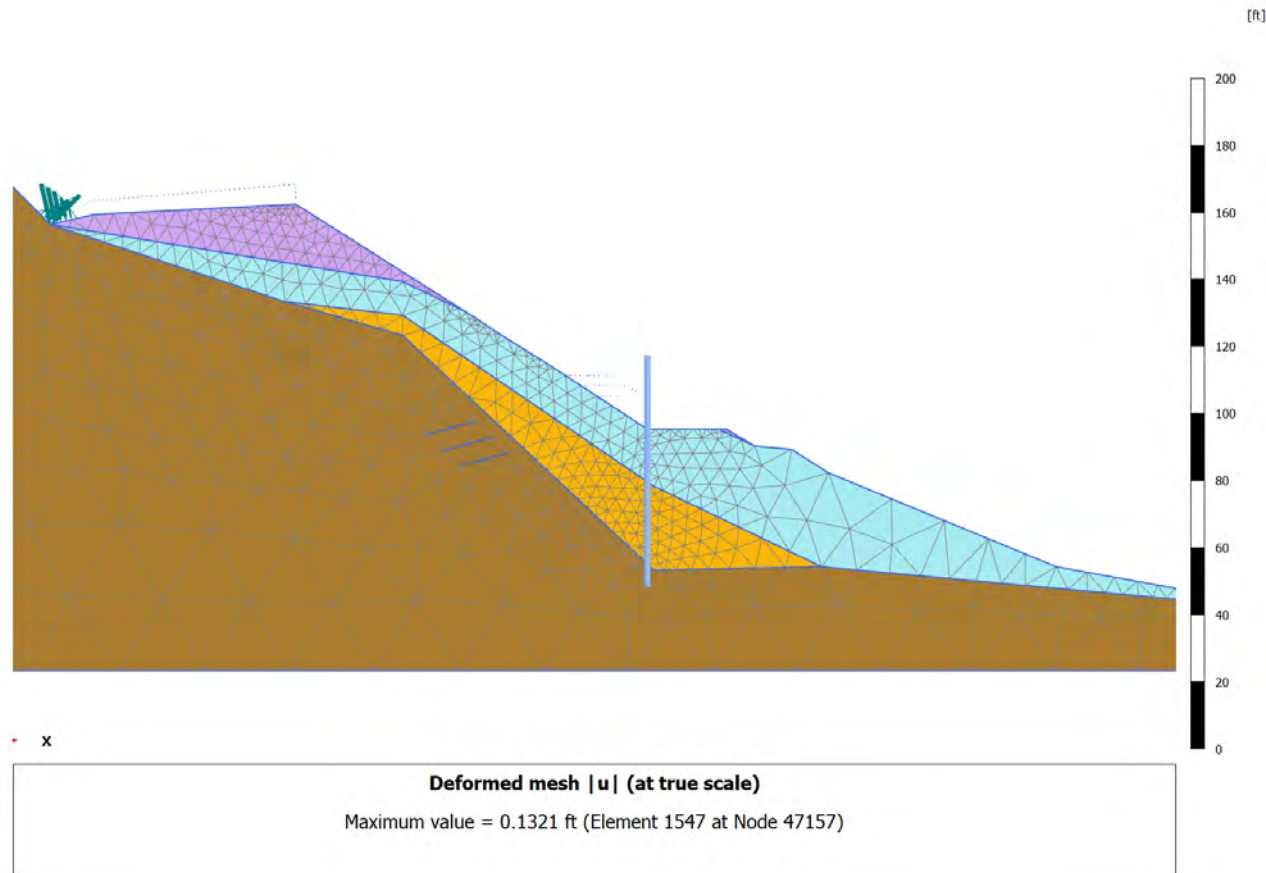
FILE NAME	C:\Users\GipnerM\OneDrive - Washington State Department of Transportation\Desktop\Wall 2 Design I X-sections & Profile 2021-06-16.dgn			
TIME	11:25:37 AM	Informational use only Not intended for Contract Plans	 Washington State Department of Transportation	Cross Sections
DATE	6/16/2021			
DESIGNED BY	GipnerM			

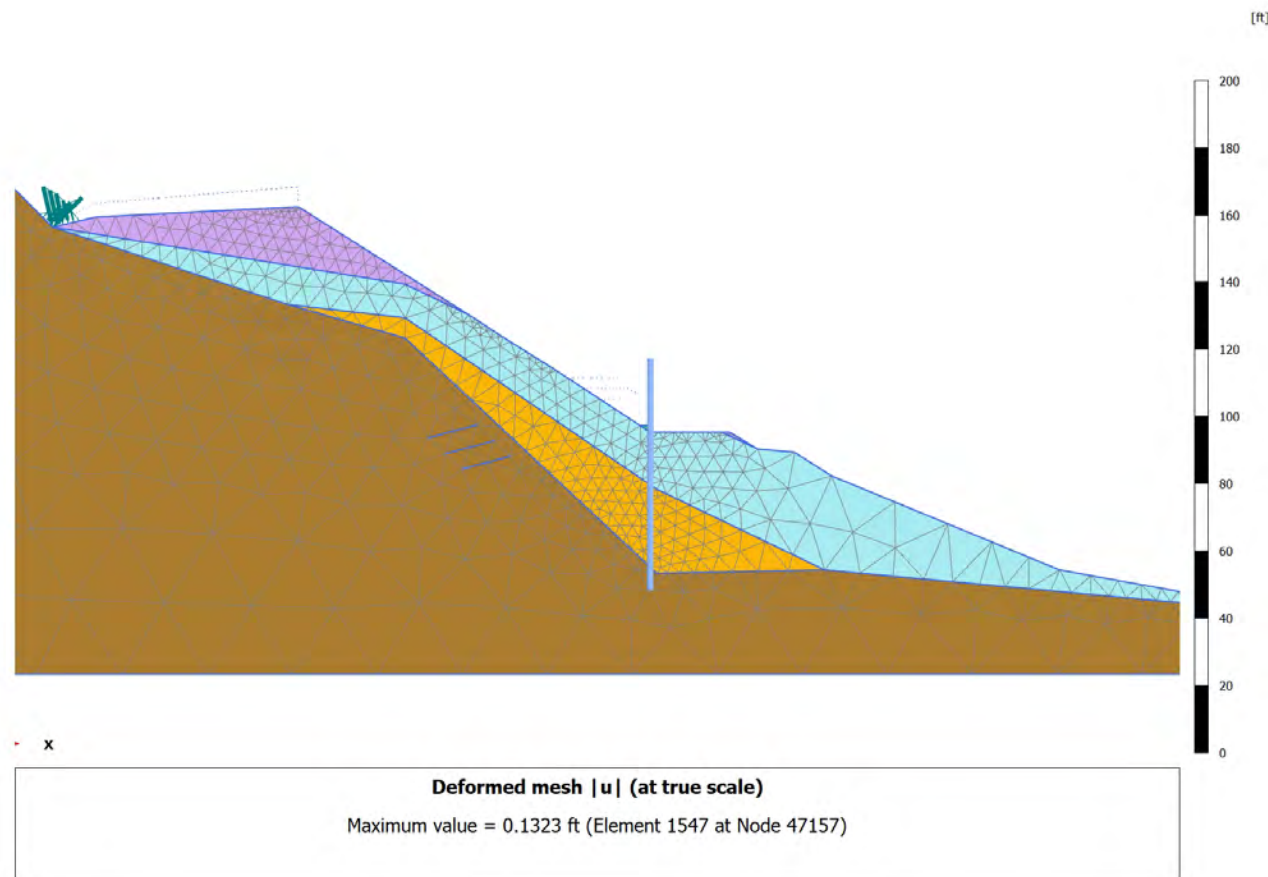
**ATTACHMENT 2: PLAXIS STORYBOARD: GEOGRID
EXAMPLE**

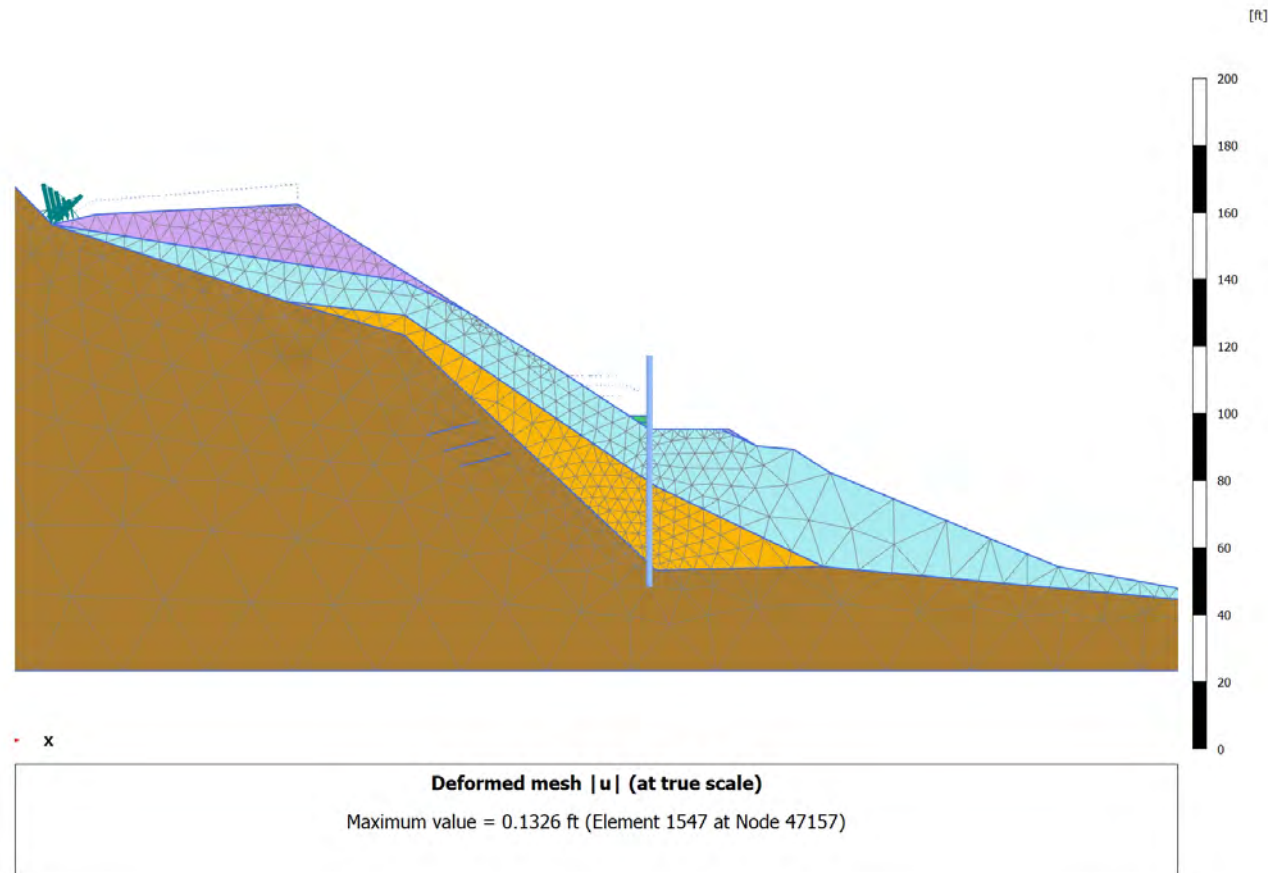
4.1.1 Calculation results, Initial phase [InitialPhase] (0/0), Deformed mesh |u|



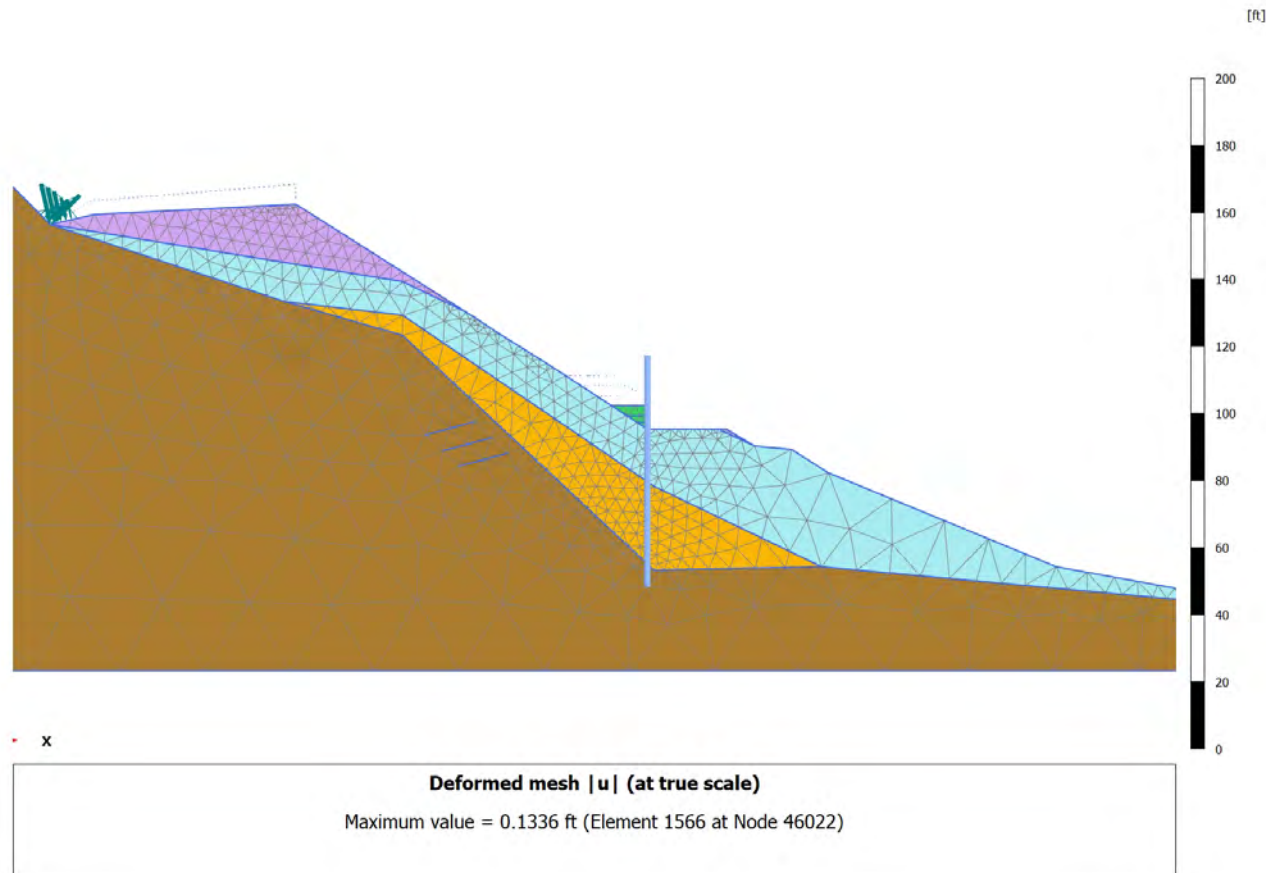
4.1.18 Calculation results, Exc to MSE [Phase_1] (1/672), Deformed mesh $|u|$ 

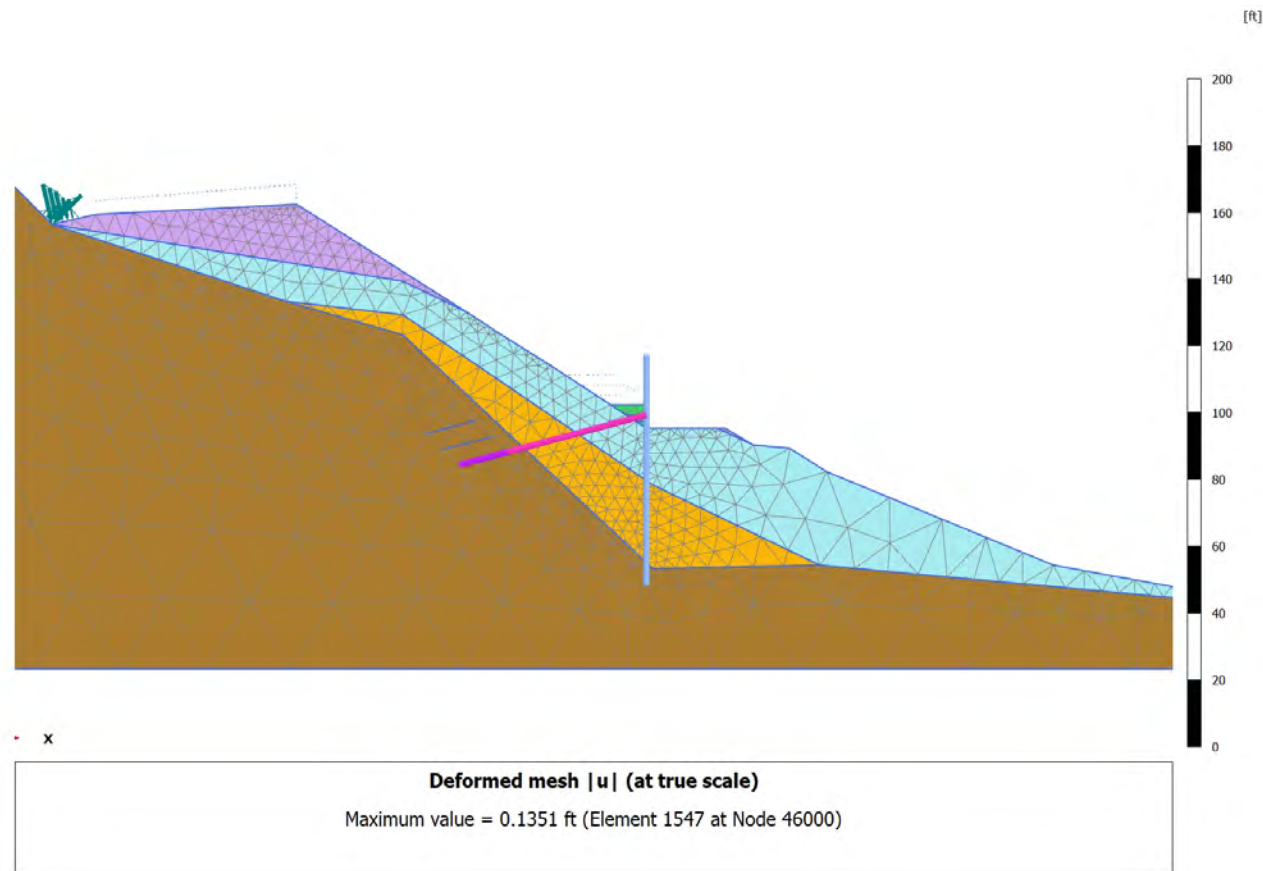
4.1.2 Calculation results, Install SP [Phase_2] (2/2), Deformed mesh $|u|$ 

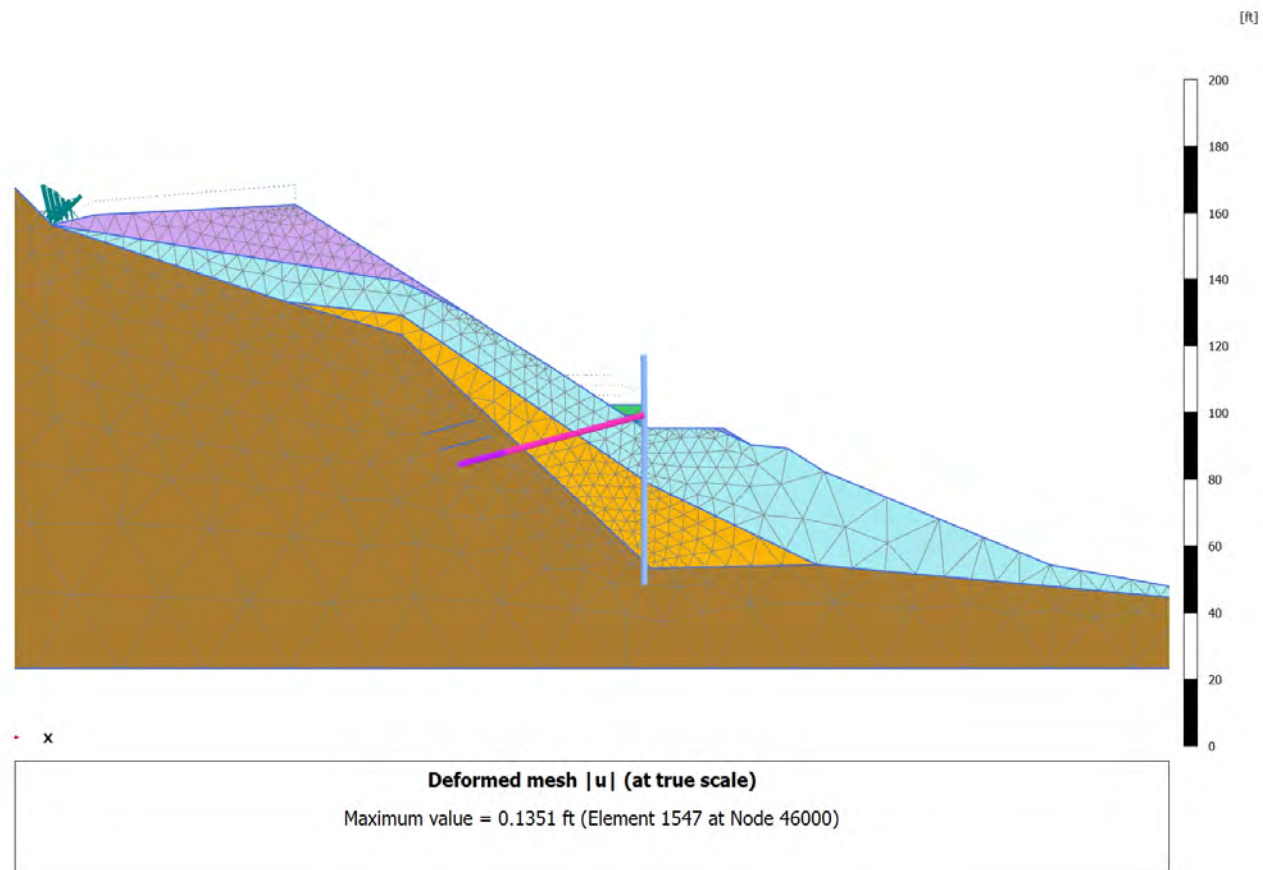
4.1.3 Calculation results, SP BF 1 [Phase_3] (3/6), Deformed mesh $|u|$ 

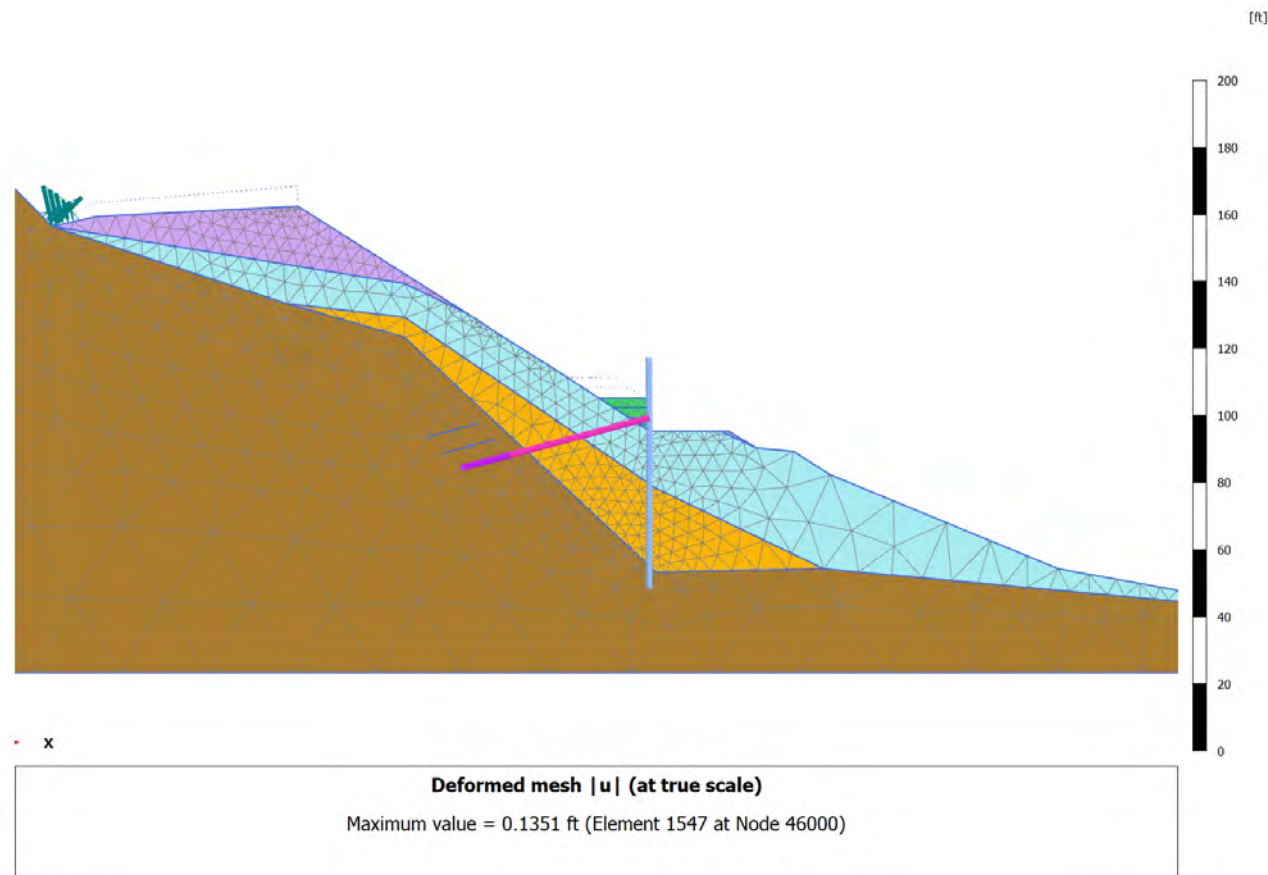
4.1.4 Calculation results, SP BF 2 [Phase_4] (4/10), Deformed mesh $|u|$ 

4.1.5 Calculation results, SP BF 3 [Phase_38] (38/15), Deformed mesh |u|

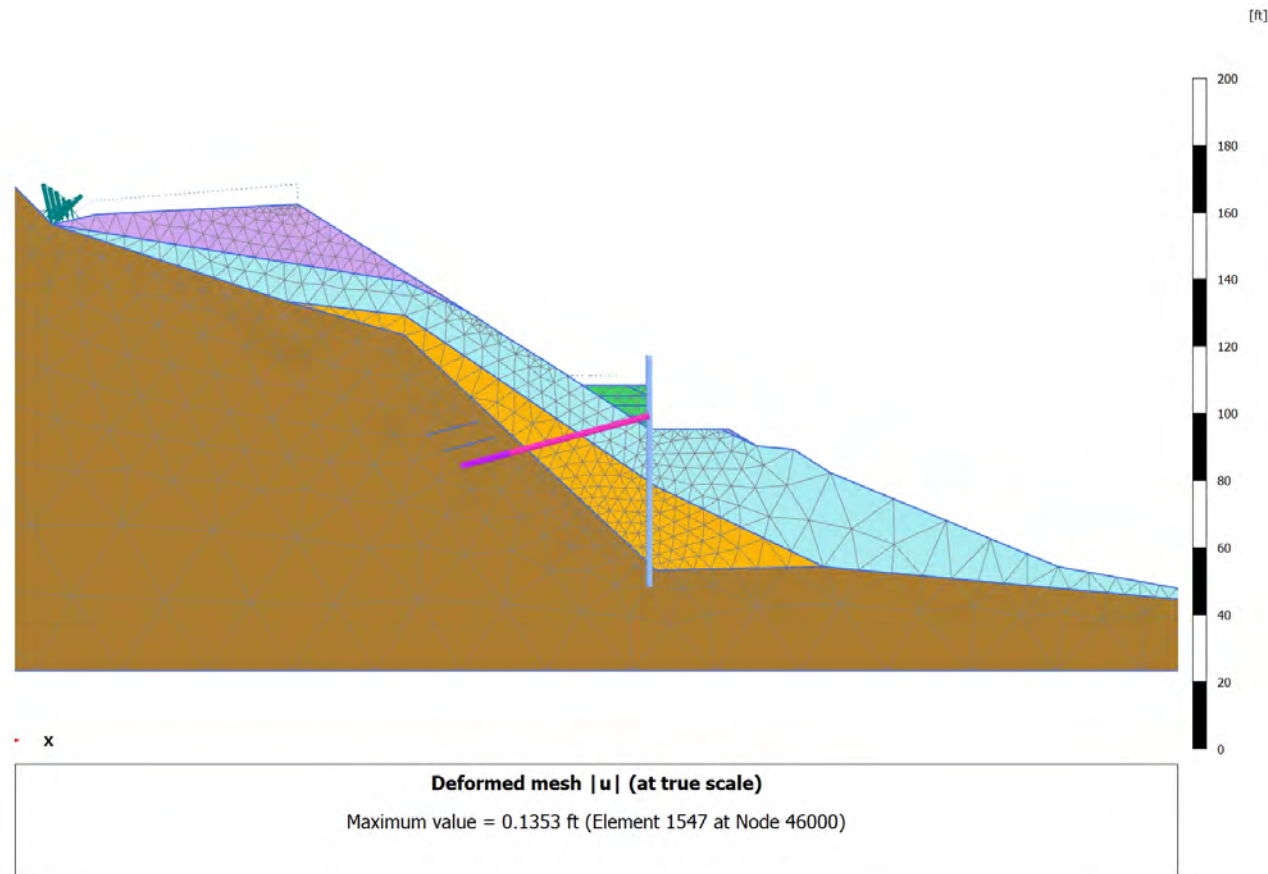


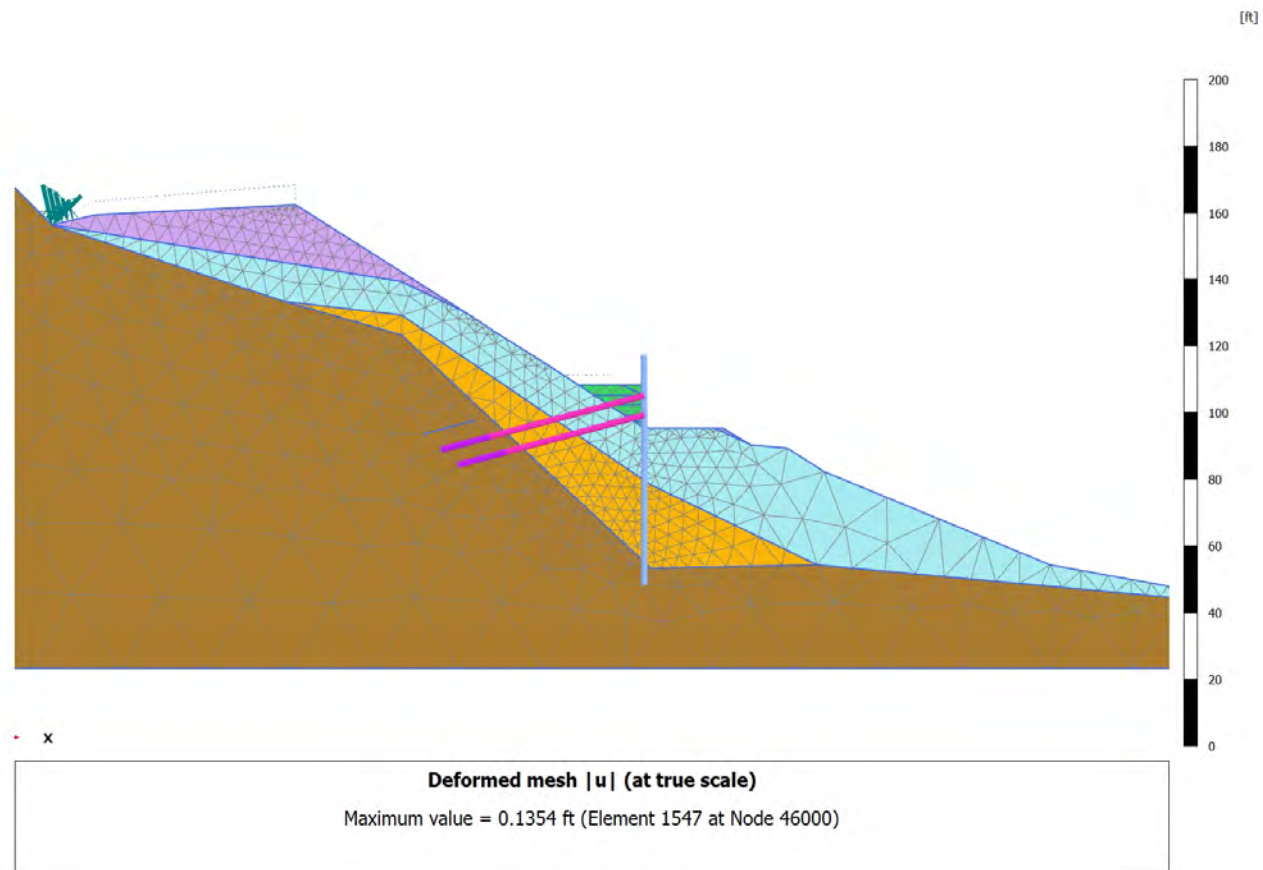
4.1.6 Calculation results, Install Tieback 1 [Phase_5] (5/194), Deformed mesh $|u|$ 

4.1.7 Calculation results, Prestress Tieback 1 [Phase_6] (6/208), Deformed mesh $|u|$ 

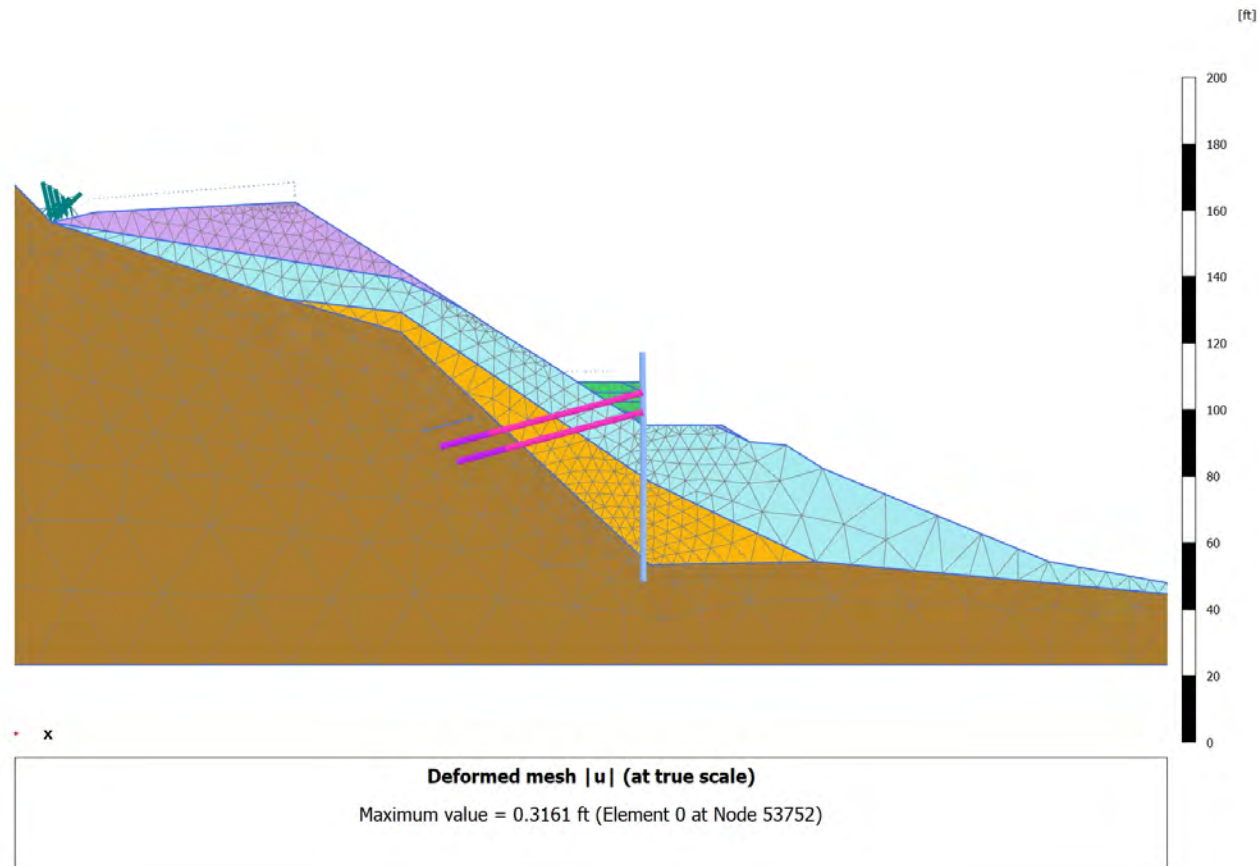
4.1.8 Calculation results, SP BF 4 [Phase_7] (7/212), Deformed mesh $|u|$ 

4.1.9 Calculation results, SP BF 5 [Phase_8] (8/219), Deformed mesh |u|

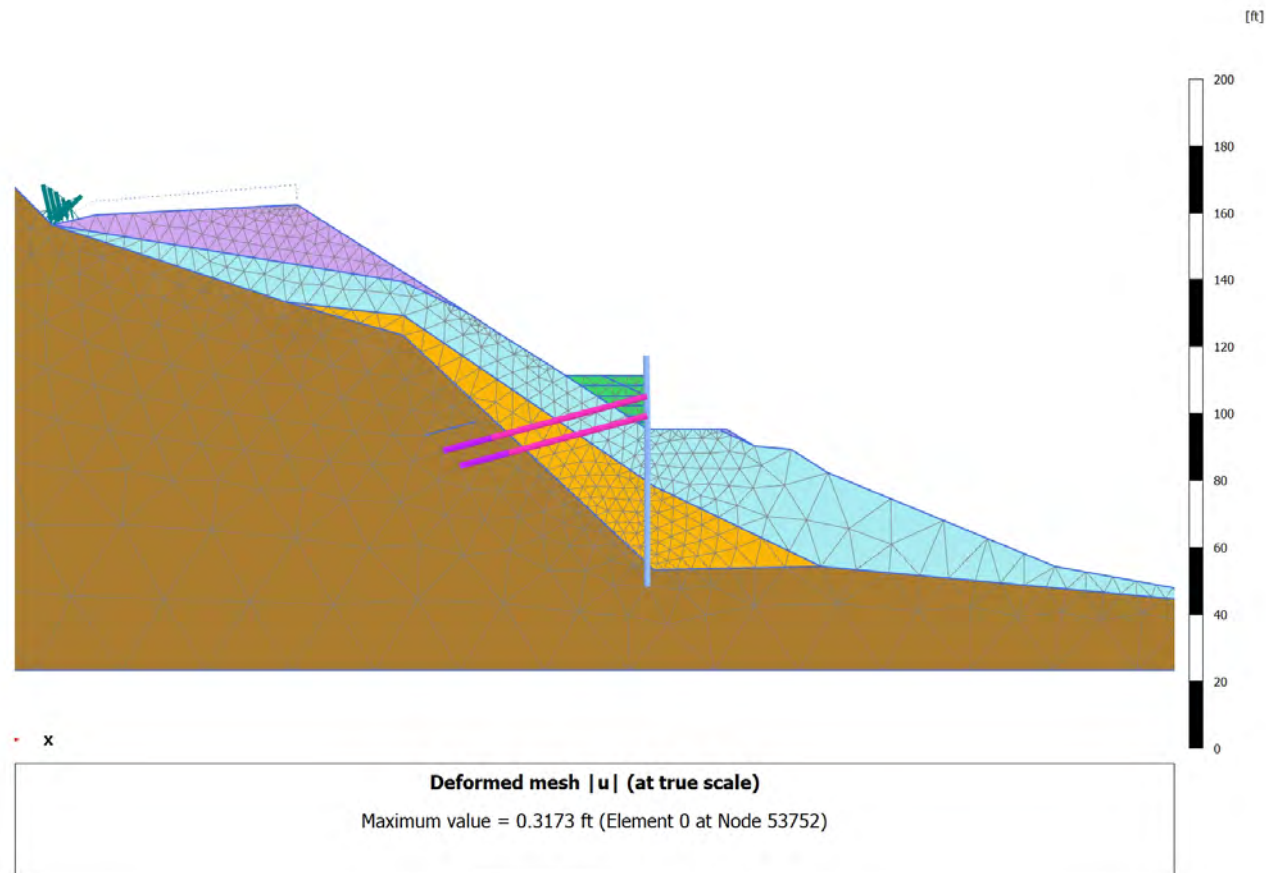


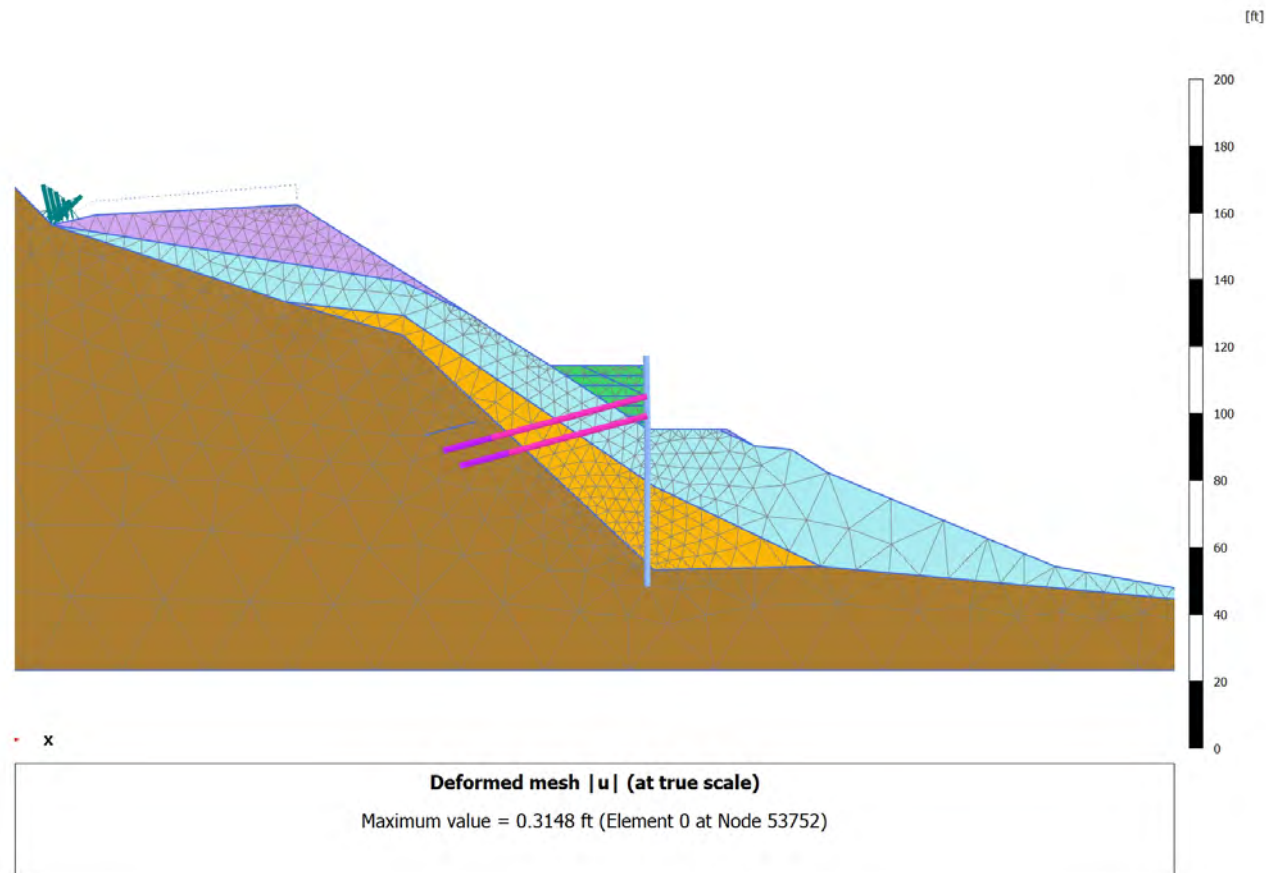
4.1.10 Calculation results, Install Tieback 2 [Phase_9] (9/222), Deformed mesh $|u|$ 

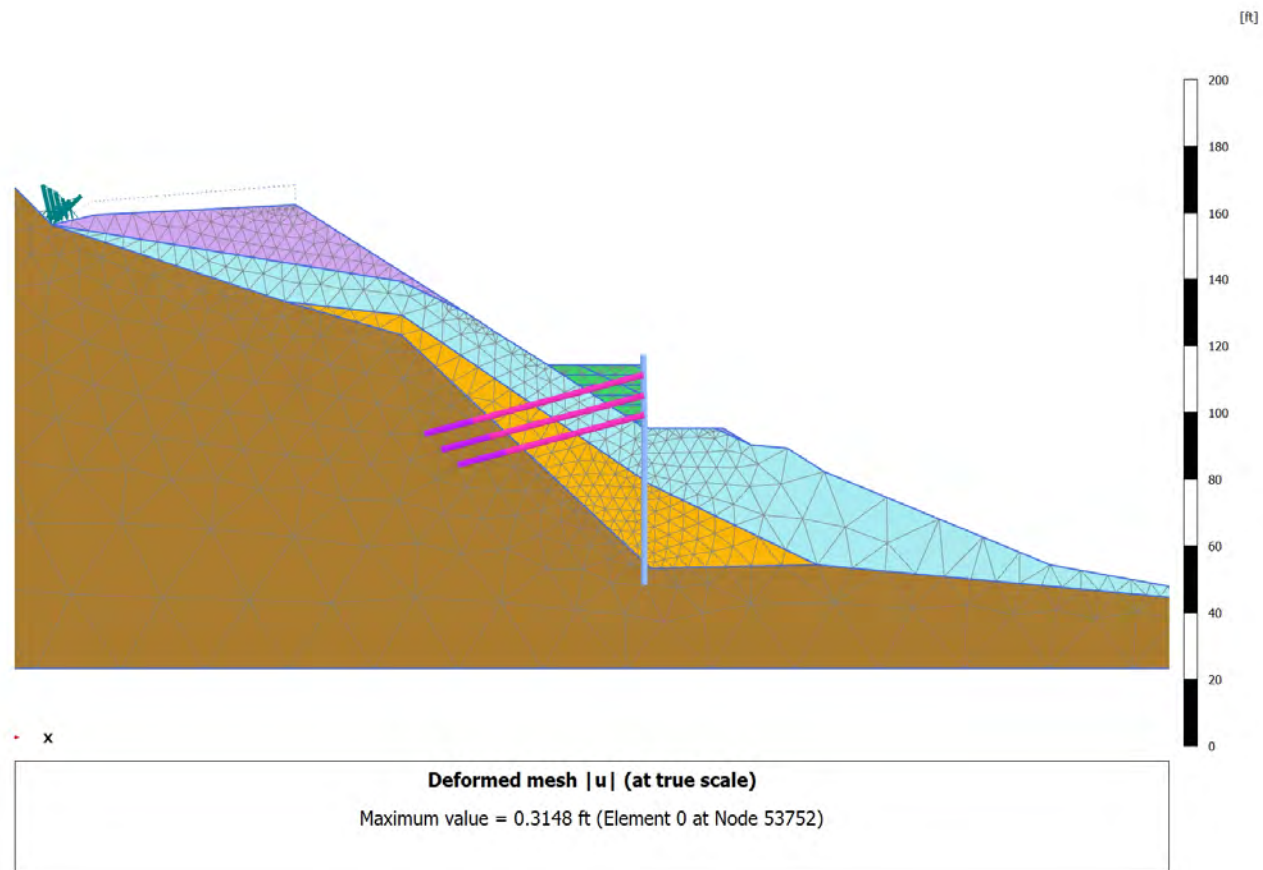
4.1.11 Calculation results, Prestress Tieback 3 [Phase_10] (10/235), Deformed mesh $|u|$



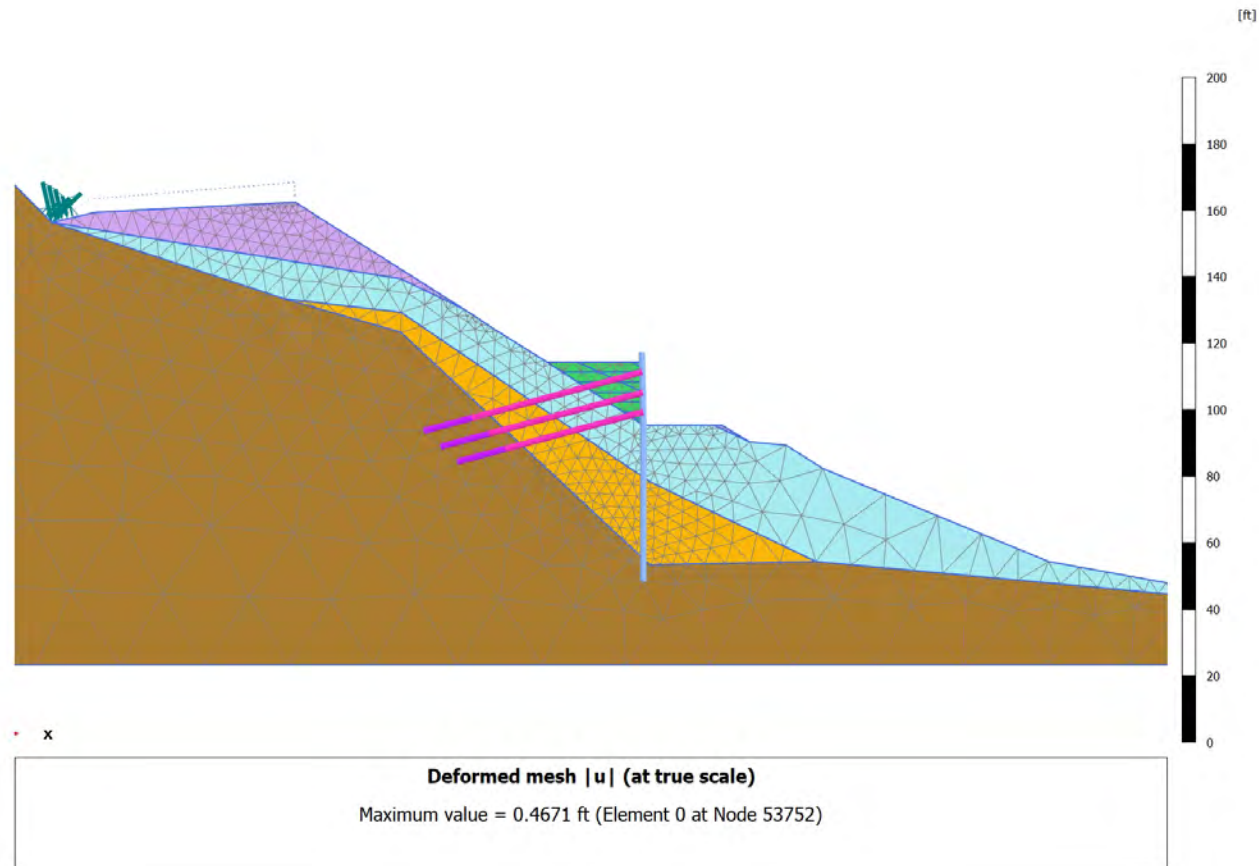
4.1.12 Calculation results, SP BF 6 [Phase_11] (11/239), Deformed mesh |u|



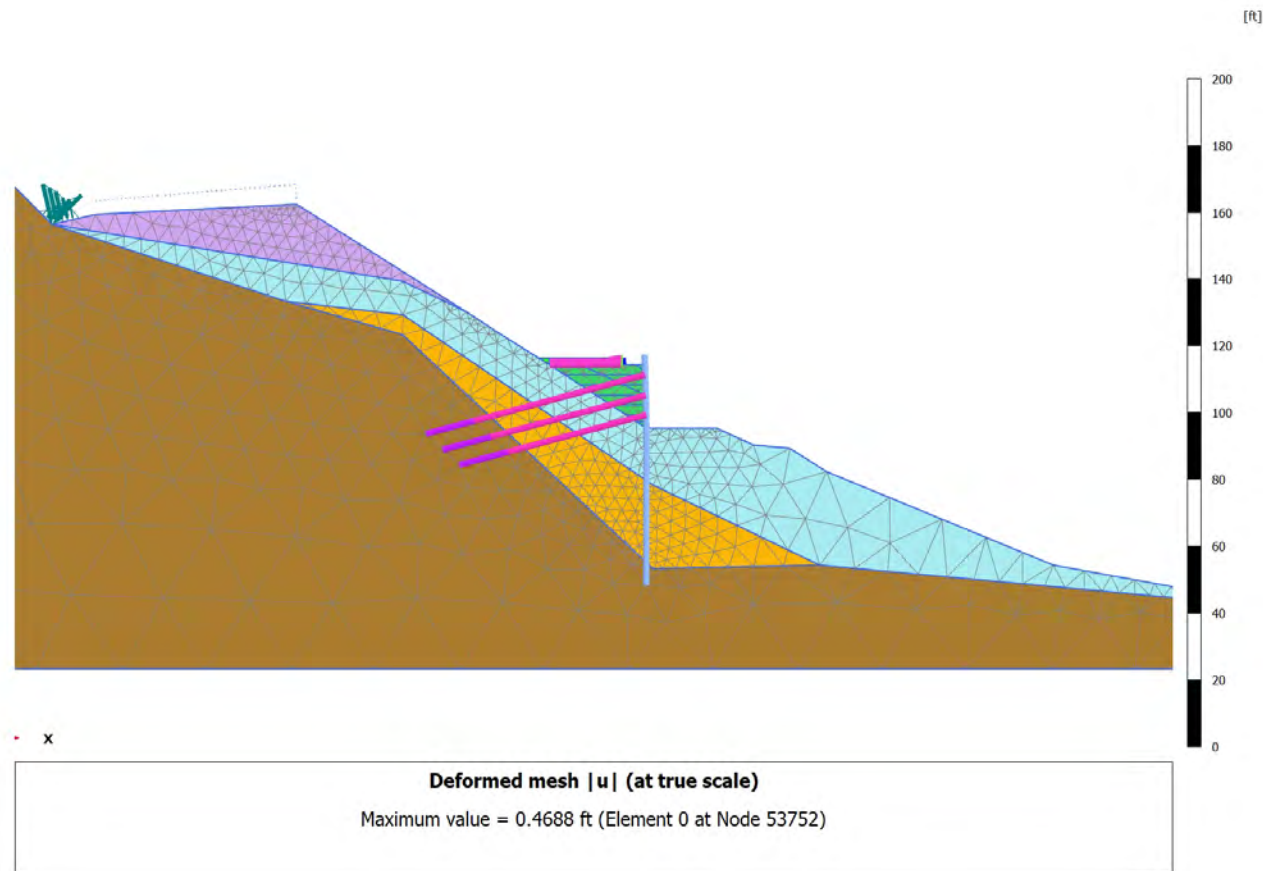
4.1.13 Calculation results, SP BF 7 [Phase_39] (39/250), Deformed mesh $|u|$ 

4.1.19 Calculation results, Install Tieback 3 [Phase_40] (40/719), Deformed mesh $|u|$ 

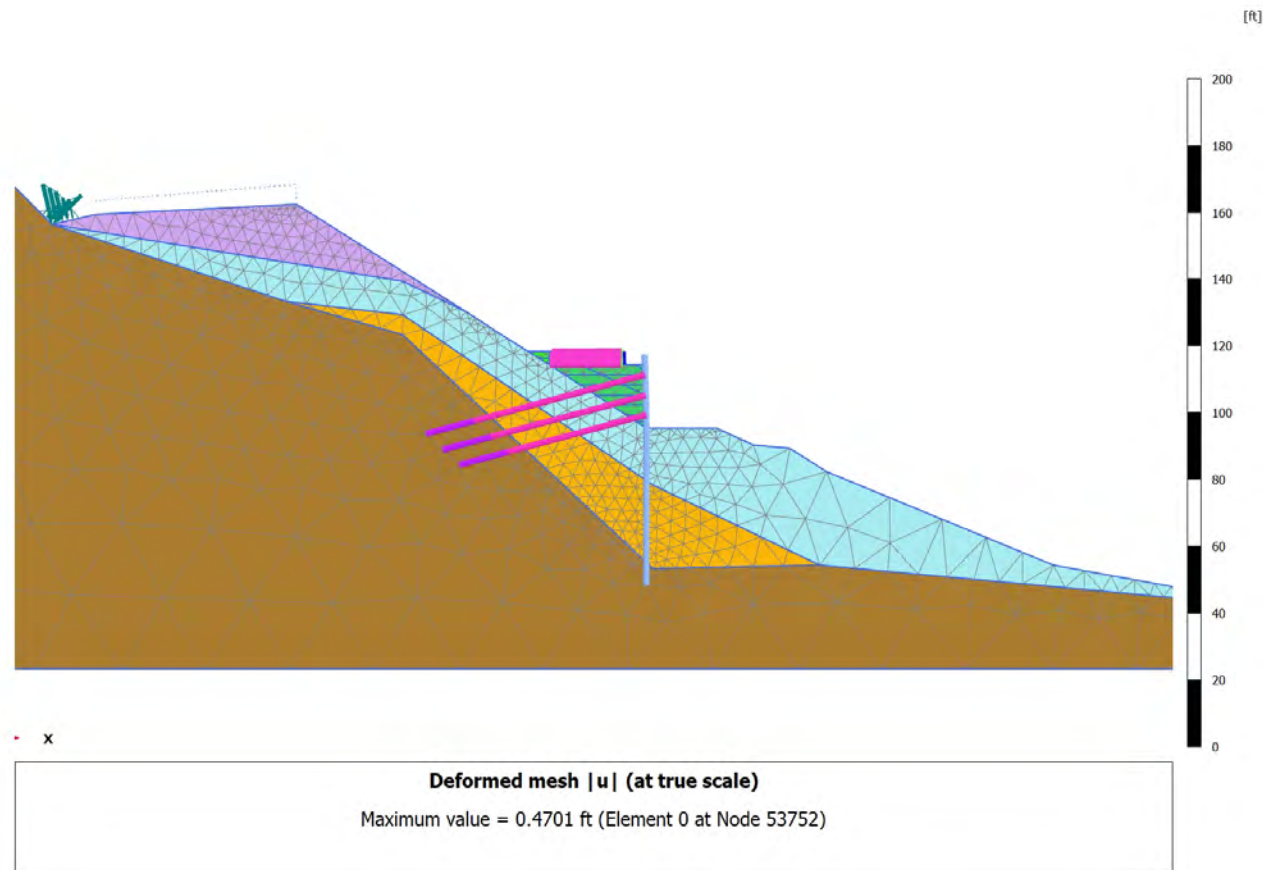
4.1.14 Calculation results, Prestress Tieback 3 [Phase_41] (41/264), Deformed mesh $|u|$



4.1.15 Calculation results, MSE Lift 1 [Phase_12] (12/270), Deformed mesh |u|

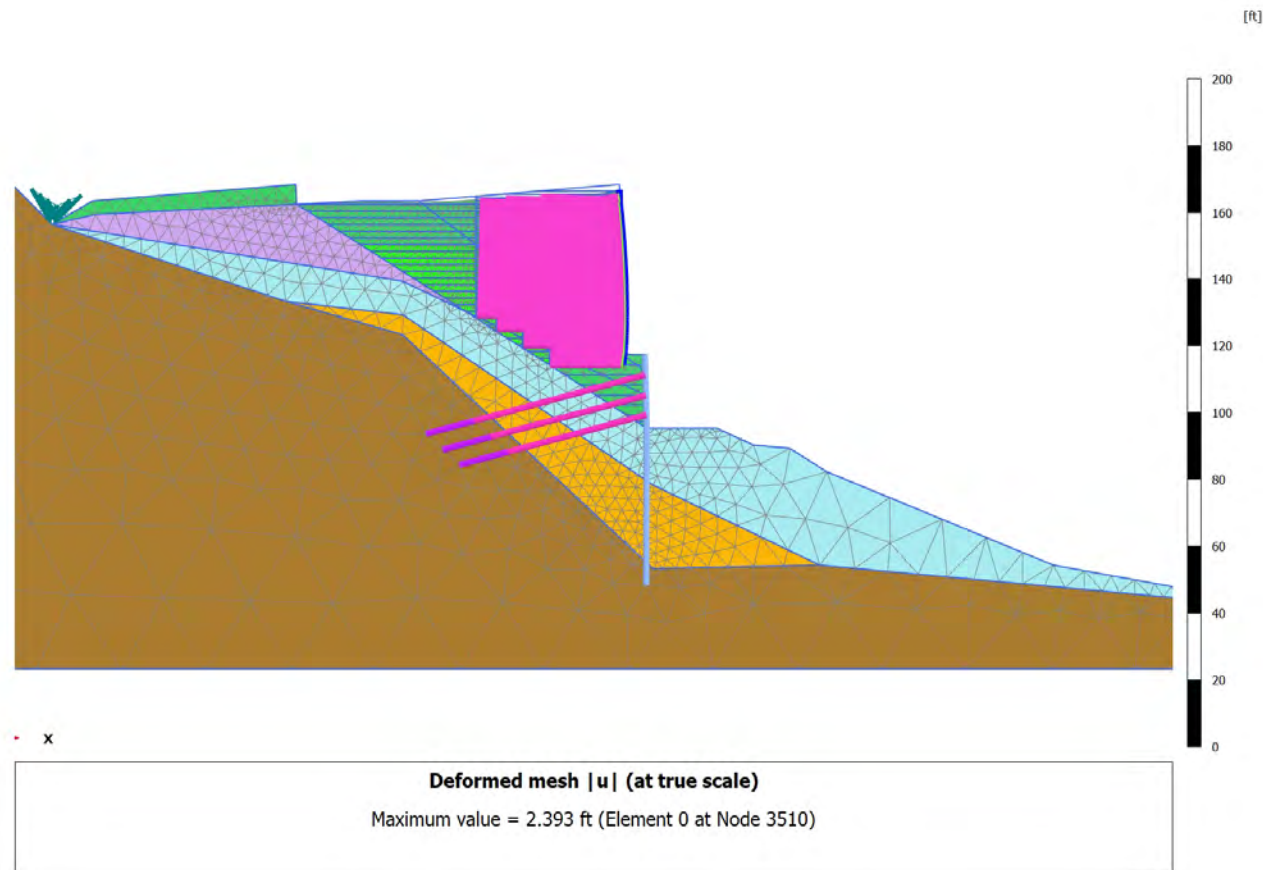


4.1.20 Calculation results, MSE Lift 2 [Phase_13] (13/726), Deformed mesh | u |

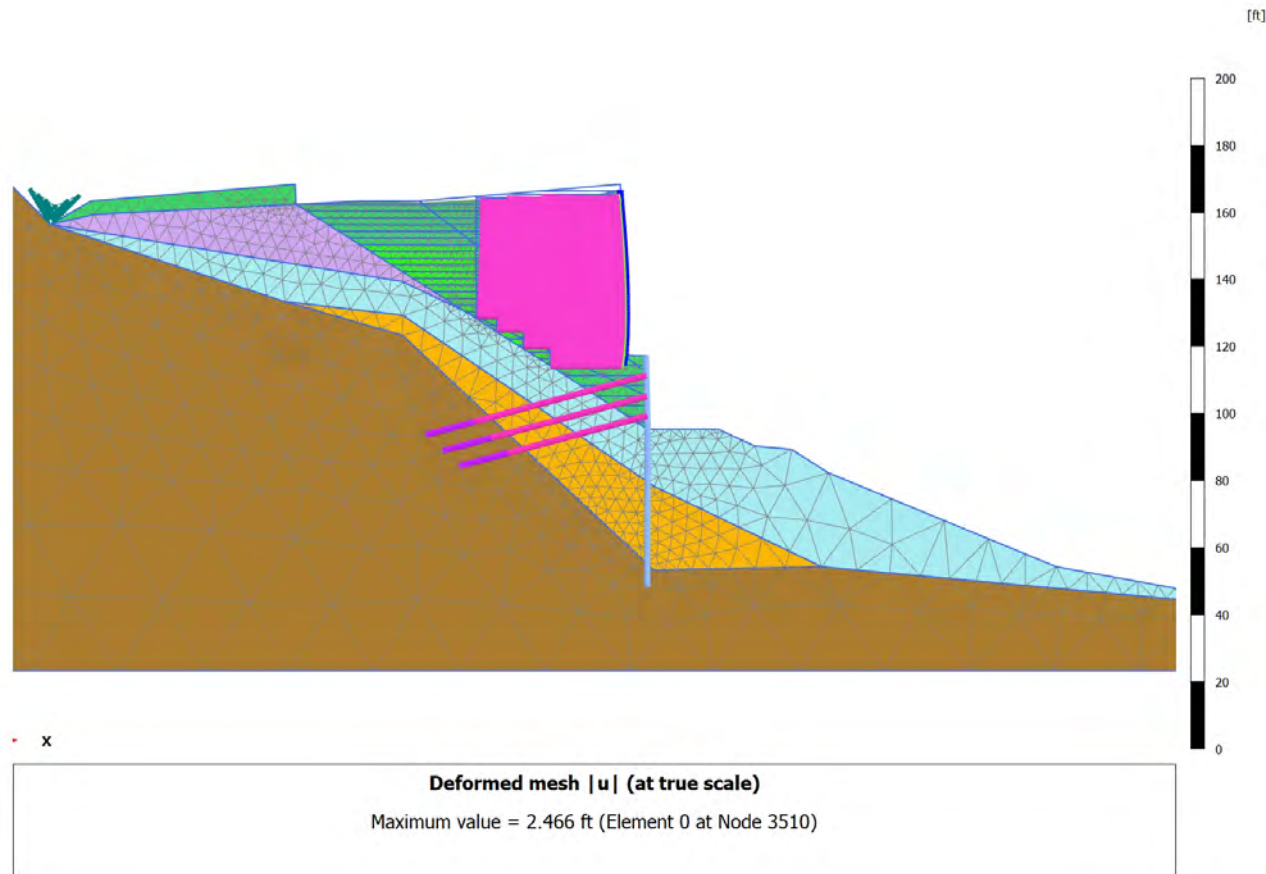


21

This sequence continues until the top of the wall is reached.

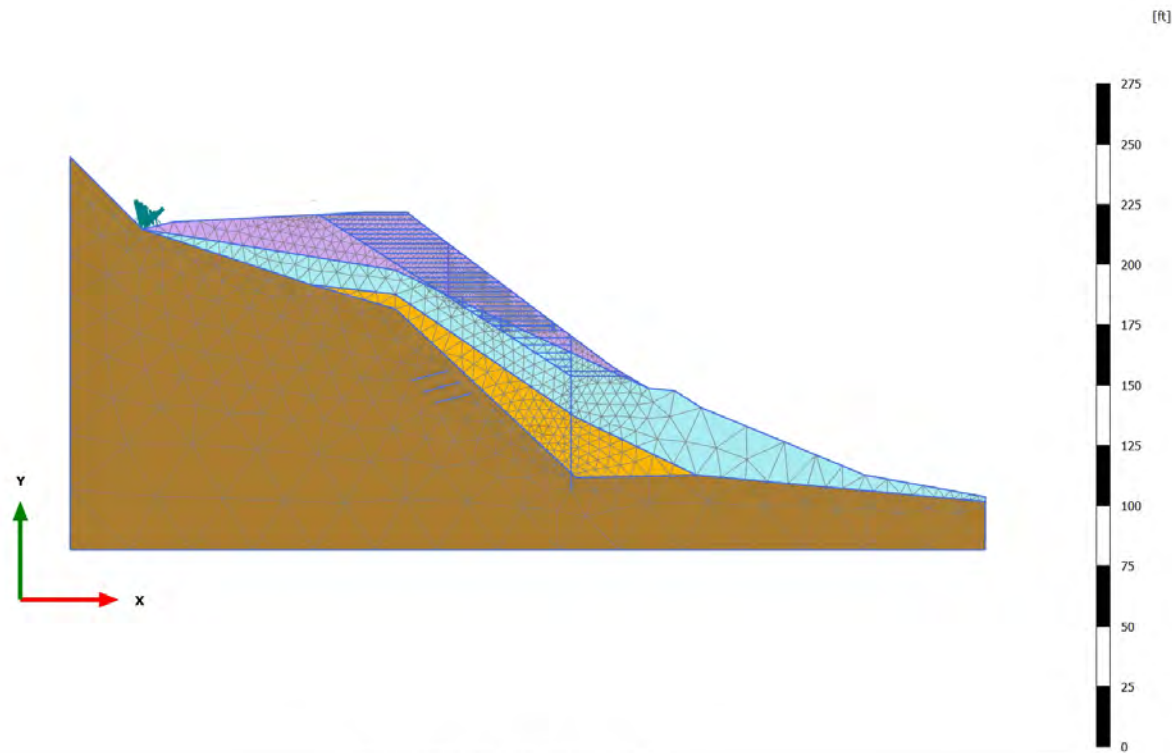
4.1.16 Calculation results, MSE Lift 26 [Phase_37] (37/564), Deformed mesh $|u|$ 

4.1.17 Calculation results, Top [Phase_42] (42/594), Deformed mesh |u|



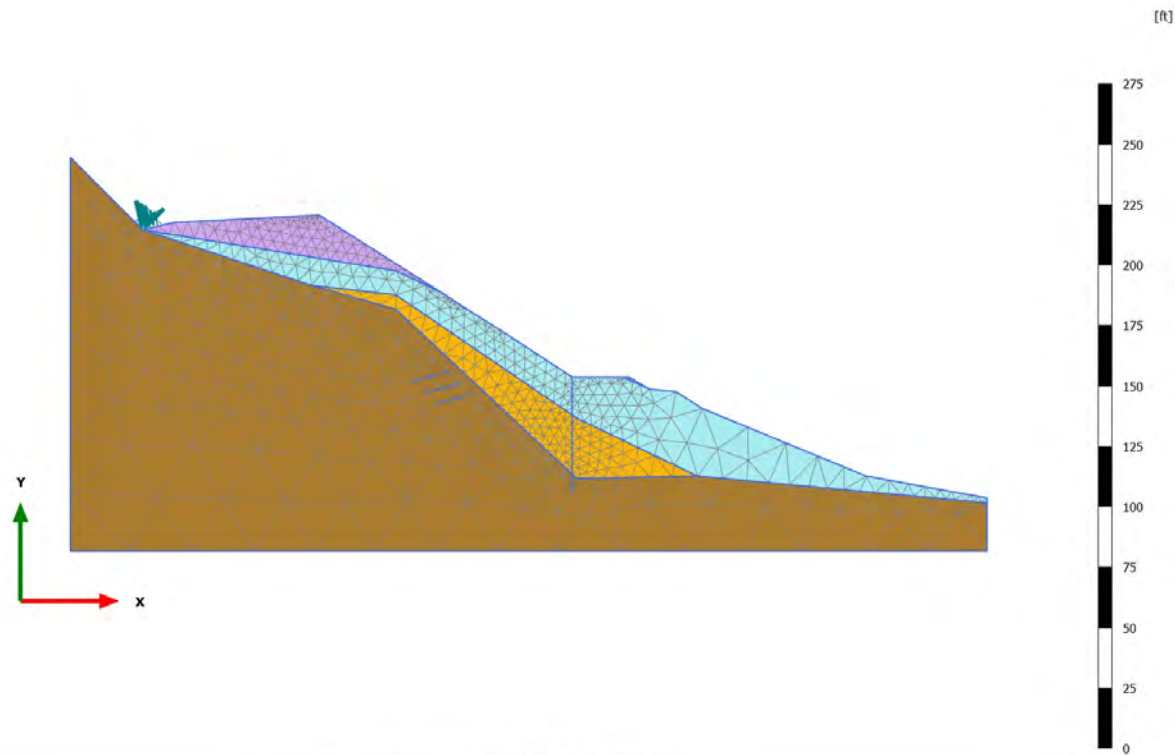
**ATTACHMENT 3: PLAXIS STORYBOARD: HILFIKER
EXAMPLE**

4.1.1 Calculation results, Initial phase [InitialPhase] (0/0), Deformed mesh |u|



Deformed mesh |u| (at true scale)

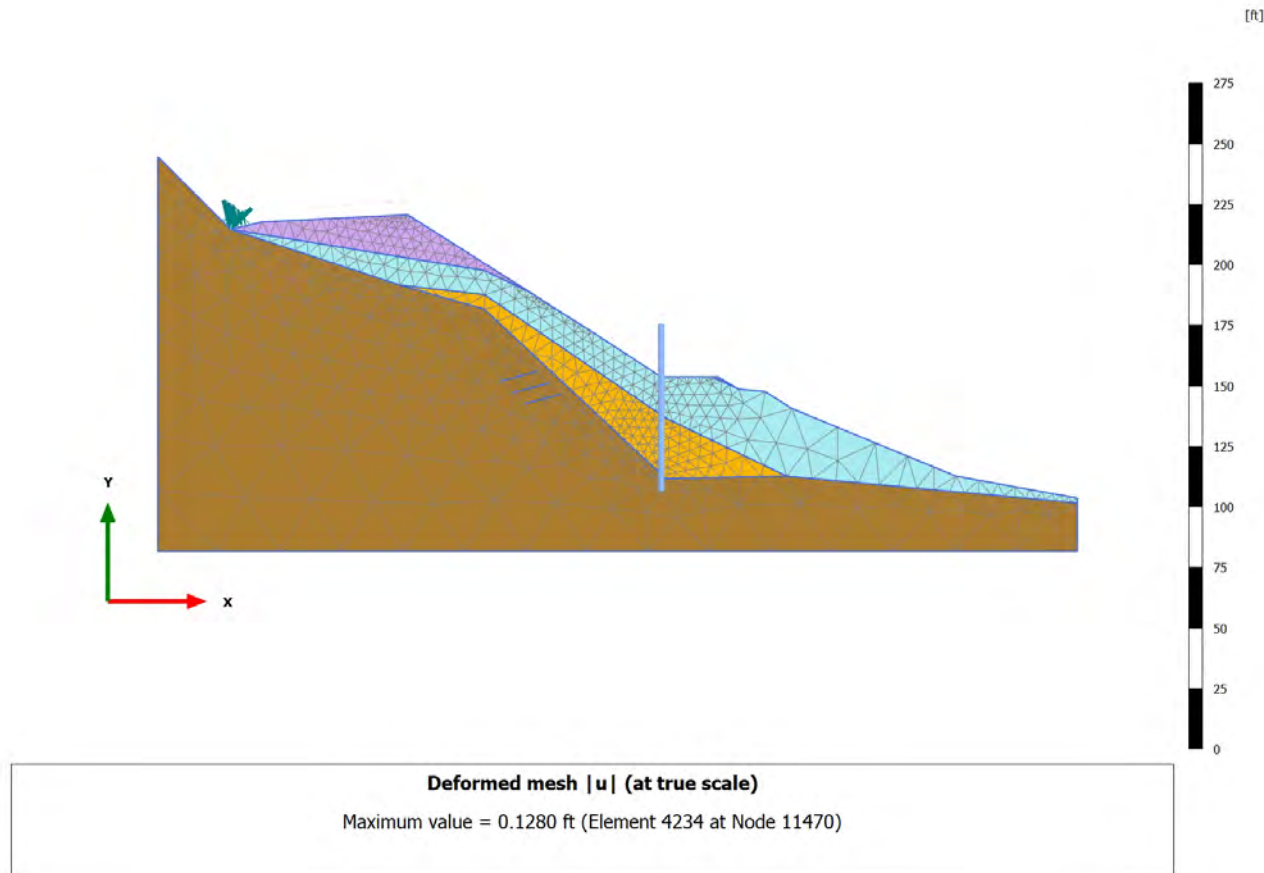
Uniform value of 0.000 ft

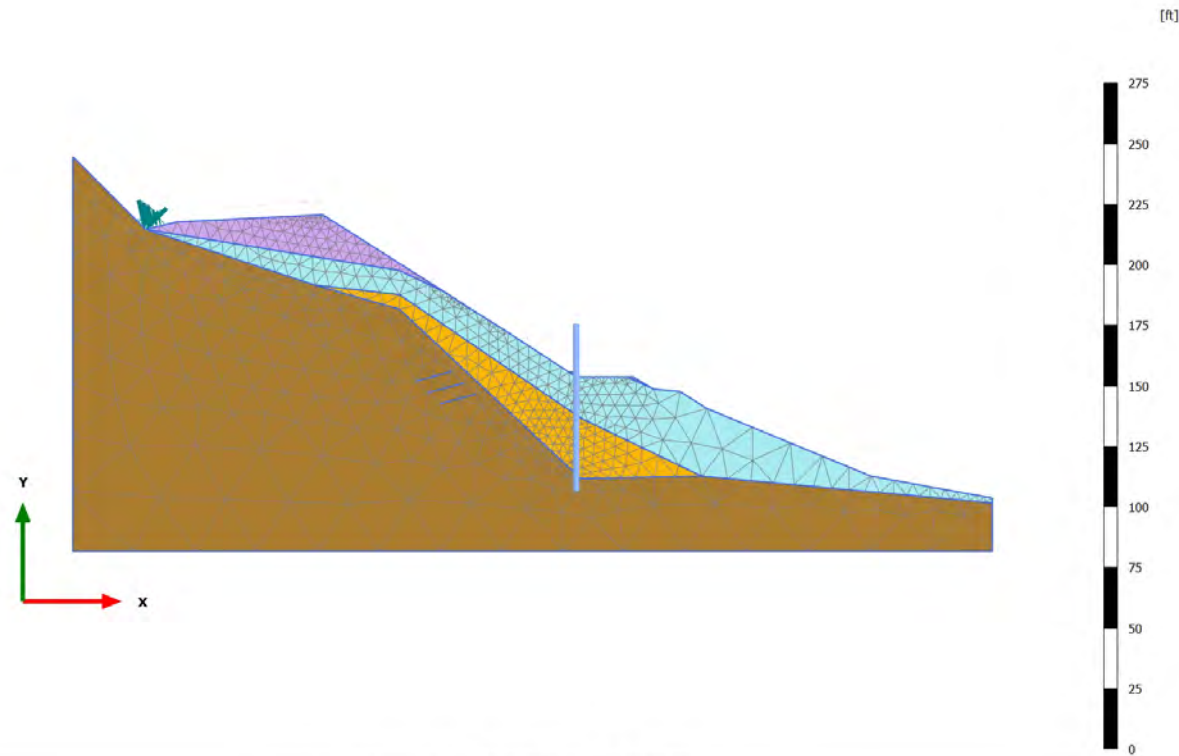
4.1.2 Calculation results, Exc to MSE [Phase_1] (1/21), Deformed mesh $|u|$ 

Deformed mesh $|u|$ (at true scale)

Maximum value = 0.1279 ft (Element 4234 at Node 11470)

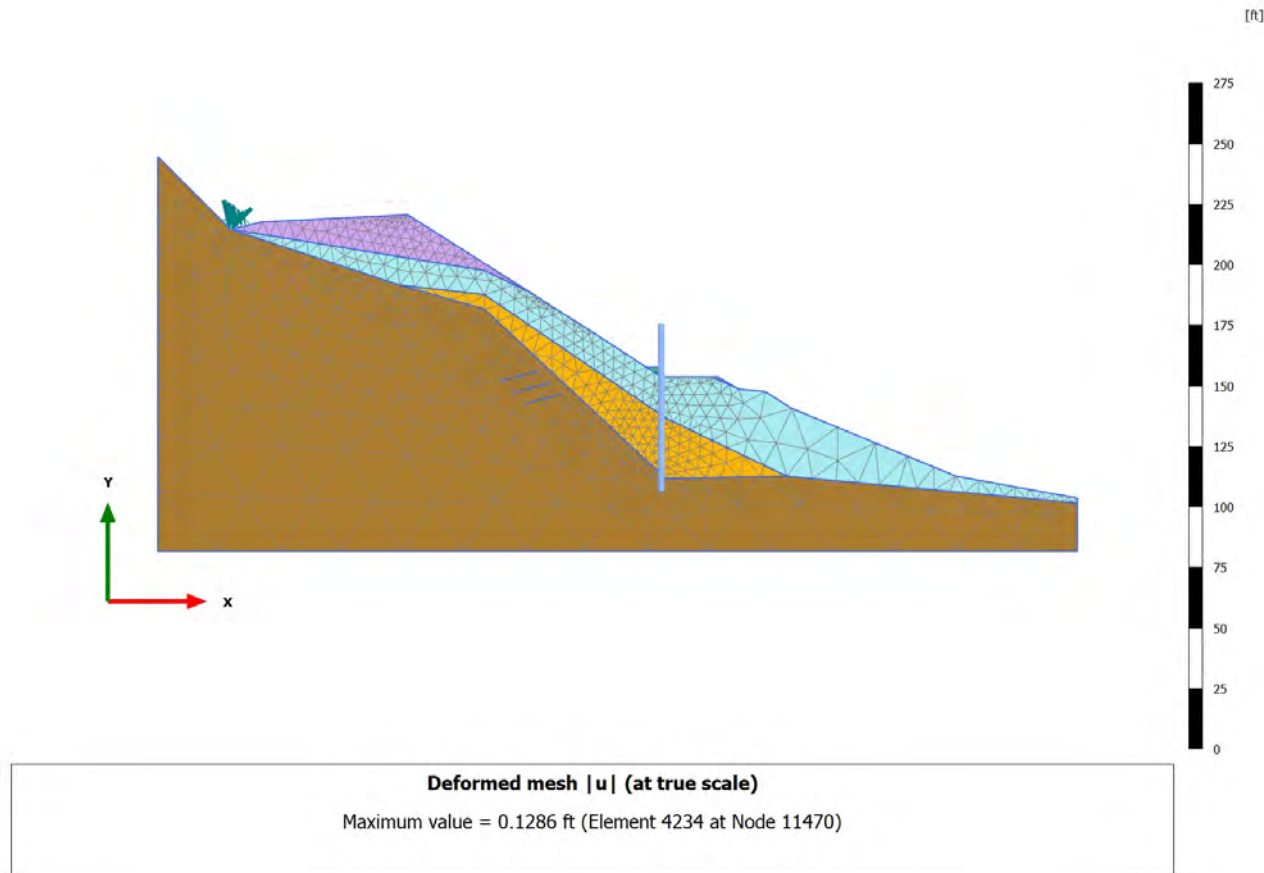
4.1.3 Calculation results, Install SP [Phase_2] (2/23), Deformed mesh |u|

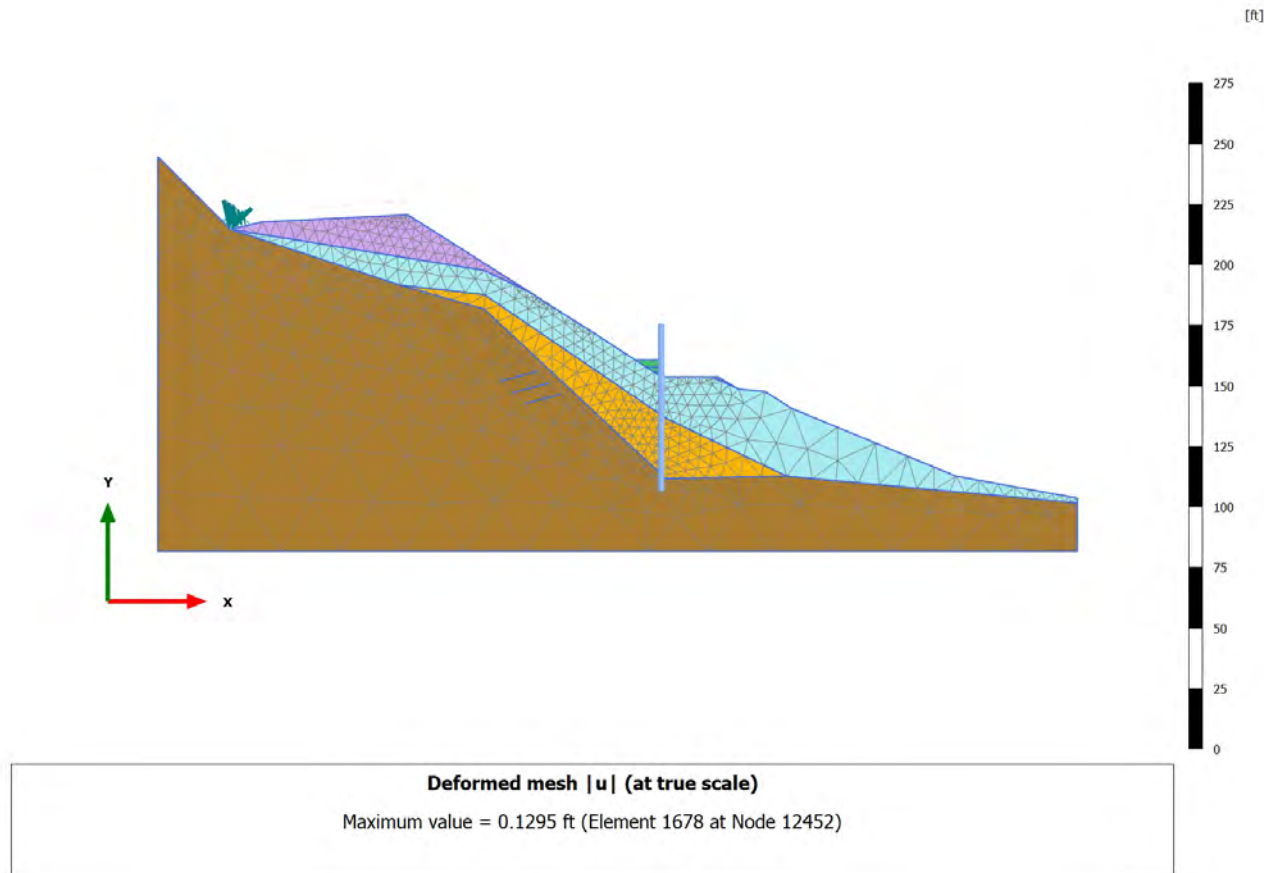


4.1.4 Calculation results, SP BF 1 [Phase_3] (3/27), Deformed mesh $|u|$ 

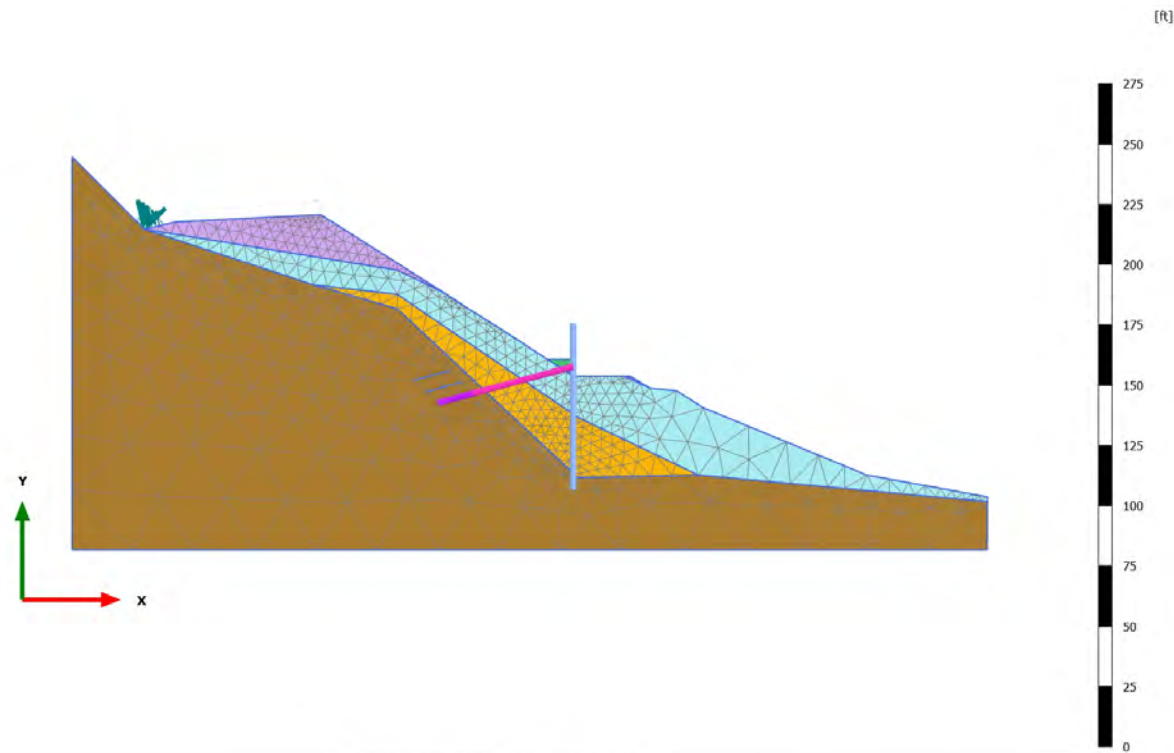
Deformed mesh $|u|$ (at true scale)

Maximum value = 0.1282 ft (Element 4234 at Node 11470)

4.1.5 Calculation results, SP BF 2 [Phase_4] (4/31), Deformed mesh $|u|$ 

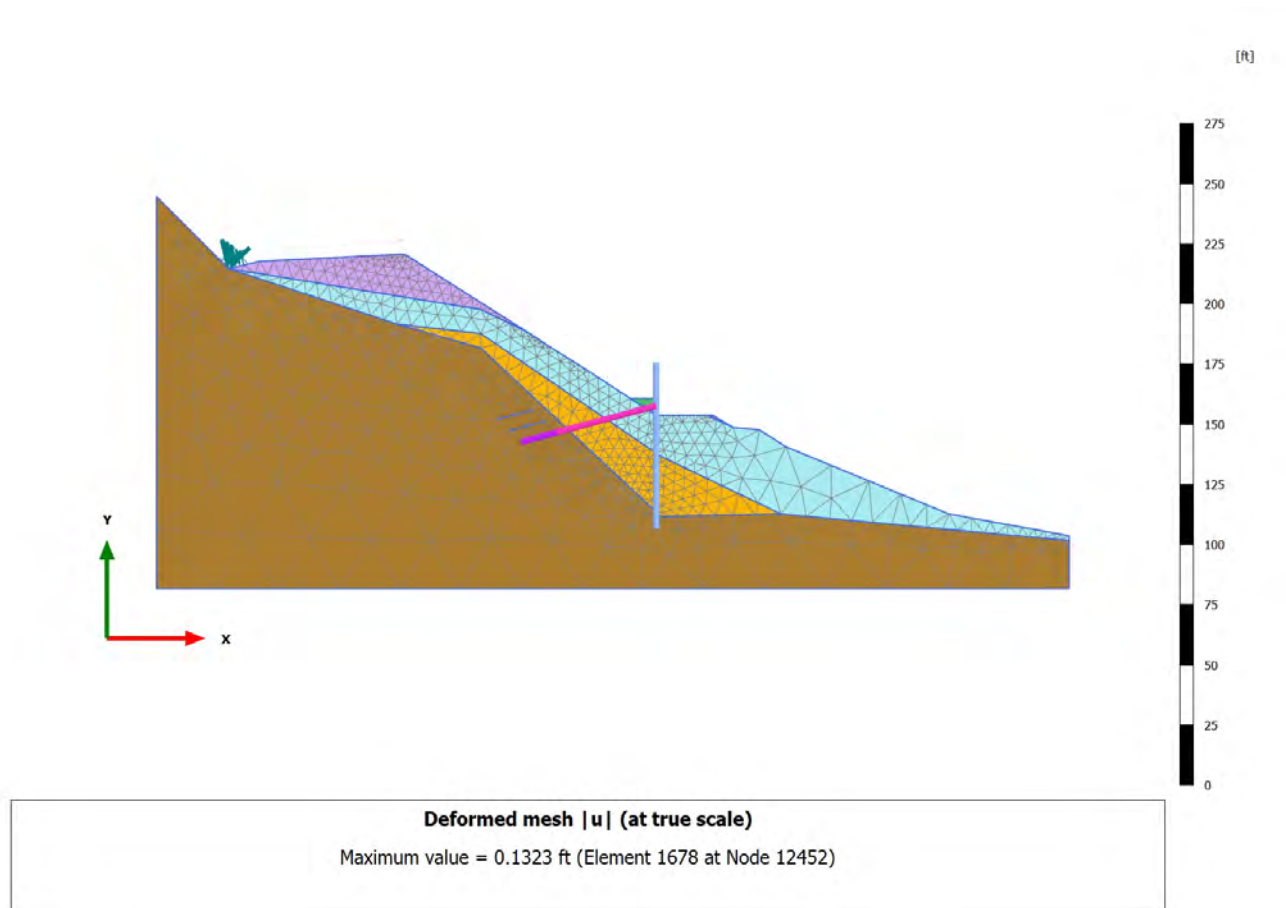
4.1.6 Calculation results, SP BF 3 [Phase_38] (38/35), Deformed mesh $|u|$ 

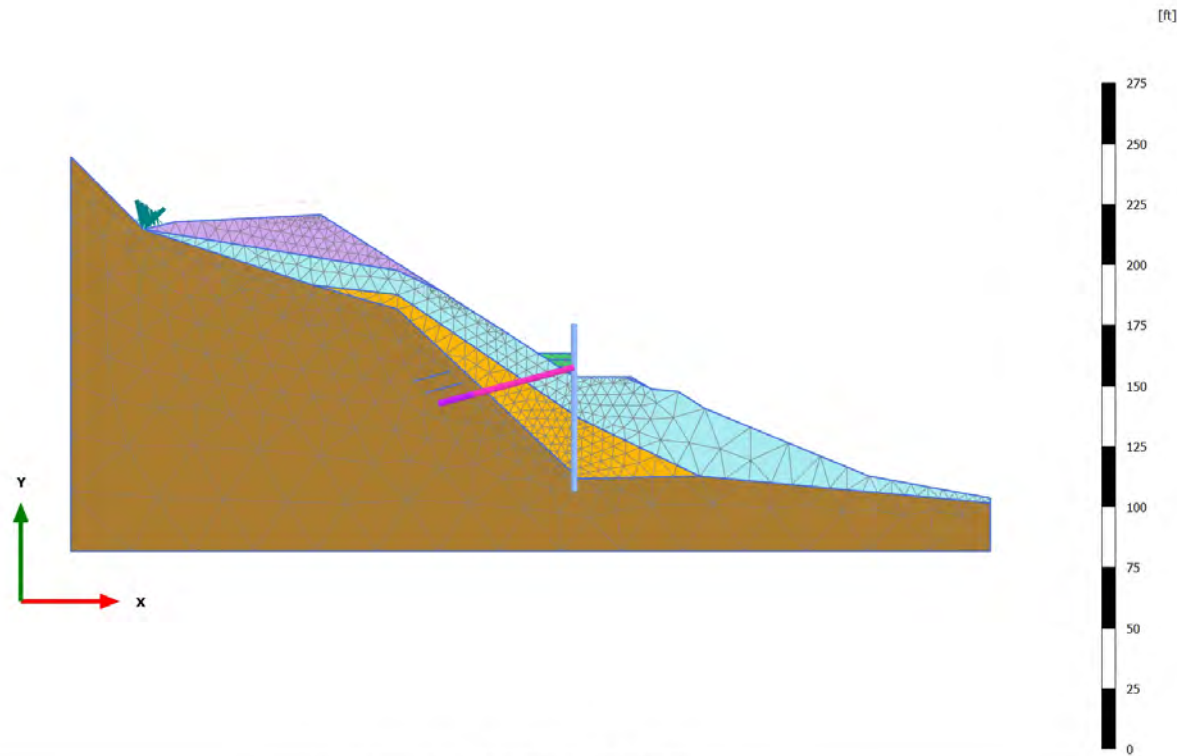
4.1.7 Calculation results, Install Tieback 1 [Phase_5] (5/222), Deformed mesh |u|



Deformed mesh |u| (at true scale)

Maximum value = 0.1324 ft (Element 1678 at Node 12452)

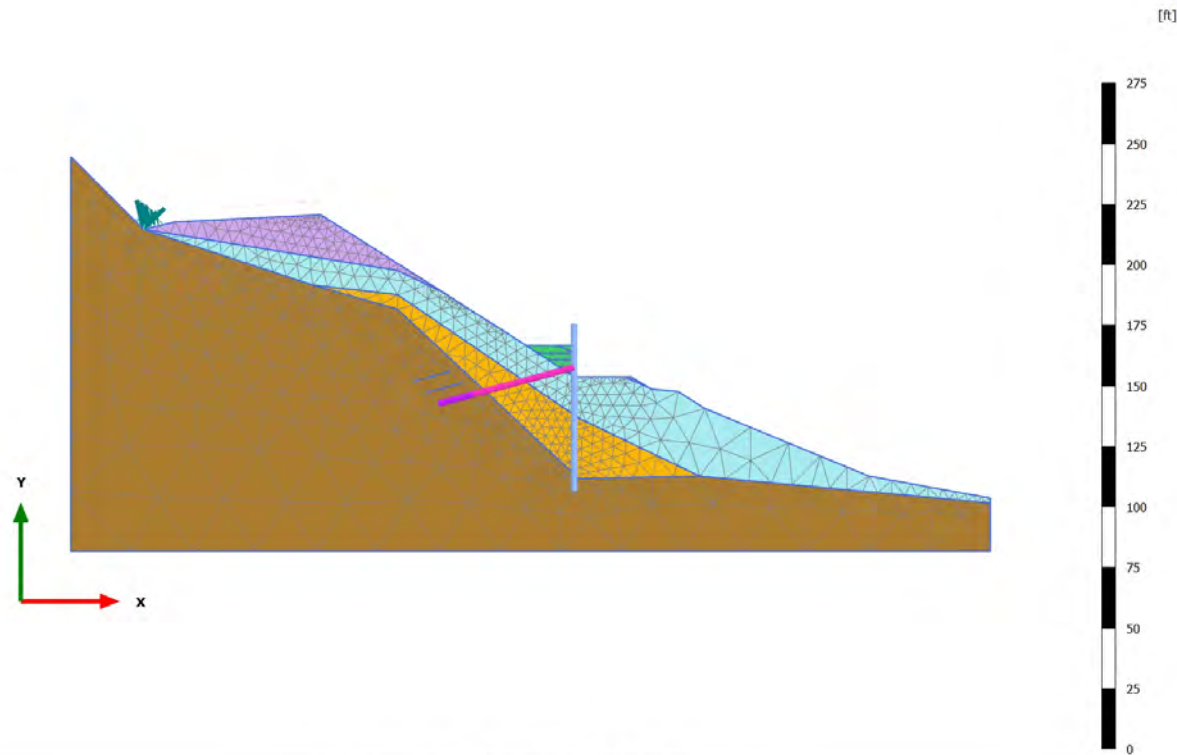
4.1.8 Calculation results, Prestress Tieback 1 [Phase_6] (6/227), Deformed mesh $|u|$ 

4.1.9 Calculation results, SP BF 4 [Phase_7] (7/231), Deformed mesh $|u|$ 

Deformed mesh $|u|$ (at true scale)

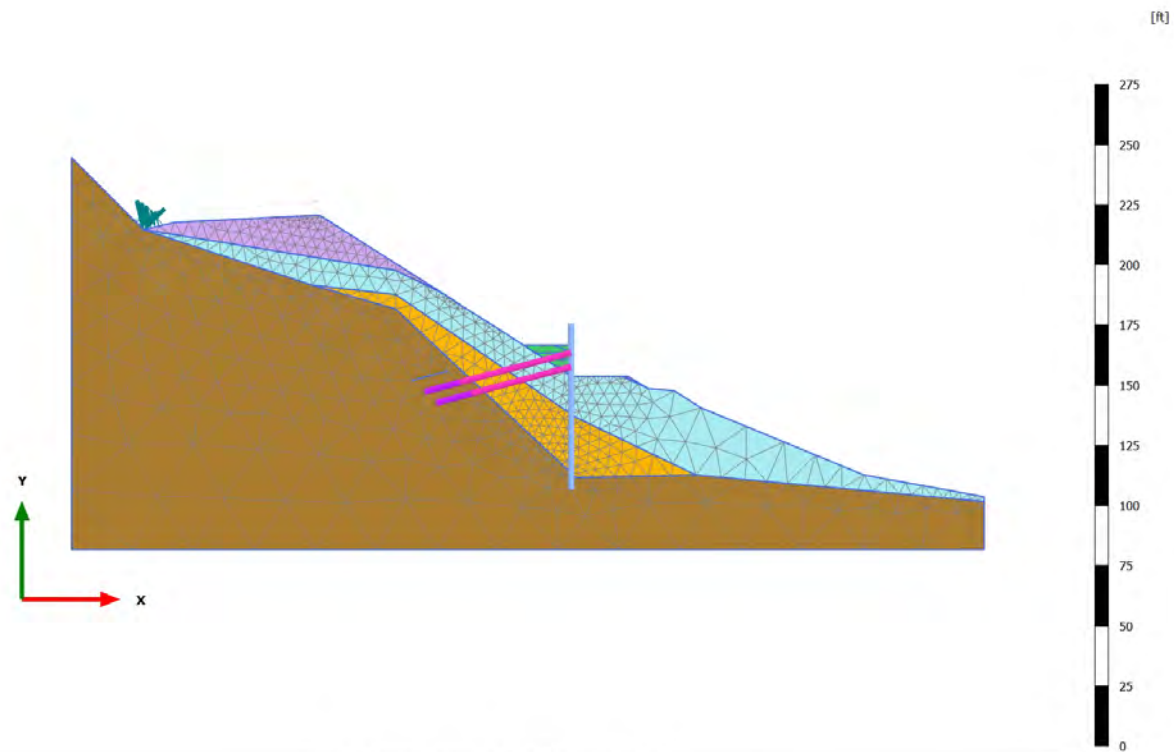
Maximum value = 0.1323 ft (Element 1678 at Node 12452)

4.1.10 Calculation results, SP BF 5 [Phase_8] (8/236), Deformed mesh |u|



Deformed mesh |u| (at true scale)

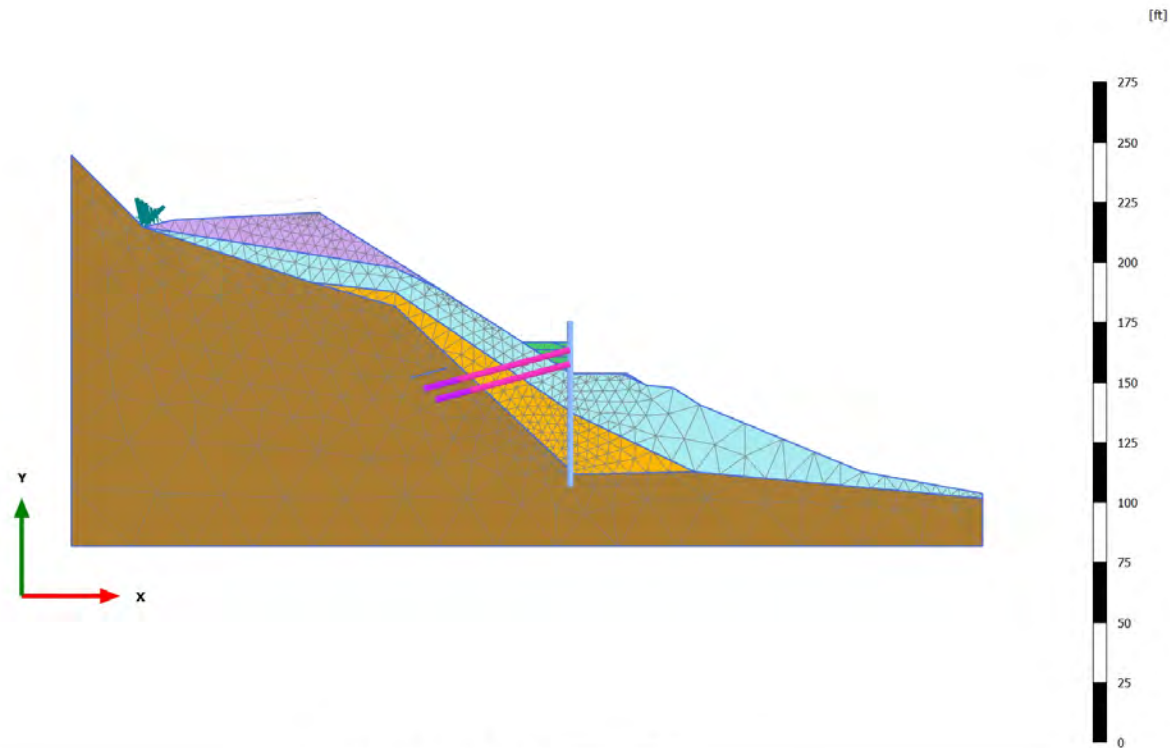
Maximum value = 0.1325 ft (Element 1678 at Node 12452)

4.1.11 Calculation results, Install Tieback 2 [Phase_9] (9/241), Deformed mesh $|u|$ 

Deformed mesh $|u|$ (at true scale)

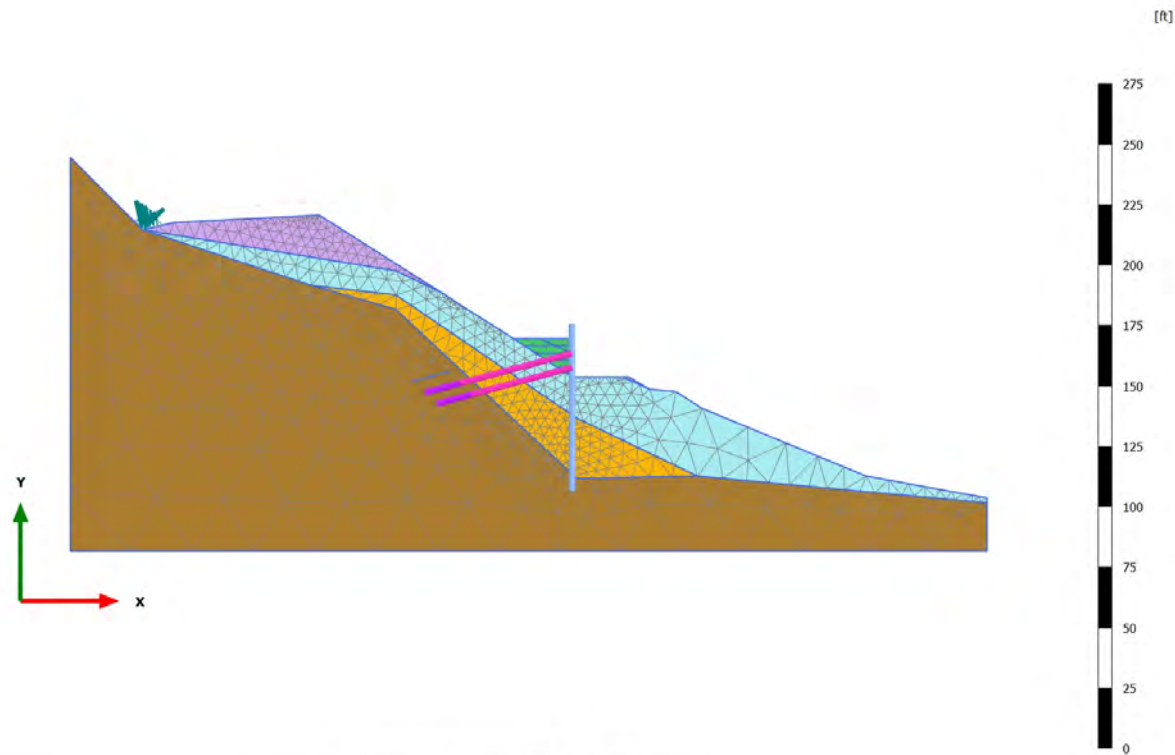
Maximum value = 0.1325 ft (Element 1678 at Node 12452)

4.1.12 Calculation results, Prestress Tieback 3 [Phase_10] (10/250), Deformed mesh $|u|$



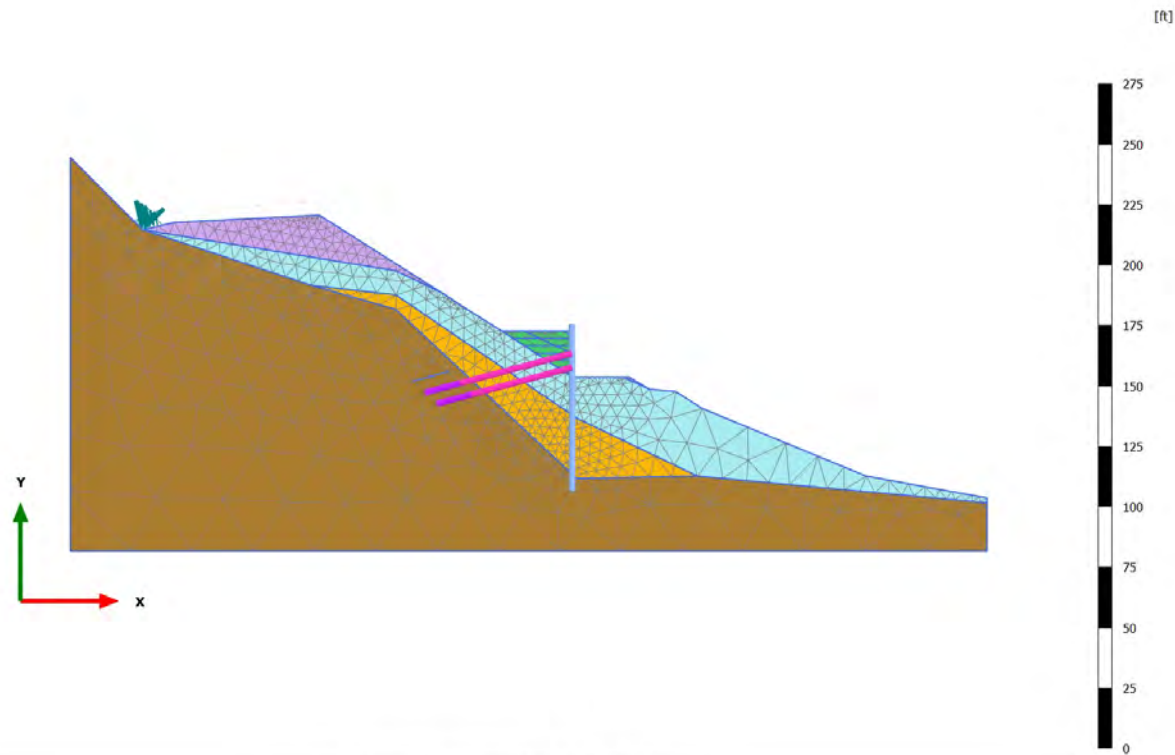
Deformed mesh $|u|$ (at true scale)

Maximum value = 0.1324 ft (Element 1678 at Node 12452)

4.1.13 Calculation results, SP BF 6 [Phase_11] (11/254), Deformed mesh $|u|$ 

Deformed mesh $|u|$ (at true scale)

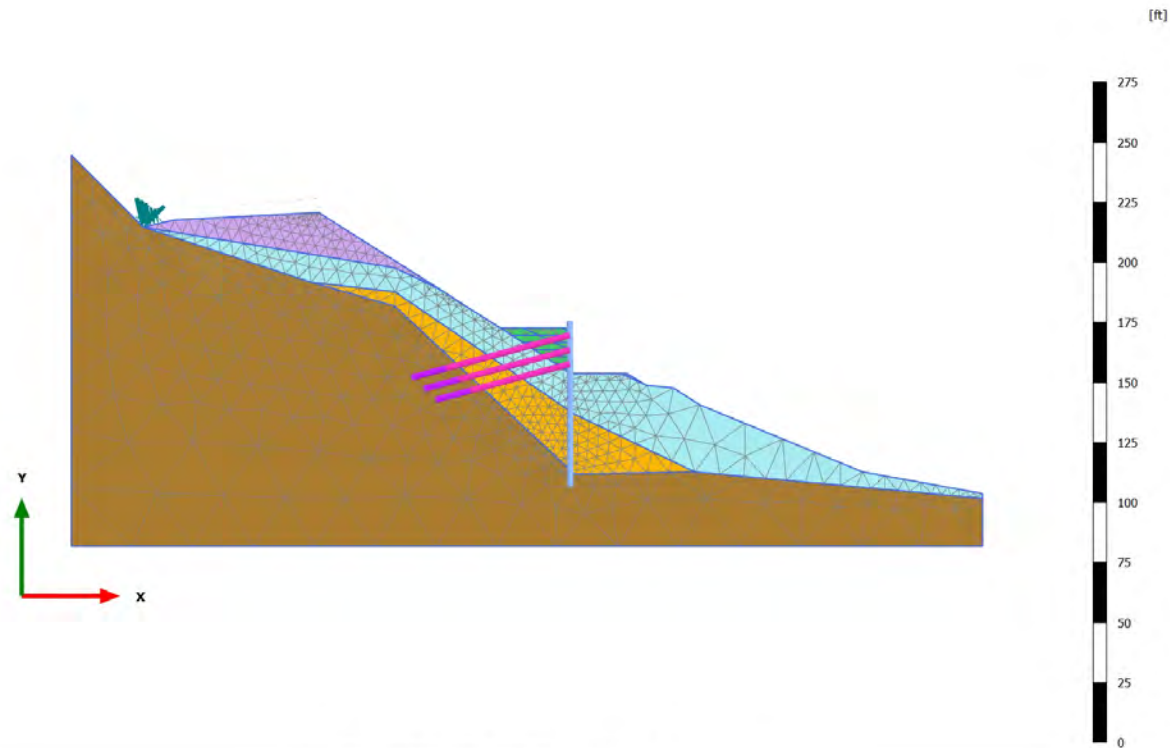
Maximum value = 0.1325 ft (Element 1678 at Node 12452)

4.1.14 Calculation results, SP BF 7 [Phase_39] (39/262), Deformed mesh $|u|$ 

Deformed mesh $|u|$ (at true scale)

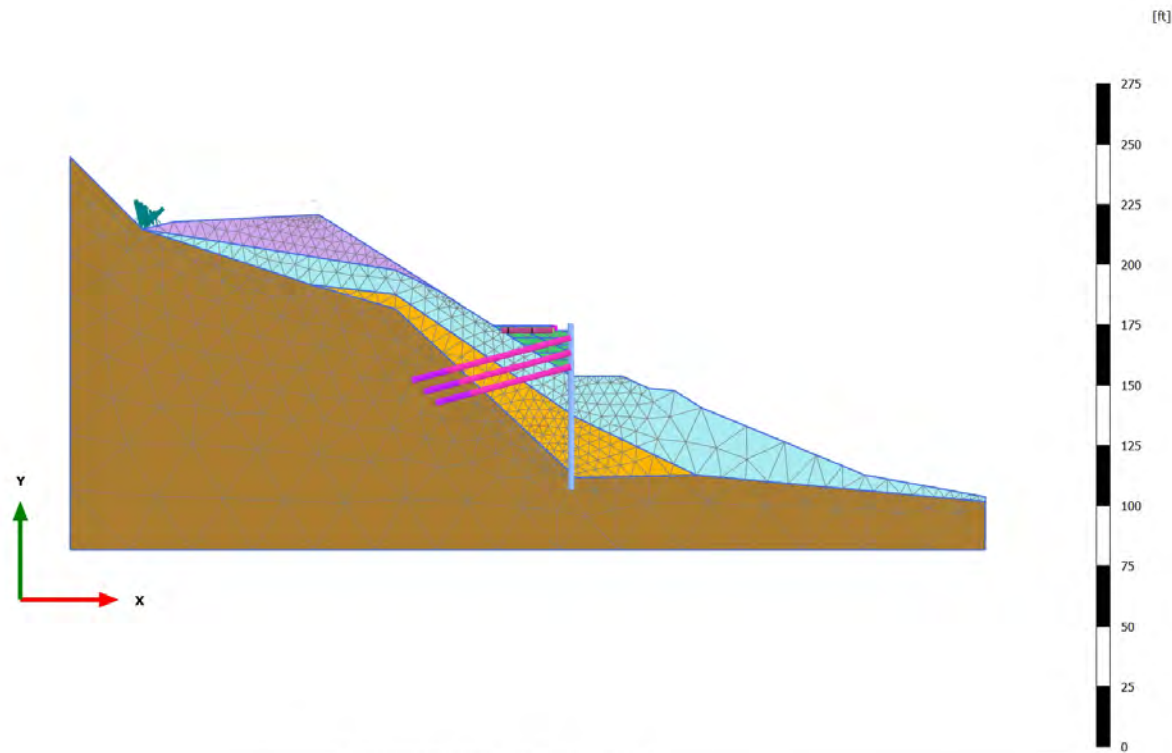
Maximum value = 0.1332 ft (Element 1678 at Node 12452)

4.1.16 Calculation results, Prestress Tieback 3 [Phase_41] (41/333), Deformed mesh $|u|$



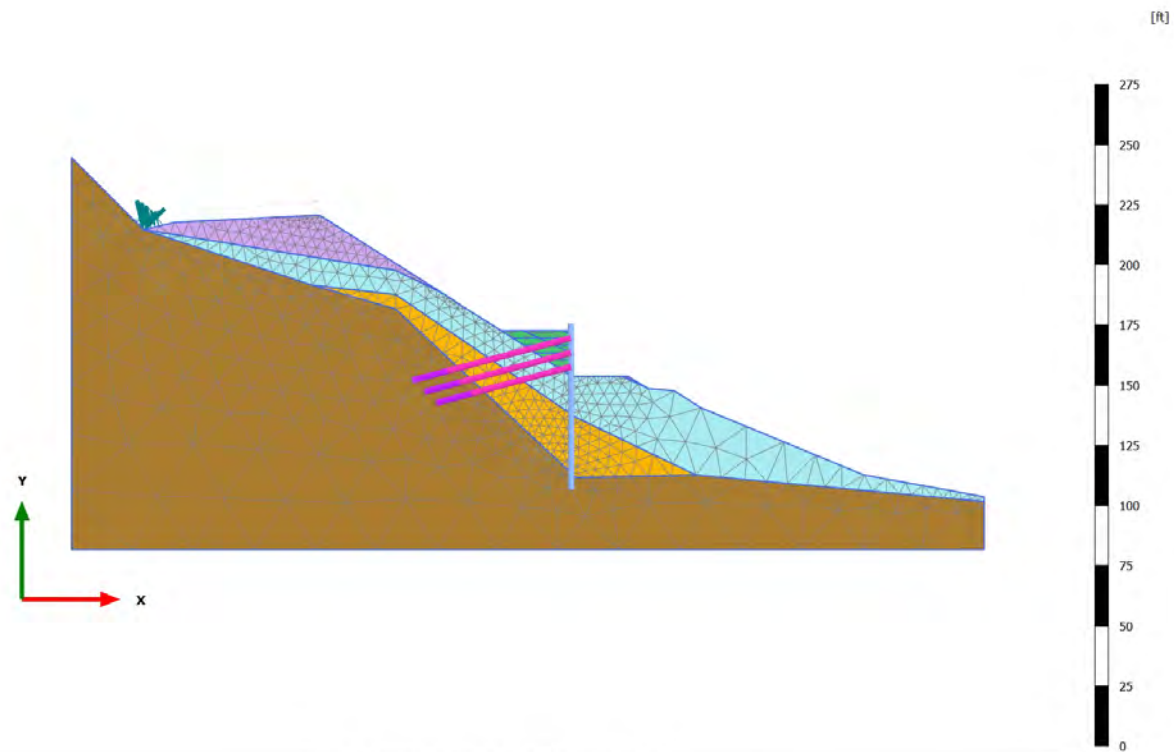
Deformed mesh $|u|$ (at true scale)

Maximum value = 0.1580 ft (Element 0 at Node 9428)

4.1.17 Calculation results, MSE Lift 1 [Phase_12] (12/337), Deformed mesh $|u|$ 

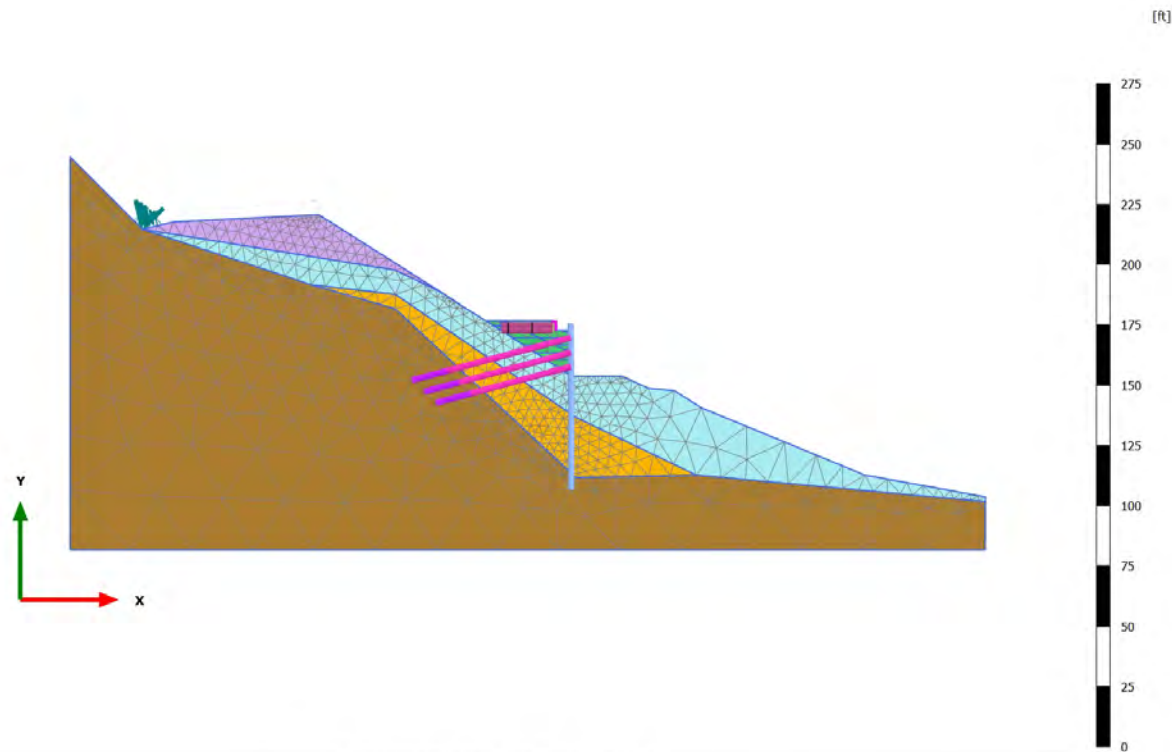
Deformed mesh $|u|$ (at true scale)

Maximum value = 0.1587 ft (Element 0 at Node 9428)

4.1.15 Calculation results, Install Tieback 3 [Phase_40] (40/324), Deformed mesh $|u|$ 

Deformed mesh $|u|$ (at true scale)

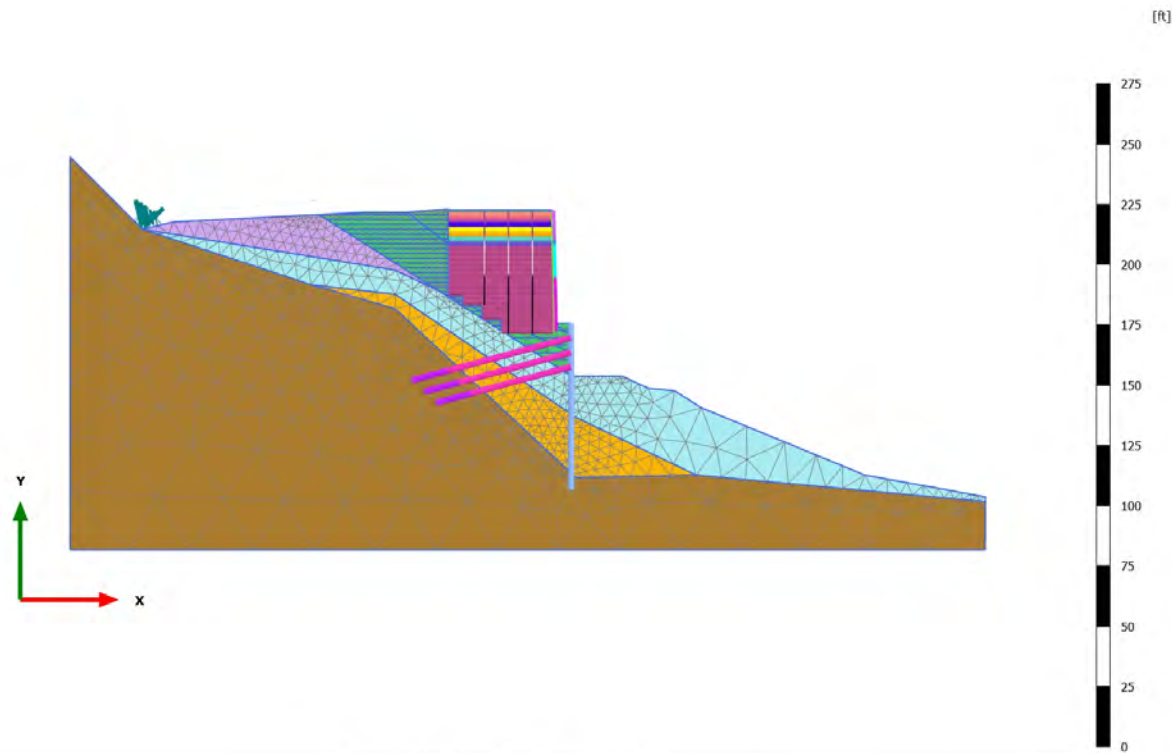
Maximum value = 0.1335 ft (Element 1678 at Node 12452)

4.1.18 Calculation results, MSE Lift 2 [Phase_13] (13/347), Deformed mesh $|u|$ 

Deformed mesh $|u|$ (at true scale)

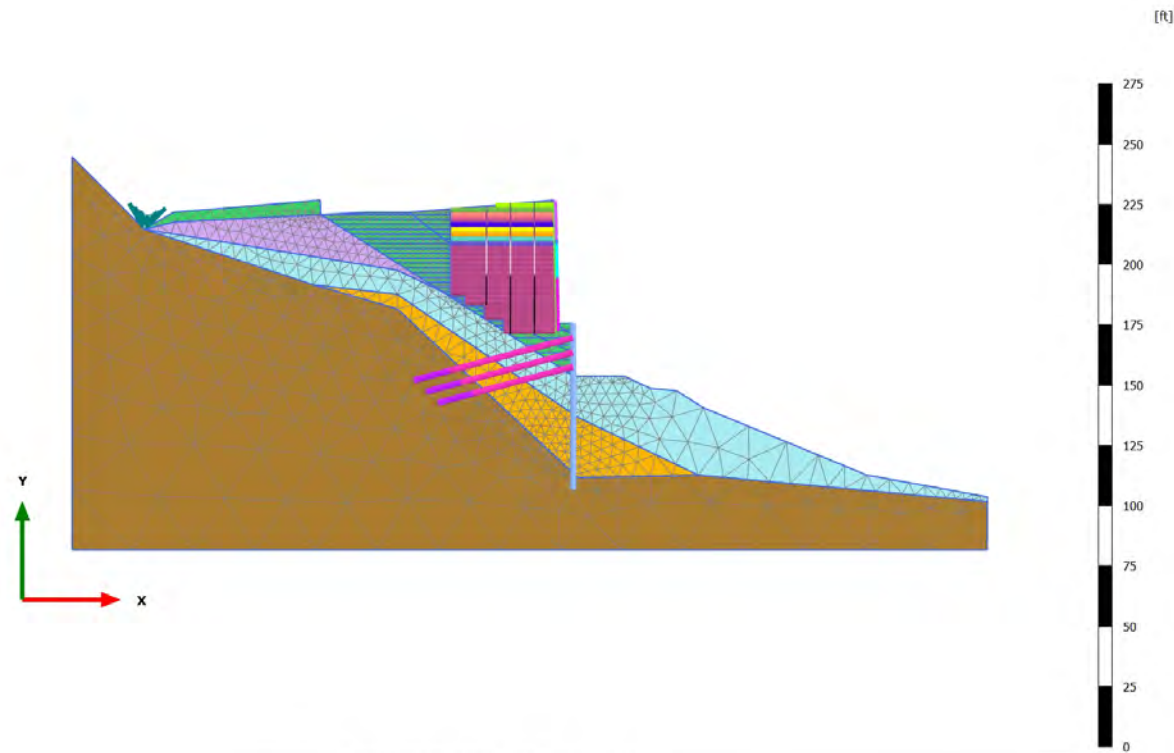
Maximum value = 0.1595 ft (Element 0 at Node 9428)

This sequence continues until the top of the wall is reached.

4.1.19 Calculation results, MSE Lift 25 [Phase_36] (36/531), Deformed mesh $|u|$ 

Deformed mesh $|u|$ (at true scale)

Maximum value = 0.4961 ft (Element 423 at Node 28618)

4.1.20 Calculation results, MSE Lift 26 [Phase_37] (37/547), Deformed mesh $|u|$ 

Deformed mesh $|u|$ (at true scale)

Maximum value = 0.5264 ft (Element 0 at Node 46926)